

THESIS

A COMBINED FIELD ANALYSIS AND MODELING APPROACH FOR ASSESSING THE
IMPACT OF GROUNDWATER PUMPING ON STREAMFLOW

Submitted by

Luke Flores

Department of Civil and Environmental Engineering

In partial fulfillment of the requirements

For the Degree of Master of Science

Colorado State University

Fort Collins, Colorado

Summer 2018

Master's Committee:

Advisor: Ryan T. Bailey

Timothy K. Gates
William E. Sanford

Copyright by Luke Flores 2018

All Rights Reserved

ABSTRACT

A COMBINED FIELD ANALYSIS AND MODELING APPROACH FOR ASSESSING THE IMPACT OF GROUNDWATER PUMPING ON STREAMFLOW

The magnitude of volumetric water exchange between streams and alluvial aquifers impacts contaminant transport rates, channel erosion and sedimentation, nutrient loading, and aquatic and riparian habitat. Quantifying the interactions between stream water and groundwater is also critically important in regions where surface water and tributary groundwater are jointly administered under a prior appropriation doctrine, such as in the western United States. Of particular concern is the effect of a nearby pumping well on streamflow. When the cone of influence of a pumping well reaches a nearby stream, the resulting hydraulic gradient can induce enhanced seepage of streamflow into the aquifer or decrease the rate of groundwater discharge to the stream. The change in these rates is often modeled using analytical or numerical solutions, or some combination of both.

Analytical solutions, although simple to apply, can produce discrepancies between field data and model output due to assumptions regarding stream and aquifer geometry and homogeneity of hydraulic parameters. Furthermore, the accuracy of such models has not been investigated in detail due to the difficulty in measuring streamflow loss in the field. In the first part of this thesis, a field experiment was conducted along a reach of the South Platte River in Denver, Colorado to estimate pumping-induced streamflow loss and groundwater head drawdown, and compare data against analytical modeling results. The analytical solutions proved accurate if streamflow was low and constant, but performed poorly if streamflow was high and variable. In particular, the

models are not capable of accurately simulating the effects of increasing stream width and bank storage due to rapid increases in streamflow. To better account for these effects a new analytical modeling framework is introduced which accounts for all major factors contributing to streamflow loss for a given site for both periods of pumping and periods between pumping. For the reach analyzed herein, the method illustrates that pumping wells often only caused half of the given streamflow loss occurring along the reach. This method can be used in other stream-aquifer systems impacted by nearby pumping.

The U.S. Geological Survey's three-dimensional finite-difference groundwater flow model, MODFLOW, was also used to assess the impacts of pumping on streamflow. While MODFLOW removes many of the restrictive assumptions that define analytical solutions, certain limitations persist when the program is applied on local, fine scales with dynamic interactions between a stream and alluvium. In particular, when the average stream width is greater than the computational grid cell size, the model will return systematically biased, grid-dependent results. Moreover, simulated streamflow loss will be limited in the range of values that can be modeled. To address these limitations, a new stream module is presented which (1) allows for streams to dynamically span multiple computational grid cells over a cross section to allow for a finer mesh; (2) computes streamflow and backwater stage along a stream reach using the quasi-steady dynamic wave approximation to the St. Venant equations, which allows for more accurate stream stages when normal flow cannot be assumed or a rating curve is not available; and (3) incorporates a process for computing streamflow loss when an unsaturated zone develops under the streambed. Streamflow loss is not assumed constant along a cross section. It is shown that most streamflow loss occurs along stream banks and over newly inundated areas after increases in upstream streamflow. The new module is tested against streamflow and groundwater data

collected in a stream-aquifer system along the South Platte River in Denver, Colorado and to estimate the impact of nearby pumping wells on streamflow. When compared with existing stream modules more accurate results are obtained from the new module. The new module can be applied to other small-scale stream-aquifer systems.

TABLE OF CONTENTS

ABSTRACT.....	ii
LIST OF FIGURES	vii
1. BACKGROUND AND MOTIVATION	1
1.1 Flow Through the Hyporheic Zone	1
1.2 Motivation	2
1.3 Pumping Wells	3
1.4 Analytical Solutions	3
1.5 Field Site Analyses	5
1.6 Numerical Modeling	6
1.7 Current Stream-Aquifer Conceptualization	7
1.8 Summary of Objectives	9
REFERENCES	12
2. AN ANALYTICAL MODELING APPROACH FOR ESTIMATING STREAMFLOW LOSS IMPACTED BY GROUNDWATER PUMPING	17
2.1 Introduction	17
2.2 Methods	22
2.2.1 <i>Study Region</i>	22
2.2.2 <i>Field Data Collection</i>	24
2.2.3 <i>Analytical Modeling of Streamflow Depletion</i>	27
2.3 Results and Discussion	28
2.3.1 <i>Groundwater Drawdown</i>	28
2.3.2 <i>Streamflow Loss</i>	33
2.3.3 <i>General Equation for Streamflow Loss</i>	40
2.4 Summary and Conclusions	45
REFERENCES	47
3. MODFLOW MODULE FOR SIMULATING STREAM-AQUIFER INTERACTIONS IN WIDTH VARIABLE STREAMS USING ST. VENANT EQUATIONS	51
3.1 Introduction	51
3.2 Development of Dynamic Streamflow Module	59
3.2.1 <i>Overview of the DSF Module</i>	59
3.2.2 <i>Determining Flow Depth</i>	60
3.2.3 <i>Determining Flowrate and Seepage</i>	62

3.2.3 DSF within MODFLOW	66
3.3 Application of DSF	68
3.3.1 Field Site	68
3.3.2 Field Data Collection	69
3.3.3 Development of MODFLOW Model	70
3.3.4 Model Results	72
3.3.4.1 Groundwater Head	72
3.3.4.2 Streamflow Loss	73
3.3.4.3 Effect of Pumping Wells	77
3.4 Conclusions	80
REFERENCES	81
4. A COMPARISON OF ANALYTICAL AND NUMERICAL METHODS: A SYNTHESIS.....	87
4.1 Introduction.....	87
4.2 Groundwater Head Distribution	87
4.3 Streamflow Loss	94
5. CONCLUSIONS AND FUTURE WORK	99
5.1 Analytical Solutions	99
5.1.1 Future Work on Analytical Solutions	99
5.2 Numerical Solutions.....	100
5.1.1 Future Work for DSF Module	100
5.3 Overall Conclusions	101

LIST OF FIGURES

Figure 1. Simulated pathlines beneath streambed (from Stonedahl et al., 2010).....	1
Figure 2. 2a (Top). Physical continuous stream-aquifer system that is losing flow through both a saturated and unsaturated soil after an increase in stream stage; 2b (Bottom). Numerical discretized stream-aquifer system in which only saturated streamflow loss occurs.....	9
Figure 3. 3a (Left): Location of study site and relative proximity to Chatfield Reservoir and City of Denver; 3b (Right): Map of South Platte River reach where streamflow and groundwater levels were monitored, showing five monitoring well locations, four pumping wells, two streamflow gauging sites, and location where river stage was monitored.....	23
Figure 4. Drawdown at the 6.10 m observation well at Location D compared with three analytical solutions (Hunt, Theis, Theis with image well).	29
Figure 5. Drawdown at the 4.25 m observation well at Location A compared with three analytical solution (Hunt, Theis, Theis with image well).	30
Figure 6. River stage compared to 0.91 m observation well at Location A.....	31
Figure 7. Drawdown at the 3.35 m observation well at Location E compared with two analytical solutions (Hunt, Theis).....	32
Figure 8. 8a (Top): Measured and predicted (with Hunt solution) streamflow depletion. Upper horizontal axis shows pumping rate; 8b (Bottom Left): Region of 6a between A and A' showing streamflow depletion (measured and predicted with Glover solution (dashed line)) on primary vertical axis and streamflow rate (solid black line) on secondary vertical axis; 8c (Bottom Right): Region of 8a figure between B and B' showing streamflow depletion and streamflow rate.	35
Figure 9. Downstream cross section illustrating large variations in stream stage and width due to variations in upstream flowrate.	37
Figure 10. Theoretical pumping period for low upstream streamflow comparing measured data with Glover (1954) and Hunt (1999) solution.	38
Figure 11. Measured data used to obtain $f(Q_u)$ with streamflow loss as a function of upstream streamflow.	41
Figure 12. Predicted streamflow loss using Eq. (2.8) compared with Hunt solution.....	42
Figure 13. Portion of streamflow loss due to pumps and changes in upstream streamflow in 2017 according to general streamflow loss model (Eq. 2.8).	43
Figure 14. Portion of streamflow loss due to pumps and changed in upstream streamflow in 2018 according to general streamflow loss model (Eq. 2.8).	44
Figure 15. 15a. Physical continuous stream-aquifer system that is losing flow through both a saturated and unsaturated soil after an increase in stream stage; 15b. Numerical discretized stream-aquifer system in which only saturated streamflow loss occurs.	55
Figure 16. Example DSF cross sections projected on MODFLOW grid. Cross sections alternate between red and blue and black cells represent largest possible stream banks over simulation period.....	60

Figure 17. Schematic of DSF cross section in relation to MODFLOW grid (after Ou et al., 2013).....	65
Figure 18. Logical flowchart illustrating the methodology of computing stream stage and flowrate within DSF.	66
Figure 19. General framework of MODFLOW-NWT when DSF module is active.....	67
Figure 20. 20a (Left): Location of study site and relative proximity to Chatfield Reservoir and City of Denver; 20b (Right): Map of South Platte River reach where streamflow and groundwater levels were monitored, showing five monitoring well locations, four pumping wells, two streamflow gauging sites, and location where river stage was monitored. MODFLOW model boundary and boundary conditions shown in red and blue, respectively.....	69
Figure 21. Hydrograph of South Platte River over the study period.	70
Figure 22. Simulated and observed groundwater heads at Location C.....	72
Figure 23. Simulated and observed groundwater heads at Location A.....	73
Figure 24. Computed streamflow loss with DSF and SFR2 modules evaluated against measured data.	74
Figure 25. 25a (Left): Inundation map of river during times of high flow at stress period hour 500; 25b (Right): Inundation map of river during times of low flow at stress period hour 550.....	75
Figure 26. 26a (Left): Inundation map of upstream reach during times of high flow at stress period hour 500; 26b (Right): Inundation map of upstream reach during times of low flow at stress period hour 550.....	76
Figure 27. 27a (Left): Inundation map of downstream reach during times of high flow at stress period hour 500; 27b (Right): Inundation map of downstream reach during times of low flow at stress period hour 550.....	77
Figure 28. Cross section over row 200 showing the transition from a losing to a gaining stream due to a decrease in streamflow.	77
Figure 29. 29a (Left): Inundation map and contour lines of groundwater head of downstream reach at stress period hour 950 when pumps are not operating; 29b (Right): Inundation map and contour lines of groundwater head of downstream reach at stress period hour 950 when pumps were modeled.	78
Figure 30. Groundwater profile over row 370 when pumps are simulated (in blue) and ignored (in red).	79
Figure 31. Pumping-induced streamflow loss.	79
Figure 32. Drawdown predictions from Hunt (1999) solution and MODFLOW DSF at Location A.	88
Figure 33. Drawdown predictions from Hunt (1999) solution and MODFLOW DSF at Location E.....	89
Figure 34. Drawdown predictions from Hunt (1999) solution and MODFLOW DSF at Location D.	90
Figure 35. Drawdown predictions from Hunt (1999) solution and MODFLOW DSF at Location C.	90
Figure 36. Contour map of the difference in drawdown (m) predictions between Hunt (1999) solution and MODFLOW DSF.	93
Figure 37. Predicted streamflow loss from the SFR2 module, the DSF module, and Eq. (2.8) compared with field collected data.	95
Figure 38 - Comparison of pumping-induced streamflow loss using DSF module and Eq. (2.8).	97

Figure 39. Portion of streamflow loss due to pumping wells when computed with Eq. (2.8) and the DSF module. ..98

LIST OF TABLES

Table 1. Hydraulic input parameters used the evaluation of drawdown curves.....	28
Table 2. Summary of collected streamflow data.	33
Table 3. Hydraulic input parameters used the evaluation of streamflow depletion equations.....	36
Table 4. Streamflow data that was classified as a ‘low flow’.....	39
Table 5. Evaluation of different MODFLOW stream modules.	57
Table 6. Necessary stream module parameters used for the DSF and SFR2 modules.....	71
Table 7. Root Mean Square Error (RMSE) of drawdown predictions of Hunt (1999) solution and MODFLOW DSF.	91
Table 8. Root Mean Square Error (RMSE) of predicted streamflow loss of the SFR2 module, DSF module, and Eq. (2.8).	96
Table 9. Root Mean Square Error (RMSE) of predicted streamflow loss of the SFR2 module, DSF module, and Eq. (2.8) when streamflow loss data collected during times of largest streamflow are neglected.	96

1. BACKGROUND AND MOTIVATION

1.1 Flow Through the Hyporheic Zone

The interaction between surface water and groundwater has long been acknowledged by hydrologists and hydrogeologists, although quantifying the magnitude and timing of water exchange fluxes remains a challenge (Kalbus et al., 2006). One such flux is the exchange of water through the hyporheic zone, or the zone directly underneath and adjacent to the stream. Hyporheic flow is unique from groundwater flow in that it is often bidirectional. That is, water moves between surface water and shallow groundwater continuously and over very short distances and times. Fig. 1 shows pathlines in the hyporheic zone beneath a channel bed where it is seen that water may leave and re-enter a stream over a single short reach.

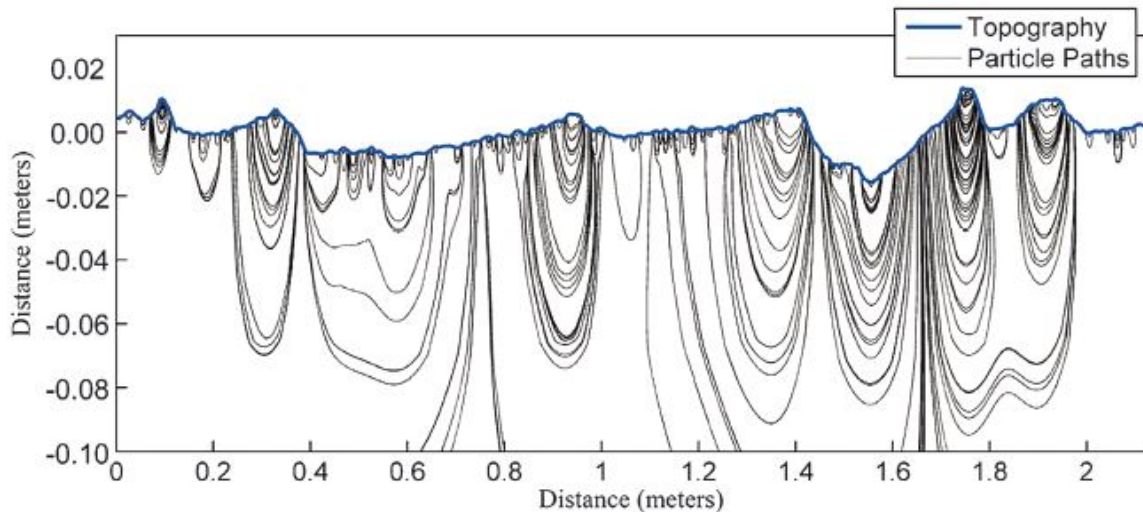


Figure 1. Simulated pathlines beneath streambed (from Stonedahl et al., 2010)

Flow through the hyporheic zone is primarily driven through hydrostatic and hydrodynamic mechanisms (Boano et al., 2014). Hydrostatic forces result from pressure gradients through the streambed and are variable upon stream topography and regional hydraulic gradients.

Hydrodynamically driven hyporheic flows are primarily due to momentum transfer resulting from directional changes in surface water flow i.e. river bends, lateral migration, vertical velocities, expanding stream width during floods, etc. Boano et al. (2014) argue hydrostatic forces will generally be more determinant in hyporheic flows.

Determining the volumetric flux of water exchange between a river and an underlying aquifer is important for water resource managers, environmental managers, and policy makers. Exchange rates between surface water and groundwater can determine phenomena including, but not limited to, contaminant transport rates (Brunke and Gonser, 1997), nutrient loads (Myers, 2013; Bailey et al., 2014), erosion and channel morphology (Keller and Kondolf, 1990; Fox et al., 2007), stream water temperature (Constantz, 1998; Hendricks and White, 1998), and wildlife habitat (Hancock et al., 2005; Beatty et al., 2010). Brunke and Gonser (1997) provide a detailed overview of various ecological, biological, chemical, and physical processes that are dependent upon exchange rates between surface water and groundwater.

1.2 Motivation

The quantification of these fluxes also has significant consequences in regions where surface water and groundwater rights are jointly administered (Colorado Water Conservation Board, 2015). In fact, in many states where the prior appropriation doctrine governs water rights and policy, tributary groundwater is defined as being hydraulically connected to surface water and is governed as such (Water Right Determination and Administration Act, 1969). Augmentation plans have been put into place which allow for a junior water rights holder to divert or remove water from fully allocated water bodies and then to replace the removed water through some other means. This necessitates the need for accurate quantification of water exchange rates.

1.3 Pumping Wells

Of particular importance is the ability to predict streamflow losses that occur due to nearby pumping wells. In general, removing groundwater from an alluvial aquifer via pumping wells disturbs the existing groundwater head equilibrium, establishing a new time-variant hydraulic gradient that can induce streamflow loss, increase the existing streamflow loss, or decrease the rate of groundwater return to stream reaches that are within the area of influence of the pumping wells. Using the language of Sec. (1.1), the well-induced hydraulic gradient creates a hydrostatic stress in the hyporheic zone around the stream. As seen in Fig. 1, a defining characteristic of the hyporheic zone is the ‘back-and-forth’ nature of the water exchange. Streamflow may exit through the streambed but will eventually re-enter the streambed at some other point along the reach. In effect, a pumping well interrupts this process and streamflow which leaves the streambed (due to the hydrostatic pressures the well induces) will not return to the stream.

The rate of exchange between stream water and groundwater can be tempered by fine sediments along the streambed that have a lower hydraulic conductivity than the underlying aquifer (Hantush, 1965; Spalding and Khaleel, 1991; Chen et al., 2008, Fox, 2011). There are three general methods for determining pumping-induced streamflow loss: analytical models, numerical models, and field site analyses.

1.4 Analytical Solutions

Several analytical models have been derived that provide estimates for pumping-induced streamflow loss under certain stream-aquifer connection conditions. Two of the most commonly used solutions are the Glover (1954) and Hunt (1999) solutions. The Glover solution, derived from the Theis (1935) solution for head drawdown due to pumping, assumes an infinitely long and straight river that fully penetrates the aquifer. Aquifer parameters (transmissivity, storage

coefficient) are assumed homogenous and groundwater head is considered initially uniform. Streamflow losses are assumed small enough that changes in stream stage and width can be neglected (the river is treated as having a width of zero) and the stream has a perfect hydraulic connection with the aquifer, i.e. stream seepage remains under saturated conditions and an unsaturated zone does not develop. Moreover, the existence of a streambed clogging layer is not accounted for. The Glover solution is a function of the complimentary error function *erfc* and is given as:

$$\frac{\Delta Q}{Q_w} = \text{erfc} \left(\sqrt{\frac{SL^2}{4Tt}} \right) \quad (1.1)$$

where ΔQ is the streamflow depletion rate [L^3/T], Q_w is the pumping rate [L^3/T], S is storativity or specific yield of the aquifer [-], T is aquifer transmissivity [L^2/T], L is the shortest distance between the pumping well and the river [L], and t is time since pumping began [T]. Eq. (1.1) approaches unity as t goes to infinity. The Hunt solution (Hunt, 1999) improves on the Glover solution by incorporating a streambed clogging layer and by modeling a partially penetrating stream, with the ratio of stream depletion rate to pumping rate given as:

$$\frac{\Delta Q}{Q_w} = \text{erfc} \left(\sqrt{\frac{SL^2}{4Tt}} \right) - \exp \left(\frac{\lambda^2 t}{4ST} + \frac{\lambda L}{2T} \right) \text{erfc} \left(\sqrt{\frac{\lambda^2 t}{4ST}} + \sqrt{\frac{SL^2}{4Tt}} \right) \quad (1.2)$$

where all parameters are identical to those in the Glover solution and λ is a conductance term, defined as the constant of proportionality between the seepage flowrate per unit length of river through the streambed and the gradient between the river stage and aquifer head [L/T]. Hunt also derived a solution for drawdown ϕ in two dimensions (x, y) in an alluvial aquifer under the same conditions:

$$\phi(x, y, t) = \frac{Q_w}{4\pi T} \left\{ E_1 \left[\frac{(L-x)^2 + y^2}{4Tt/S} \right] - \int_0^\infty e^{-\theta} E_1 \left[\frac{\left(L + |x| + \frac{2T\theta}{\lambda} \right)^2 + y^2}{\frac{4Tt}{S}} \right] d\theta \right\} \quad (1.3)$$

where all parameters are identical to those in Eq. (1.2) and θ is a variable of integration. While analytical solutions are relatively fast and easy to use (in comparison to more advanced numerical models) and essentially free (in comparison to obtaining field measurements) the accuracy of Eqs. (1.1) - (1.3) are largely dependent upon representatively correct input parameters (T , S , λ). Moreover, the assumptions made in the derivation of these analytical solutions are inherently always violated in the field. Biased results can be obtained that model a mathematical conceptualization of the problem and not the physical real world problem.

1.5 Field Site Analyses

Field analyses consist of *in situ* methods of direct measurement of parameters either directly or indirectly influencing streamflow loss. Field techniques include using seepage meters (Lee, 1977; Woessner and Sullivan, 1984), heat and solute tracers (Constantz et al., 2001; Constantz and Stonestrom, 2003; Anderson, 2005), grain size analyses (Hazen, 1892; Shepherd, 1989), and permeameter tests (Sophocleous et al., 1988; Fox et al., 2011). Although perhaps the most straightforward approach is through direct measurement of streamflow during pumping periods.

Hunt et al. (2001) tested his own solution (Hunt, 1999) against both measured streamflow data and observed groundwater levels on a small drainage canal area in New Zealand. The solution yielded good fits for both sets of data by calibrating λ ; however, the length of the pumping period was only 10 hours and the flowrate in the canal was less than approximately 0.05 m³/s. Therefore, the validity of the solution over a longer pumping period and for a larger stream is not known. The study also had difficulties in determining a known upstream flowrate

that was not within the zone of influence of the pumping well. Nyholm et al. (2000) performed a similar study on a headwater stream in Denmark where the Hunt (1999) solution was evaluated against field-collected streamflow data. However, both streamflow rates and pumping well rates were on the order of $0.01 \text{ m}^3/\text{s}$. Fox (2004) tested the validity of the Hunt drawdown solution with delayed yield effects (Hunt, 2003) along the South Platte River in eastern Colorado. He obtained a satisfactory match between observed and simulated head drawdown patterns by modifying Hunt's streambed conductance term, however model results were not compared to measured streamflow loss.

Using field measurements is perhaps the most accurate method of determining pumping-induced streamflow loss, as it does not involve any parameter estimation and removes the bias often associated with modeling. However it is often costly, labor intensive, and time consuming. Moreover in some cases it may not be practical if streamflow rates are high or if groundwater pumping rates are small compared to streamflow rates.

1.6 Numerical Modeling

As the demand for more integrated water management practices increases, so does the demand for increased modeling capabilities, especially in regard to surface water-groundwater interactions (Sophocleous, 2000). In terms of accuracy, numerical models are the standard in hydrologic monitoring and modeling as they are based on the discretization of exact partial differential equations. Unlike analytical models, numerical models can account for parameter heterogeneity, physical nonlinearities, and problem geometry so that solutions only lose accuracy due to numerics and not oversimplified assumptions.

There are a plethora of numerical models that seek to model surface water-groundwater interactions applying varying levels of complexity. Many fully-coupled models have been

developed which jointly solve a form of the St. Venant equations and the variably-saturated Richard's equation which are then cast into a single global matrix and solved simultaneously. Examples of such models include ParFlow (Maxwell et al., 2014), CATHY (Camporese et al. 2010), HydroGeoSphere (Therrien et al., 2006, Aquanty Inc., 2013), MODHMS (HydroGeoLogic, Inc.), and FIHM (Kumar et al. 2009). While the physical veracity of these models are the benchmark in hydrologic modeling, they typically require large input data sets (that are often unavailable to the modeler), require a high level of model understanding, and in some cases require payment for use. For these reasons, simpler, more manageable, and free open-source models are often resorted to.

Due to its wide spread availability as an open-source code, abundance of documentation, ease-of-use, and industry acceptance, MODFLOW (Harbaugh, 2005) has become the most commonly used numerical hydrologic model (Furman, 2008). Strictly speaking, MODFLOW is exclusively a groundwater flow model and all surface water-groundwater interactions are linked with MODFLOW in an uncoupled manner. However, the uncoupled nature of MODFLOW is arguably what makes it appealing as a hydrologic model. External modules can be independently created and easily combined with the existing MODFLOW framework with relative ease. In this sense, the uncoupled nature of MODFLOW can be seen as a benefit over more sophisticated coupled models; so long as the external modules are physically-based and provide accurate external stresses applied to the model.

1.7 Current Stream-Aquifer Conceptualization

Consider the simple conceptual alluvial system in Fig 2a. The system is in equilibrium with a flow stage of H_l and the stream is losing flow to the aquifer as the stream stage is greater than the groundwater head in the underlying aquifer. As the alluvium under the stream is saturated

along the entire wetted perimeter of the stream, the loss is assumed to occur through a saturated soil. If the stage in the stream were to rapidly increase to H_2 , in general, the increase in stage could not be instantaneously matched by the groundwater head as groundwater moves orders of magnitude slower than surface water. As a result, despite the groundwater conditions remaining unchanged, an unsaturated zone develops along the stream banks. This unsaturated zone will induce streamflow loss with a greater magnitude than under saturated conditions. Using the language of Sec. (1.1), the increase in streamflow results in a hydrodynamic stress which is not dependent on the hydrostatic conditions in the subsurface but on the surface water. Under this circumstance, the flow through the hyporheic zone then becomes primarily driven by hydrodynamic, and not hydrostatic, stresses.

If this same conceptual system were to be modeled numerically using the primary MODFLOW stream modules, so that the continuous physical system must become a discrete analog of itself, then the system illustrated in Fig. 2b will result. Similarly to the physical continuous system, the discrete system implies that the stream is losing flow under saturated conditions because the groundwater head H_a is below the stream stage but above the streambed. However, now if the stream stage increases from H_1 to H_2 a problem develops because the stream is implicitly assumed to be rectangular and contained to its cell so that all increases in stage cannot manifest in a wider stream.

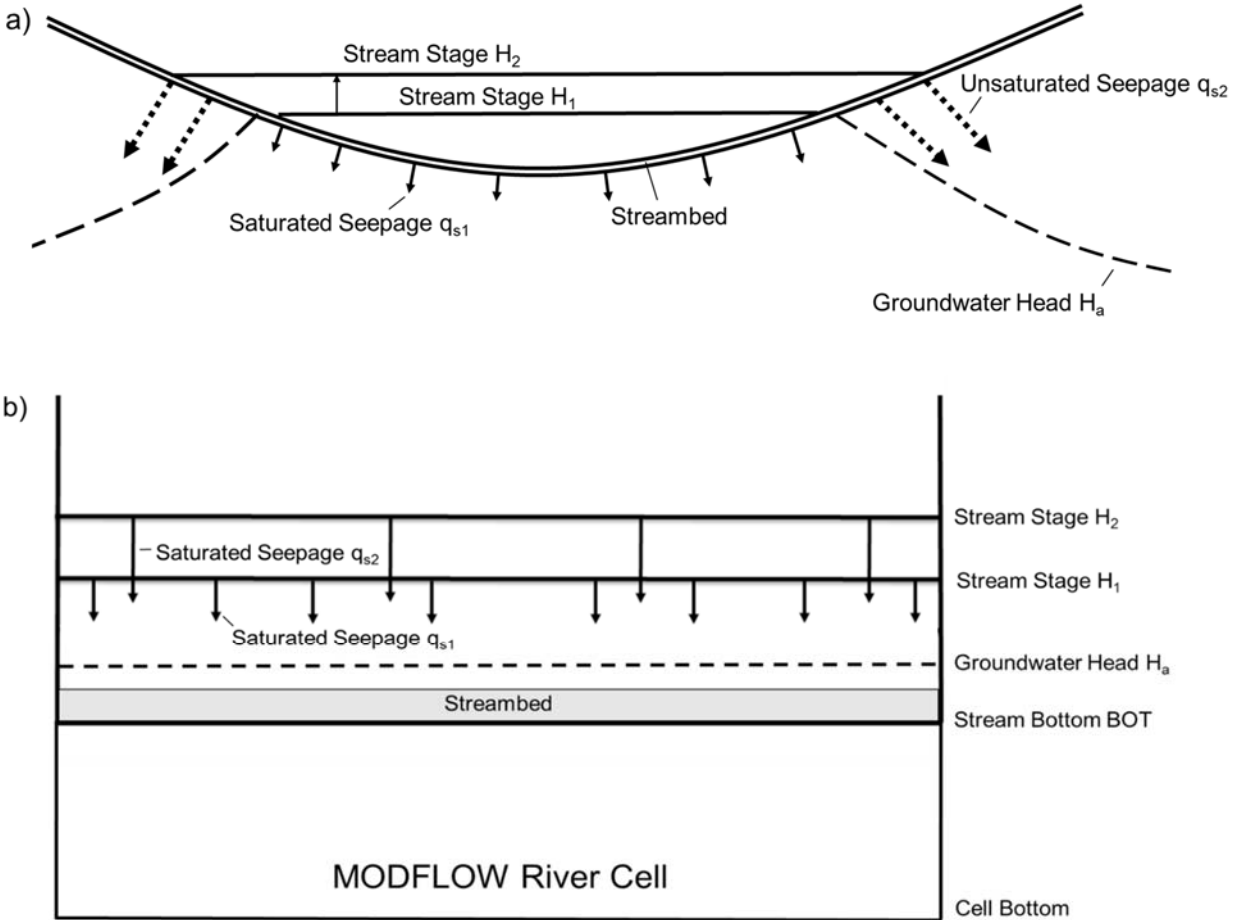


Figure 2. 2a (Top). Physical continuous stream-aquifer system that is losing flow through both a saturated and unsaturated soil after an increase in stream stage; 2b (Bottom). Numerical discretized stream-aquifer system in which only saturated streamflow loss occurs.

As a result, the unsaturated zone flow that occurs in reality will not be captured in the discrete counterpart and streamflow loss will be under-predicted. In effect, this implies that commonly used MODFLOW stream modules are not designed to model streamflow loss due to hydrodynamic stresses and exclusively were developed to capture hydrostatic stresses. For large scale regional models this is satisfactory but for reach scale models this becomes problematic when hydrodynamic stresses are prevalent.

1.8 Summary of Objectives

In light of the previous discussion, a field study was conducted along a 2 km reach of the South Platte River in the south Denver metro-area to quantify the effects of a nearby pumping

well field. During the study period, streamflow fluctuated greatly due to variable releases from an upstream dam and a waste water treatment plant. This led to a variable stream width that created conditions that made it difficult to quantify pumping-induced streamflow loss using conventional methods. In particular, analytical methods are obsolete in modeling this phenomena as commonly used streamflow depletion equations (such as the Glover and Hunt solutions) do not model a stream with a physical width, let alone a variable width. Likewise, for the reasons addressed in Sec. 1.7, the current MODFLOW stream modules are not well suited to capture large increases in stream width.

The question then becomes: How can the effects of hydrostatic and hydrodynamic mechanisms be separated in the quantification of hyporheic flows? Put more simply, how can streamflow losses due to pumping wells (losses due to hydrostatic forces) be identified and separated from streamflow losses due to changing streamflow and stream width (losses due to hydrodynamic forces)? To this end, a combined field work, analytical, and numerical methodology is presented which consists of the following:

1. Quantify pumping-induced streamflow loss along a reach of a river using a groundwater and in-stream flow monitoring network, with groundwater monitoring wells used to observe the propagation of pumping-induced water table drawdown and in-stream flow measurements used to measure total streamflow loss (Chapter 2).
2. Test the Glover and Hunt analytical solutions against measured streamflow loss. To perform the comparison, a new analytical method is developed that determines the fraction of streamflow loss attributed to groundwater pumping and other natural processes through periods of pumping and non-pumping (Chapter 2).

3. The development of a new MODFLOW stream module that is capable of computing more accurate stream infiltration fluxes for streams that undergoes regular changes in stream width. This is done primarily through two mechanisms. First, streams are not modeled as static boundary conditions and can adaptively change width based on variable flowrate, flow stage, and channel geometry. The module calculates river stage from the quasi-steady dynamic wave approximation to the St. Venant equation using an implicit scheme for improved stability. Based on the river's spatially variable channel geometry the flow's top width is computed which in turn determines the cells that are inundated by the stream and therefore where stream-aquifer interactions occur. That is, streams are not modeled as a single line of cells and can span multiple cells over a cross section. Second, each inundated cell has its own interaction with the river under either saturated or unsaturated conditions depending in the location of the aquifer directly beneath the cell. By allowing infiltration fluxes to be variable across a given cross section more accurate streamflow loss rates can be computed (Chapter 3).
4. A comparison of the two modeling frameworks (numerical and analytical) to assess each's validity and accuracy when applied for the purpose of evaluating pumping-induced streamflow loss (Chapter 4).

It is anticipated that this combined field/modeling method can be used in other stream-aquifer systems to measure streamflow loss and quantify differences between natural streamflow loss and pumping-induced streamflow loss.

REFERENCES

- Anderson, M.P., 2005, "Heat as a Ground Water Tracer." *Ground Water*, vol. 43, no. 6, pp. 951–968, doi:10.1111/j.1745-6584.2005.00052.x.
- Bailey, R.T., T.K. Gates, M. Admadi, 2014, Simulating Reactive Transport of Selenium Coupled with Nitrogen in a Regional-Scale Irrigated Groundwater System. *Journal of Hydrology*, vol. 515, pp. 29–46., doi:10.1016/j.jhydrol.2014.04.039.
- Beatty, S.J., D.L. Morgan, F.J. McAleer, A.R. Ramsay, 2010, Groundwater contribution to baseflow maintains habitat connectivity for *Tandanus bostocki* (Teleostei: Plotosidae) in a south-western Australian river. *Ecology of Freshwater Fish* 19, pp. 595-608., doi:10.1111/j.1600-0633.2010.004400.x
- Boano, F., et al., 2014, "Hyporheic flow and transport processes: Mechanisms, models, and biogeochemical implications." *Review of Geophysics*, 52, 603-679, doi:10.1002/2012RG000417.
- Brunke, M., and Tom Gonser., 1997, The Ecological Significance of Exchange Processes between Rivers and Groundwater. *Freshwater Biology*, vol. 37, no. 1, pp. 1–33., doi:10.1046/j.1365-2427.1997.00143.x.
- Camporese, M., et al., 2010, "Surface-Subsurface Flow Modeling with Path-Based Runoff Routing, Boundary Condition-Based Coupling, and Assimilation of Multisource Observation Data." *Water Resources Research*, vol. 46, no. 2, doi:10.1029/2008wr007536.

- Chen, X., M. Burbach, C. Cheng, 2008, Electrical and Hydraulic Vertical Variability in Channel Sediments and Its Effects on Streamflow Depletion Due to Groundwater Extraction. *Journal of Hydrology*, vol. 352, no. 3-4, pp. 250–266, doi:10.1016/j.jhydrol.2008.01.004.
- Colorado Water Conservation Board 2016 Colorado's Water Plan
(www.colorado.gov/pacific/cowaterplan/plan) (Accessed: 8 December 2016).
- Constanz, J., 1988, Interaction between stream temperature, streamflow, and groundwater exchanges in alpine streams. *Water Resources Research*, 34(7), pp. 1609-1615.
- Fox, G. A., G.V. Wilson, A. Simon, E.J. Langendoen, O. Akay, J.W. Fuchs., 2007, Measuring streambank erosion due to ground water seepage: correlation to bank pore water pressure, precipitation, and stream stage. *Earth Surface Processes and Landforms*. 32, pp. 1558-1573, doi:10.1002/esp.1490
- Fox, G. A., D.M. Heeren, M.A. Kizer, 2011, Evaluation of a Stream-Aquifer Analysis Test for Deriving Reach-Scale Streambed Conductance. *Transactions of the American Society of Agricultural and Biological Engineers*. 54(2): 473-479.
- Furman, A., 2008, Modeling coupled surface-subsurface flow processes: A review, *Vadoze Zone J.*, 7(2), 741-756, doi:10.2136/vzj2007.0065.
- Glover, R. E., and G. G. Balmer., 1954, River Depletion Resulting from Pumping a Well near a River. *Transactions, American Geophysical Union*, vol. 35, no. 3, p. 468.,
doi:10.1029/tr035i003p00468
- Hantush, M. S., 1965, Wells near Streams with Semipervious Beds. *Journal of Geophysical Research*, vol. 70, no. 12, pp. 2829–2838., doi:10.1029/jz070i012p02829.

- Hancock, P. J., A.J. Boulton, W.F. Humphreys, 2005, Aquifers and Hyporheic Zones: Towards an Ecological Understanding of Groundwater. *Hydrogeology Journal*, vol. 13, no. 1, pp. 98–111., doi:10.1007/s10040-004-0421-6.
- Harbaugh, A.W., 2005, MODFLOW-2005, the U.S. Geological Survey modular ground-water model -- the Ground-Water Flow Process: U.S. Geological Survey Techniques and Methods 6-A16.
- Hazen, A., 1892, Some physical properties of sands and gravels. Mass. State Board of Health, Ann. Rept. pp. 539-556.
- Hendricks, S.P., and D.S White., 1988, Hummocking by Lotic *Chara*: Observations on Alterations of Hyporheic Temperature Patterns. *Aquatic Botany*, vol. 31, no. 1-2, pp. 13–22., doi:10.1016/0304-3770(88)90036-8.
- Hunt, B., J. Weir, B. Clausen, 2001, A Stream Depletion Field Experiment. *Ground Water*, vol. 39, no. 2, pp. 283–289., doi:10.1111/j.1745-6584.2001.tb02310.x.
- Hunt, B., 2003, Unsteady Stream Depletion When Pumping from Semiconfined Aquifer. *Journal of Hydrologic Engineering*, vol. 8, no. 1, pp. 12–19., doi:10.1061/(asce)1084-0699(2003)8:1(12).
- Kalbus, E., et al. “Measuring Methods for Groundwater, Surface Water and Their Interactions: a Review.” *Hydrology and Earth System Sciences Discussions*, vol. 3, no. 4, 2006, pp. 1809–1850., doi:10.5194/hessd-3-1809-2006.
- Keller, Edward A., and G.M. Kondolf., 1990, Chapter 15. Groundwater and Fluvial Processes; Selected Observations. *Groundwater Geomorphology; The Role of Subsurface Water in Earth-Surface Processes and Landforms Geological Society of America Special Papers*, pp. 319–340., doi:10.1130/spe252-p319.

- Kumar, Mukesh, Christopher J. Duffy, and Karen M. Salvage. "A second-order accurate, finite volume-based, integrated hydrologic modeling (FIHM) framework for simulation of surface and subsurface flow." *Vadose Zone Journal* 8, no. 4, 2009: 873-890.
- Lee, David Robert. "A Device for Measuring Seepage Flux in Lakes and Estuaries." *Limnology and Oceanography*, vol. 22, no. 1, 1977, pp. 140–147., doi:10.4319/lo.1977.22.1.0140.
- Maxwell, R.M., et al., ParFlow User's Manual. Integrated GroundWater Modeling Center Report GWM1 2016-01, 167p.
- Myers, Tom, 2013, Remediation scenarios for selenium contamination, Blackfoot watershed, southeast Idaho, USA. *Hydrogeology Journal*, 21, pp. 655-671., doi:10.1007/s10040-013-0953-8.
- Niswonger, R.G. and Prudic, D.E., 2005, Documentation of the Streamflow-Routing (SFR2) Package to include unsaturated flow beneath streams--A modification to SFR1: U.S. Geological Survey Techniques and Methods, Book 6, Chap. A13, 47 p.
- Nyholm, T., S. Christensen, K.R. Rasmussen, 2002, Flow Depletion in a Small Stream Caused by Ground Water Abstraction from Wells. *Ground Water*, 40(4), pp. 425-437.
- Shepherd, Russell G. "Correlations of Permeability and Grain Size." *Ground Water*, vol. 27, no. 5, 1989, pp. 633–638., doi:10.1111/j.1745-6584.1989.tb00476.x.
- Sophocleous, Marios, M.A. Townsend, L.D. Vogler, T.J. McClain, E.T. Marks, G.R. Coble, 1988, Experimental Studies in Stream-Aquifer Interaction along the Arkansas River in Central Kansas" Field Testing and Analysis. *Journal of Hydrology*, vol. 98, no. 3-4, 1988, pp. 249–273., doi:10.1016/0022-1694(88)90017-0.
- Spalding, Charles P., and Raziuddin Khaleel., 1991, Review of Analytical Models to Stream Depletion Induced by Pumping: Guide to Model Selection. *Egyptian Journal of Medical*

Human Genetics, Elsevier, 6 Apr.,

www.sciencedirect.com/science/article/pii/S0022169418302683.

Stonedahl, S.H. (2010) “A multiscale model for integrating hyporheic exchange from rippled to meanders.” *Water Resources Research*, 46, W12539, doi:10.1029/2009WR008865.

Stonestrom, David Arthur., and Jim Constantz. *Heat as a Tool for Studying the Movement of Ground Water near Streams*. U.S. Dept. of the Interior, U.S. Geological Survey, 2003.

Sophocleous, M. “From Safe Yield to Sustainable Development of Water Resources; the Kansas Experience.” *Journal of Hydrology*, vol. 235, no. 1-2, 2000, pp. 27–43.,
doi:10.1016/s0022-1694(00)00263-8

Theis, C. V., 1935, The Relation between the Lowering of the Piezometric Surface and the Rate and Duration of Discharge of a Well Using Ground-Water Storage. *Transactions, American Geophysical Union*, vol. 16, no. 2, p. 519., doi:10.1029/tr016i002p00519.

Therrien, R., R.G. McLaren, E.A. Studickym and S.M Panday. 2006. *Hydrogeosphere*.
Waterloo, Canada: Groundwater Simulations Group, University of Waterloo.

Woessner, William W., and Kevin E. Sullivan. “Results of Seepage Meter and Mini-Piezometer Study, Lake Mead, Nevada.” *Ground Water*, vol. 22, no. 5, 1984, pp. 561–568.,
doi:10.1111/j.1745-6584.1984.tb01425.x.

2. AN ANALYTICAL MODELING APPROACH FOR ESTIMATING STREAMFLOW LOSS IMPACTED BY GROUNDWATER PUMPING

2.1 Introduction

Determining the volumetric flux of water exchange between a river and an underlying aquifer is important for water resource managers, environmental managers, and policy makers. The quantification of these fluxes has significant consequences in regions where surface water rights and groundwater rights are jointly administered (Colorado Water Conservation Board, 2015). Exchange rates between surface water and groundwater can determine phenomena including, but not limited to, contaminant transport rates (Brunke and Gonser, 1997), nutrient loads (Myers, 2013; Bailey et al., 2014), erosion and channel morphology (Keller and Kondolf, 1990; Fox et al., 2007), stream water temperature (Constantz, 1998; Hendricks and White, 1998), and wildlife habitat (Hancock et al., 2005; Beatty et al., 2010). Brunke and Gonser (1997) provide a detailed overview of various ecological, biological, chemical, and physical processes that are dependent upon exchange rates between surface water and groundwater.

Of particular importance is the ability to predict streamflow losses that occur due to nearby pumping wells. In general, removing groundwater from an alluvial aquifer via pumping wells disturbs the existing groundwater head equilibrium, establishing a new time-variant hydraulic gradient that can induce streamflow loss, increase the existing streamflow loss, or decrease the rate of groundwater return to stream reaches that are within the area of influence of the pumping well. The rate of exchange between stream water and groundwater can be tempered by fine sediments along the streambed that have a lower hydraulic conductivity than the underlying aquifer (Hantush, 1965; Spalding and Khaleel, 1991; Chen et al., 2008, Fox, 2011).

Several studies have used numerical modeling to quantify the effects of pumping on streamflow. Sophocleous and Perkins (2000) linked MODFLOW (Harbaugh, 2005) with the watershed surface water model SWAT (Arnold et al., 1998) to evaluate the effects of groundwater-irrigated agricultural regions on surface water systems in southern Kansas. The linked model was highly accurate and provided insight into developing sustainable water management practices, although the authors acknowledged that the model was complex and expensive to make. A similar study was developed for an agricultural watershed in Korea (Kim et al., 2008) to provide a broad view into catchment scale effects of pumping. Reach scale effects were not evaluated.

However, due to the intricacies and the effort required to develop numerical models, the most common method to quantify pumping-induced streamflow loss has been through the use of analytical models (Sophocleous et al., 1988; Hunt, 2003; Fox, 2004; Fox, 2011). Several analytical models have been derived that provide estimates for pumping-induced streamflow loss under certain stream-aquifer connection conditions. Two of the most commonly used solutions are the Glover (1954) and Hunt (1999) solutions. The Glover solution, derived from the Theis (1935) solution for head drawdown due to pumping, assumes an infinitely long and straight river that fully penetrates the aquifer. Aquifer parameters (transmissivity, storage coefficient) are assumed homogenous and groundwater head is considered initially uniform. Streamflow losses are assumed small enough that changes in stream stage and width can be neglected (the river is treated as having a width of zero) and the stream has a perfect hydraulic connection with the aquifer, i.e. stream seepage remains under saturated conditions and an unsaturated zone does not develop. Moreover, the existence of a streambed clogging layer is not accounted for. The Glover solution is a function of the complimentary error function $erfc$ and is given as:

$$\frac{\Delta Q}{Q_w} = \operatorname{erfc} \left(\sqrt{\frac{SL^2}{4Tt}} \right) \quad (2.1)$$

where ΔQ is the streamflow depletion rate [L^3/T], Q_w is the pumping rate [L^3/T], S is storativity or specific yield of the aquifer [-], T is aquifer transmissivity [L^2/T], L is the shortest distance between the pumping well and the river [L], and t is time since pumping began [T]. Eq. (2.1) approaches unity as t goes to infinity. The Hunt solution (Hunt, 1999) improves on the Glover solution by incorporating a streambed clogging layer and by modeling a partially penetrating stream, with the ratio of stream depletion rate to pumping rate given as:

$$\frac{\Delta Q}{Q_w} = \operatorname{erfc} \left(\sqrt{\frac{SL^2}{4Tt}} \right) - \exp \left(\frac{\lambda^2 t}{4ST} + \frac{\lambda L}{2T} \right) \operatorname{erfc} \left(\sqrt{\frac{\lambda^2 t}{4ST}} + \sqrt{\frac{SL^2}{4Tt}} \right) \quad (2.2)$$

where all parameters are identical to those in the Glover solution and λ is a conductance term, defined as the constant of proportionality between the seepage flowrate per unit length of river through the streambed and the gradient between the river stage and aquifer head [L/T]. Hunt also derived a solution for drawdown ϕ in two dimensions (x, y) in an alluvial aquifer under the same conditions:

$$\phi(x, y, t) = \frac{Q_w}{4\pi T} \left\{ E_1 \left[\frac{(L-x)^2 + y^2}{4Tt/S} \right] - \int_0^\infty e^{-\theta} E_1 \left[\frac{\left(L + |x| + \frac{2T\theta}{\lambda} \right)^2 + y^2}{\frac{4Tt}{S}} \right] d\theta \right\} \quad (2.3)$$

where all parameters are identical to those in Eq. (2.2) and θ is a variable of integration. These models have been applied to several field studies to determine their accuracy. Perhaps the first comprehensive pumping-induced streamflow loss analysis was conducted by Sophocleous et al. (1988) along a 30 km reach of the Arkansas River in Kansas. They provided estimates of streambed hydraulic conductivity obtained from infiltrometer experiments, with streamflow loss

measured and compared to streamflow depletion curves given by Jenkins (1968). Measured streamflow loss was significantly less than modeled streamflow loss which was attributed to the partial penetration of the river into a semiconfined aquifer. Similarly, Fox et al. (2011) obtained estimates of streambed hydraulic conductivity from direct measurements with sieve tests and falling-head permeameters along the North Canadian River in Oklahoma and used the measurements in the evaluation of Hunt's equation for drawdown. The estimated values for hydraulic conductivity implied that the streambed did not add any significant resistance to the infiltration flux, i.e. a clogging layer was nonexistent and the streamflow depletion equation reduced to the Glover solution. However, while drawdown data was collected to assess the validity of the measurement, streamflow was not measured during the experiment and so was not compared to output from the Hunt and Glover solutions.

Hunt et al. (2001) tested his own solution (Hunt, 1999) against both measured streamflow data and observed groundwater levels on a small drainage canal area in New Zealand. The solution yielded good fits for both sets of data by calibrating λ ; however, the length of the pumping period was only 10 hours and the flowrate in the canal was less than approximately $0.05 \text{ m}^3/\text{s}$. Therefore, the validity of the solution over a longer pumping period and for a larger stream is not known. The study also had difficulties in determining a known upstream flowrate that was not within the zone of influence of the pumping well. Nyholm et al. (2000) performed a similar study on a headwater stream in Denmark where the Hunt (1999) solution was evaluated against field-collected streamflow data. However, both streamflow rates and pumping well rates were on the order of $0.01 \text{ m}^3/\text{s}$. Fox (2004) tested the validity of the Hunt solution with delayed yield effects (Hunt, 2003) along the South Platte River in eastern Colorado. He obtained a satisfactory match between observed and simulated head drawdown patterns by modifying

Hunt's streambed conductance term, however model results were not compared to measured streamflow loss.

Using field measurements is perhaps the most accurate method of determining pumping-induced streamflow loss, as it does not involve any parameter estimation and removes the bias often associated with modeling. However it is often costly, labor intensive, and time consuming. Moreover in some cases it may not be practical if streamflow rates are high or if groundwater pumping rates are small compared to streamflow rates. Despite the importance of quantifying actual influence of groundwater pumping on streamflow loss, there has been a lack of studies devoted to measuring pumping-induced streamflow loss in rivers. Furthermore, studies employing analytical models to quantify streamflow loss have failed to adequately compare the model's primary system-response variable (streamflow loss rate) with field data, instead relying on secondary variables (drawdown) to confirm model performance (e.g. Fox, 2004; Fox et al., 2011). A direct comparison between measured and simulated streamflow loss rate is needed. However, this is complicated by the following points:

1. Streamflow rates are often much higher than pumping rates, resulting in pumping-induced streamflow loss rates that can be within the range of instrument measurement error when streamflow is high;
2. Streamflow loss occurs naturally in many rivers due to an existing hydraulic gradient between the stream and the alluvial aquifer, direct precipitation or evaporation, or bank storage due to stream width rapidly increasing. Thus, when the pumps are operating, streamflow loss likely is a combination of background losses, i.e. losses that would occur in the absence of pumping, and pumping-induced losses.

Therefore, an approach should be derived that can adequately test analytical models while accounting for losses due to natural processes and groundwater pumping. If analytical models are to continue to be used as a tool in water resources engineering, there is a need for a simple modeling approach that accomplishes this goal.

This study presents a combined field and analytical modeling methodology to accomplish two main objectives: 1) Quantify pumping-induced streamflow loss along a reach of a river using a groundwater and in-stream flow monitoring network, with groundwater monitoring wells used to observe the propagation of pumping-induced water table drawdown and in-stream flow measurements used to measure streamflow loss; and 2) Test the Glover and Hunt analytical solutions against measured streamflow loss. To perform the comparison, a new analytical method is developed that determines the fraction of streamflow loss attributed to groundwater pumping and other natural processes through periods of pumping and non-pumping. The method is applied to a 2 km reach of the South Platte River in the south Denver metro-area, downstream of an urban reservoir. We anticipate that this combined field/modeling method can be used in other stream-aquifer systems to measure streamflow loss, test analytical models for a particular system, and quantify differences between natural streamflow loss and pumping-induced streamflow loss.

2.2 Methods

2.2.1 Study Region

A reach of the South Platte River running through the South Suburban Park in Littleton, Colorado served as the field site for the study (Fig. 3a). The South Platte River flows from south to north, with a shallow alluvial aquifer formed along its length. The alluvium thickness in the study reach ranges from 4 to 16 m, with an average depth to bedrock of 14 m. Drill logs indicate

that the alluvium primarily consists of fine gravels and coarse sands with small patches of finer clays. The reach is 2 km downstream of Chatfield Reservoir (Fig. 3a), controlled and operated by the United States Army Corps of Engineers to release water into the South Platte River.



Figure 3. 3a (Left): Location of study site and relative proximity to Chatfield Reservoir and City of Denver; 3b (Right): Map of South Platte River reach where streamflow and groundwater levels were monitored, showing five monitoring well locations, four pumping wells, two streamflow gauging sites, and location where river stage was monitored.

The releases from Chatfield Reservoir were, in general, fluctuating greatly during much of the study period, with releases ranging from 0 to 23 m³/s. In addition, the Centennial Waste Water Treatment Plant (WWTP) released water downstream of the dam but upstream of the study site. While the variations in the dam's release varied over weeks, the WWTP release varied over the course of a day, ranging from approximately 0.15 to 0.55 m³/s. Four high-capacity pumping wells (Fig. 3b) owned and operated by the Centennial Water and Sanitation District (CWSD) are located in the alluvial aquifer, between 122 and 259 m from the River.

2.2.2 Field Data Collection

The streamflow and groundwater monitoring network used to quantify the influence of groundwater pumping on streamflow and groundwater in the South Platte River stream-aquifer system is shown in Fig. 3b. Data were collected between December 2016 and April 2018. Eleven monitoring wells were drilled at five locations. Locations A and B each had three nested wells drilled with screens located at 0.91, 2.40, and 4.25 m below ground surface. Locations C and D each had two nested wells drilled with screens at 6.10 and 9.14 m. A final well was drilled at Location E on the opposite side of the river to determine if drawdown occurred beyond the river, and therefore if the river was acting as a boundary to the influence of the pumping wells. The well at Location E had a screen located at 3.35 m below the ground surface. Groundwater levels were monitored with HOBO Onset Data Loggers (pressure transducers). Atmospheric pressure was also monitored with a data logger and was subtracted from the pressure readings from the observation wells to calculate the depth of water atop the loggers and the associated groundwater head. Groundwater data from the wells at Locations A, B, and E were recorded from December 2016 to April 2017 at 15 minutes intervals. These wells were then removed, as mandated by the management of South Suburban Park so as not to disturb the riparian vegetation. Groundwater data from the wells at Locations C and D were recorded from December 2016 to April 2018, also at 15 minutes intervals. River stage was monitored using a pressure transducer at a point directly adjacent to Location A (Fig. 3b).

Streamflow loss was estimated in the field by taking the difference between measured upstream and downstream streamflow rates, approximately 1.2 km apart in river reach distance. Upstream streamflow was measured by a stream gauge (“US Gauging Site” in Fig. 3b) operated by the City of Littleton, with readings recorded every 15 minutes. The stream gauge is

downstream of both Chatfield Dam and the effluent release from the WWTP. The downstream streamflow rate was measured at the location (“DS Gauging Site”) shown in Fig. 3b. No surface water inflows occurred between the upstream and downstream gauging sites. Streamflow at the downstream site was measured using an acoustic Doppler velocimeter (ADV). The three point velocity method was used to determine the average velocity along a vertical line and measurements were taken every two feet (~ 0.6 m) along a cross section. River cross section widths varied between 4.5 and 24 m depending on streamflow and location along the reach.

As the reach was prone to frequent changes in streamflow rate, water storage along the reach could not be assumed constant. The storage S [L^3] along the reach with length L and top width T_w is computed as:

$$S = T_w L \left(\frac{h_u + h_d}{2} \right) \quad (2.4)$$

where the stream stage at the downstream and upstream locations are labeled as h_1 and h_2 , respectively. L and T_w are assumed constant both in time and space. Eq. (2.4) implies that the channel is nearly rectangular and that all increases in streamflow only manifest in a stream with a greater stage, and that stream width is constant for all streamflow rates. While this assumption is inherently invalid, a more thorough analysis would be necessary to determine a function or relationship between flowrate and stream width over the entire reach. It follows that the time rate of change of S is:

$$\frac{dS}{dt} = T_w L \left(\frac{\frac{dh_u}{dt} + \frac{dh_d}{dt}}{2} \right) \quad (2.5)$$

The derivatives of h_1 and h_2 are approximated with a four-point finite difference method given below:

$$\frac{dh}{dt} \approx \frac{-h_{i-2} + 8h_{i-1} - 8h_{i+1} + h_{i+2}}{12\Delta t} \quad (2.6)$$

The i indices on h refer to the time at which the stream was recorded. The difference between successive measurements was 15 minutes. To account for the speed of the flood wave (celerity) through the reach, the Kleitz-Seddon Law was applied in conjunction with Manning's equation to approximate travel time t_c between the upstream and downstream gauge sites. The wide channel assumption was made so that the flood wave celerity could be approximated by $c = 5u/3$, where u is the mean flow velocity (Singh, 1996), taken to be constant along the entire reach. u was measured at the downstream location by the ADV with measurements ranging between approximately 0.15 m/s and 0.52 m/s. Once c was calculated, the time for the flood wave to propagate through the reach was computed. Streamflow loss ΔQ was then calculated to be the difference between the upstream flowrate Q_u and downstream flowrate Q_d , with Q_u corresponding to a time t_c before the recorded downstream flowrate:

$$\Delta Q(t) = Q_u(t - t_c) - Q_d(t) - \frac{dS}{dt} \quad (2.7)$$

Q_d were taken at discrete times and typically when the streamflow was low (less than 3.40 m³/s). Flowrates larger than this typically resulted in combined flow depths and velocities that produced unsafe conditions for data collection with the ADV. Two sets of measurements were taken: the first from January 2017 to February 2017 and the second from March 2018 to April 2018. In all, 23 streamflow measurements were taken over the two periods, with the majority during period of pumping. Over the study period, the four pumping wells operated over continuous periods of 1 to 5 weeks with combined yields ranging from 0.09 to 0.28 m³/s.

2.2.3 Analytical Modeling of Streamflow Depletion

The Glover and Hunt analytical streamflow depletion solutions were used to quantify pumping-induced streamflow loss and compare with field-measured streamflow loss. Model results also are compared against groundwater drawdown at the monitoring wells to corroborate analytical model accuracy and provide estimates of aquifer parameters (transmissivity T , specific yield S_y). The Glover and Hunt equations are given in Eqs. (2.1) and (2.2), respectively. To account for time-variable pumping rates from the four pumping wells, the Glover and Hunt equations were applied using the principle of superposition in time.

The Hunt drawdown equation in Eq. (2.3) is applied to simulate drawdown at the locations of the monitoring wells. The Theis solution (Theis, 1935), used in the original derivation of the Glover model (Theis, 1941; Glover, 1954), is used to simulate drawdown for comparison:

$$\phi(r, t) = \frac{Q_w}{4\pi T} W \left(\frac{r^2 S}{4Tt} \right) \quad (2.8)$$

where W is the Theis well function, or exponential integral. Drawdown was calculated using Eq. (2.8), and also a version of Eq. (2.8) that assumes the river is a recharge boundary, with a perfect hydraulic connection between the stream and the aquifer. This second analysis employs image well theory, with a set of image injection wells positioned opposite of the four actual pumping wells.

Other factors besides pumping can contribute to streamflow loss along the study reach. If a function can be obtained describing the effect of these factors, and assuming linear independence of solutions, then applying superposition provides a new encompassing solution to estimate total streamflow loss ΔQ :

$$\Delta Q(pumps, \varepsilon) = g(pumps) + f(\varepsilon) \quad (2.9)$$

where $g(pumps)$ is a function describing the contribution to streamflow loss from pumping (e.g. Glover solution, Hunt solution, or another method of computing pumping-induced streamflow loss) and $f(\epsilon)$ is a function describing the contribution to streamflow loss from other external factors. $f(\epsilon)$ can be an equation describing losses due to a changing upstream flowrate inducing bank storage, background regional gradients, inflows/outflows from diversions, direct precipitation or evaporation, etc. For generality, this function is simply dependent upon a lumped variable ϵ .

2.3 Results and Discussion

2.3.1 Groundwater Drawdown

The observed transient drawdown is shown for Location D (Fig. 4), Location A (Fig. 5), and Location E (Fig. 7). These three wells were chosen for detailed analysis due to their location: D is close to the pumping wells, A is on the river bank, and E is on the opposite side of river. Table 1 presents the aquifer parameters (T , S_y , λ) that yield the best fit between the simulated and observed drawdown values at the observation well (OW) locations. λ is used only for the Hunt solution.

Table 1. Hydraulic input parameters used the evaluation of drawdown curves.

Location and Well	Transmissivity T (m ² /day)	Specific Yield S_y	Streambed Conductance λ (m/day)
Location D – 6.10 m OW	1,900	0.2	10
Location A – 4.25 m OW	2,500	0.15	10
Location E – 3.35 m OW	2,500	0.2	60

Each location was independently calibrated with a trial-and-error curve fitting approach, yielding different parameter values due to aquifer heterogeneity and the treatment of the river as a straight line whereas this reach of the South Platte River is best characterized by an arc (see Fig. 3b). However, all three parameter sets are within the same order of magnitude. For the

results shown in Figs. (4), (5), and (6) all four pumping wells were turned on at 11:00 AM MT on 13 January 2017 and turned off at 10:00 AM MT on 30 January 2017. The average collective pumping rate of all four wells over this time was approximately $0.21 \text{ m}^3/\text{s}$.

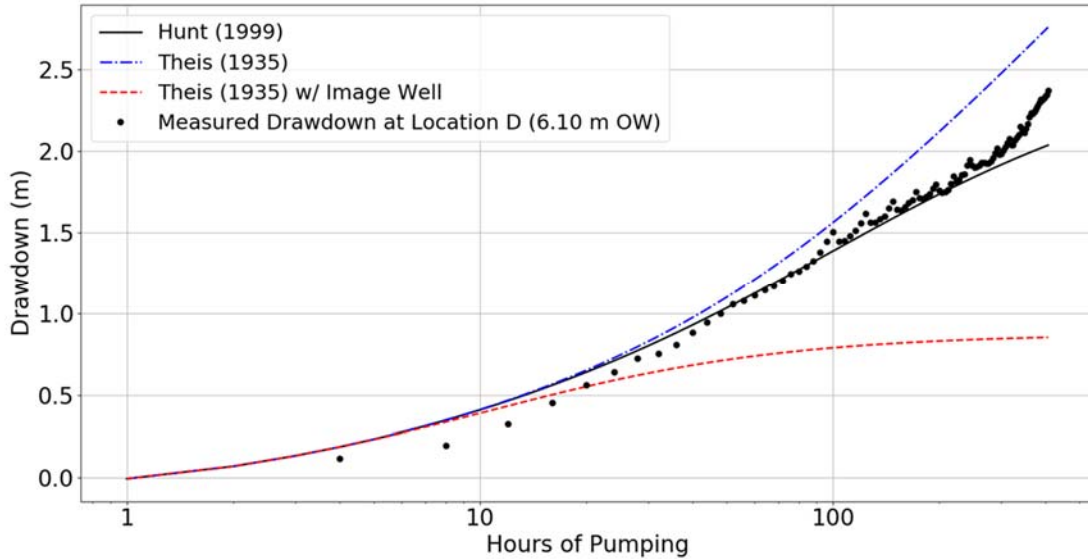


Figure 4. Drawdown at the 6.10 m observation well at Location D compared with three analytical solutions (Hunt, Theis, Theis with image well).

Fig. 4 shows results for the 6.10 m observation well at Location D. Three curves were fit to the data to provide insight into how groundwater head responded to pumping. The Hunt drawdown equation given by Eq. (2.3) provides the best results, due to its ability to simultaneously account for river recharge and drawdown at the river. The close fit of the model to the data suggests that the river is supplying water to the aquifer, thereby decreasing the rate of drawdown. The original Theis solution, which does not account for river recharge, over-predicts drawdown as there is no other source of water to replenish the aquifer. Finally, the Theis solution with image wells under-predicts drawdown, as the river is treated as a constant recharge boundary with an endless supply of water.

The same analysis was applied to the 4.25 m observation well at Location A (Fig. 5), which is located only 0.5 m from the river's edge. The field data demonstrates that while drawdown does occur at the river, the non-monotonic nature of the drawdown is the result of a strong hydraulic connection between the river and alluvium. That is, hyporheic flows, that are dependent upon hydrodynamic forces, are active close to the stream bank.

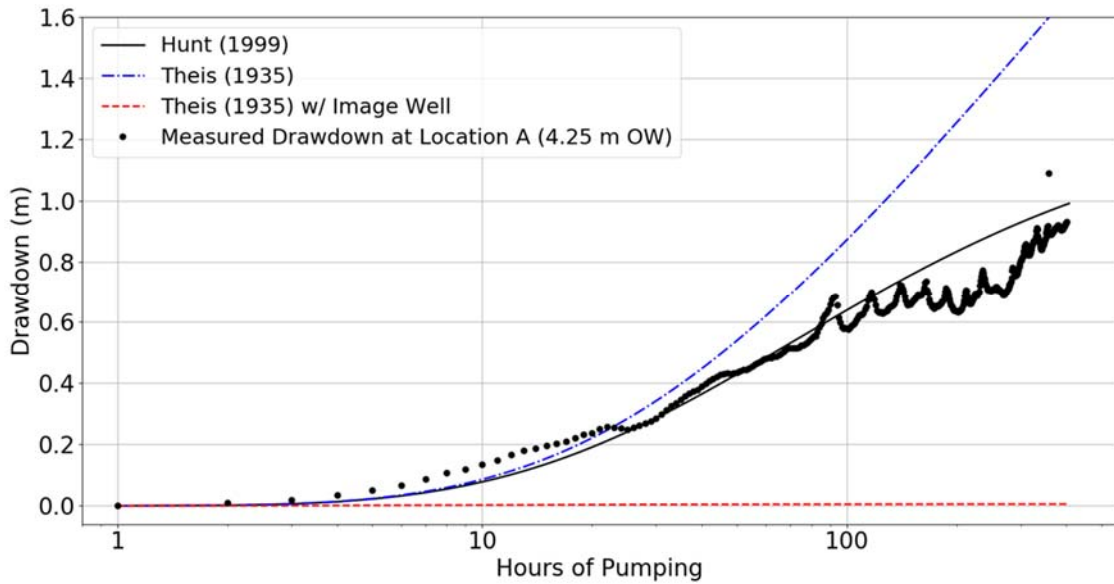


Figure 5. Drawdown at the 4.25 m observation well at Location A compared with three analytical solution (Hunt, Theis, Theis with image well).

This is further confirmed in Figure 6 which shows fluctuations in groundwater head at Location A (0.91 m observation well) and river stage over the same pumping period. The fluctuations in river stage are the result of a variable streamflow rate, which influences shallow groundwater levels almost instantaneously.

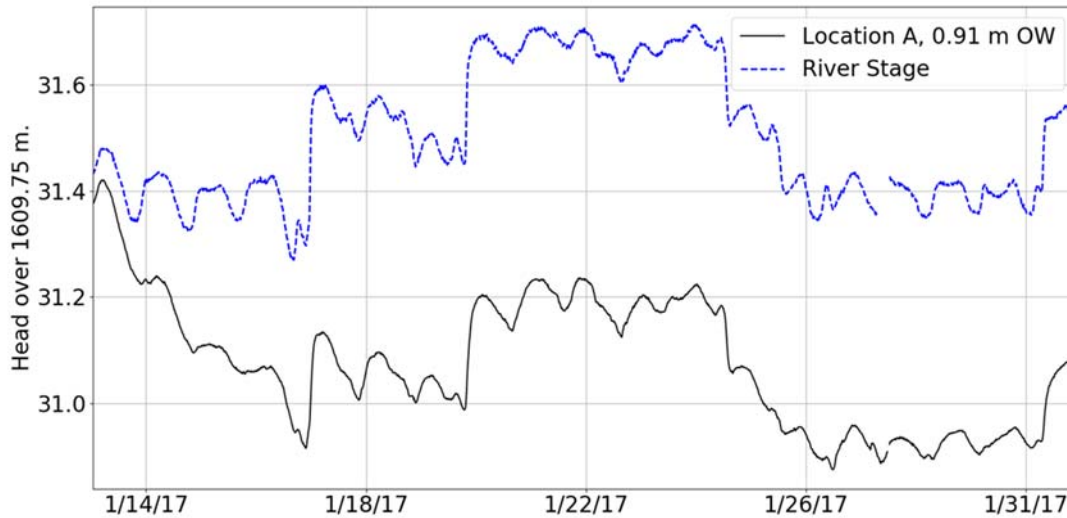


Figure 6. River stage compared to 0.91 m observation well at Location A.

This suggests that not only is the river losing water to the alluvium, but that the losses are nearly linearly related to the river's stage and that the (possible) existence of a clogging layer does not significantly increase the travel time of the water from the river to the 0.91 m groundwater well. Moreover, while pumping-induced drawdown (hydrostatic effect) is clearly occurring, flow through the hyporheic zone is also very dependent on the hydrodynamic effects from the stream. As with Location D, the Hunt solution provides the best results (Fig. 5), particularly at later times ($t > 20$ hours) when the river likely is supplying water to the aquifer and thus preventing more significant drawdown. Of course, the Theis image well solution predicts a drawdown of nearly 0 m due to the treatment of the river as a recharge boundary. The original Theis solution over-predicts drawdown, as no recharge source is modeled.

The observed drawdown at Location E (Fig. 7) shows that the effects of pumping on groundwater head propagate to the aquifer on the other side of the river, a condition that is not included in the Theis or Glover solutions. However, while this indicates that the stream does not act as a constant head boundary condition, the drawdown at Location E is significantly less than

that of Location A despite being separated by only approximately one river width (~10 m), i.e. the river acts as a flux boundary that is capable of mitigating some of the drawdown effects.

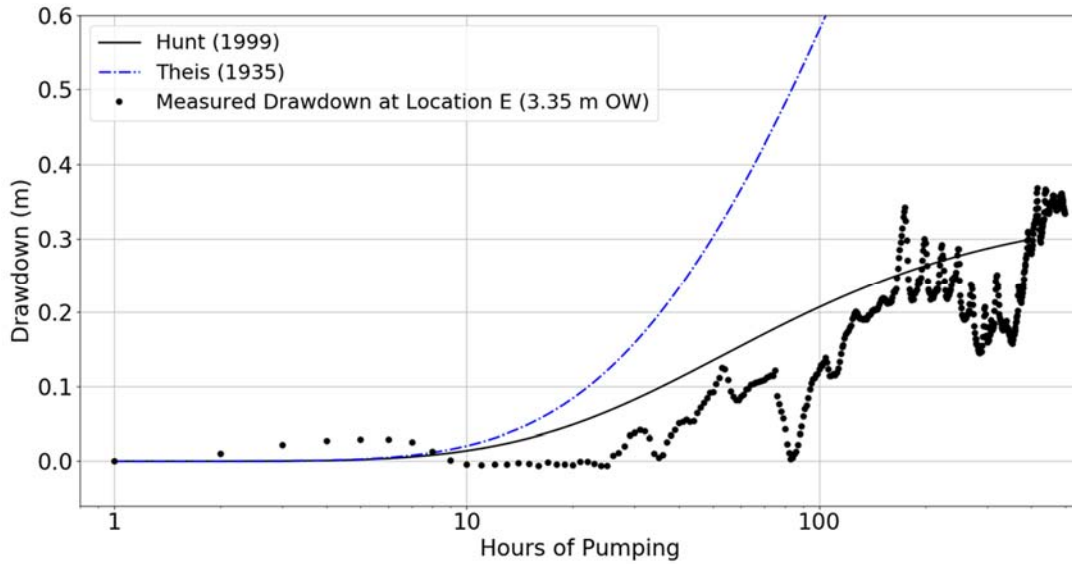


Figure 7. Drawdown at the 3.35 m observation well at Location E compared with two analytical solutions (Hunt, Theis).

Furthermore, the data suggests a delayed-yield effect with early times not experiencing significant drawdown. This is most likely due to the river supplying enough water so that the effects of the pumping wells are not propagated across the river. However, after approximately 100 hours of pumping, the water table decreases rapidly, indicating that the stream was not capable of replenishing the aquifer at the same rate as the pumping rates.

Overall, the groundwater head data suggest that pumping-induced streamflow loss is occurring along the reach.

2.3.2 Streamflow Loss

Table 2 presents details of the collected streamflow data (date, upstream streamflow, downstream streamflow, streamflow loss). Fig. 8a shows the measured streamflow loss data (as points) for the two sample periods (designated by dashes A-A' and B-B'), along with the time-varying combined pumping rate from the four pumping wells throughout the study period.

Table 2. Summary of collected streamflow data.

Date	Time	Upstream Streamflow (m ³ /s)	Downstream Streamflow (m ³ /s)	Change in Storage (m ³ /s)	Streamflow Loss (m ³ /s)
1/10/2017	10:00 AM	3.182	2.73	0.008	0.442
1/13/2017	9:00 AM	0.305	0.306	0.094	-0.095
1/13/2017	11:00 AM	0.462	0.459	0.053	-0.05
1/13/2017	1:00 PM	0.509	0.459	0.009	0.041
1/16/2017	12:00 PM	0.44	0.375	0.024	0.041
1/16/2017	1:00 PM	0.485	0.404	0.015	0.066
1/20/2017	9:00 AM	1.26	1.05	-0.021	0.228
1/20/2017	10:00 AM	1.33	1.06	-0.04	0.308
1/20/2017	11:00 AM	1.33	1.03	-0.034	0.33
1/28/2017	8:00 AM	0.533	0.426	-0.009	0.116
1/28/2017	9:00 AM	0.658	0.474	0.036	0.149
1/28/2017	10:00 AM	0.711	0.551	0.009	0.151
2/4/2017	8:00 AM	0.911	0.785	0.027	0.098
2/4/2017	9:00 AM	0.971	0.804	0.024	0.142
2/11/2017	8:00 AM	1.58	1.23	0.005	0.343
2/11/2017	9:00 AM	1.66	1.29	0.024	0.336
3/2/2018	9:00 AM	0.365	0.201	0.087	0.077
3/3/2018	10:00 AM	0.223	0.069	0.042	0.113
3/7/2018	10:00 AM	0.485	0.295	0.076	0.114
3/7/2018	11:00 AM	0.509	0.331	0.004	0.174
3/17/2018	7:00 AM	0.277	0.087	0.042	0.148
3/30/2018	7:00 AM	0.241	0.162	0.019	0.06
4/2/2018	7:00 AM	0.2503	0.222	0.042	-0.014

Figs. 8b and 8c show streamflow loss and streamflow rate at the upstream gauging site for the A-A' and B-B' time periods, respectively, showing the large fluctuation in streamflow due to

releases from Chatfield Reservoir and the daily changes in WWTP release. The figures also show estimated streamflow loss from the Glover and Hunt solutions, based on the time series of pumping rates. The aquifer parameter data used in the Glover and Hunt streamflow solutions are given in Table 3.

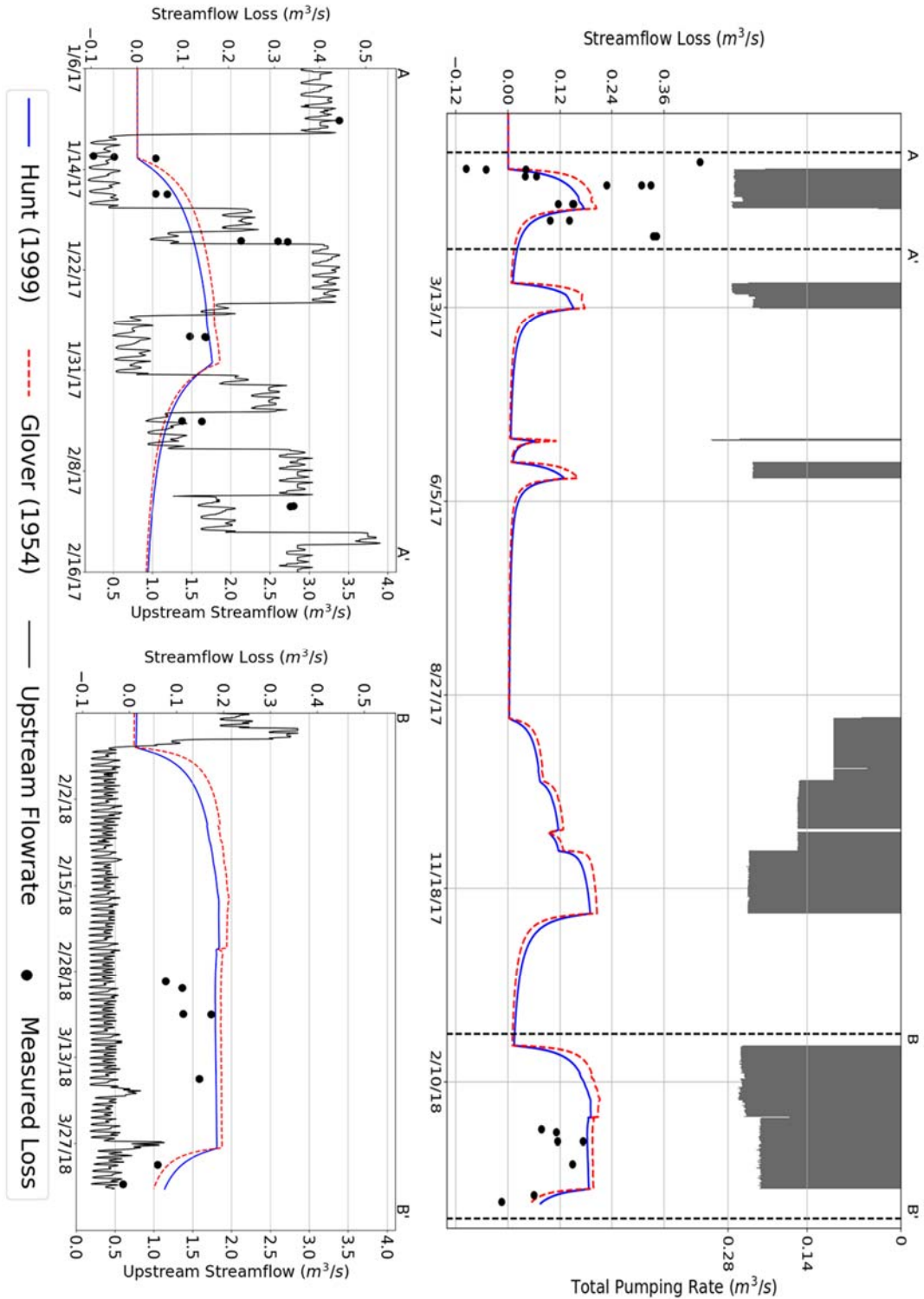


Figure 8. 8a (Top): Measured and predicted (with Hunt solution) streamflow depletion. Upper horizontal axis shows pumping rate; 8b (Bottom Left): Region of 6a between A and A' showing streamflow depletion (measured and predicted with Glover solution (dashed line)) on primary vertical axis and streamflow rate (solid black line) on secondary vertical axis; 8c (Bottom Right): Region of 8a figure between B and B' showing streamflow depletion and streamflow rate.

They differ from the aquifer parameter data used to evaluate the drawdown equations because the arced river was approximated as a straight line. In the case of evaluating drawdown, the location of the linear river was approximated relative to the point at which drawdown was being evaluated. When evaluating the streamflow depletion equations, the approximated linear river was measured relative to the four pumping wells. Because the parameters were fit for each location, they differ from the parameters used in the drawdown evaluations because input parameters (specifically, location of the river relative to the pumping well) changed slightly. However both parameter sets are similar in magnitude.

Table 3. Hydraulic input parameters used the evaluation of streamflow depletion equations.

Solution	Transmissivity T (m ² /day)	Specific Yield S _y	Streambed Conductance λ (m/day)
Glover	2,500	0.15	-
Hunt	2,500	0.15	10

If more resolute parameter approximations are desired then a multiple linear regression model should be applied in an attempt to calibrate all parameters at once. However, Nyholm et al. (2002) showed that this can often be impossible due to the non-linearity of the problem.

Fig. 8b suggests that while the Glover and Hunt solutions perform adequately while the pumps are on, models perform poorly during recovery in comparison to measured streamflow loss data. As the magnitude of streamflow loss appears to coincide with the magnitude of streamflow rate (Fig 8b), likely this is due to streamflow loss being dependent on the magnitude of streamflow in the reach as well as pumping rate. Hence, the Glover and Hunt solutions predict a streamflow depletion rate of 0 m³/s prior to the pumps turning on, when in fact a large rate of streamflow loss was measured (first point in Fig. 8b). Moreover, pump shut-off (30 January 2017) coincided with an increase of flow from approximately 0.5 m³/s to 2.5 m³/s, such that

streamflow losses remained relatively constant after the wells turned off (as seen on 4 January 2017) and even increased at later times (as seen on 11 January 2017) as streamflow continued to increase. This likely is due to a corresponding increase in stream width and associated bank storage and infiltration in the unsaturated zone along the banks of the river. As an example (Fig. 9), a decrease in flow rate (3.25 to 0.35 m³/s) from 13 January 2017 to 14 January 2017 resulted in a decrease in stream stage (0.22 m) and stream width (1.8 m). An increase in flow rate would cause an opposite response, with an increase in stream stage and stream width.

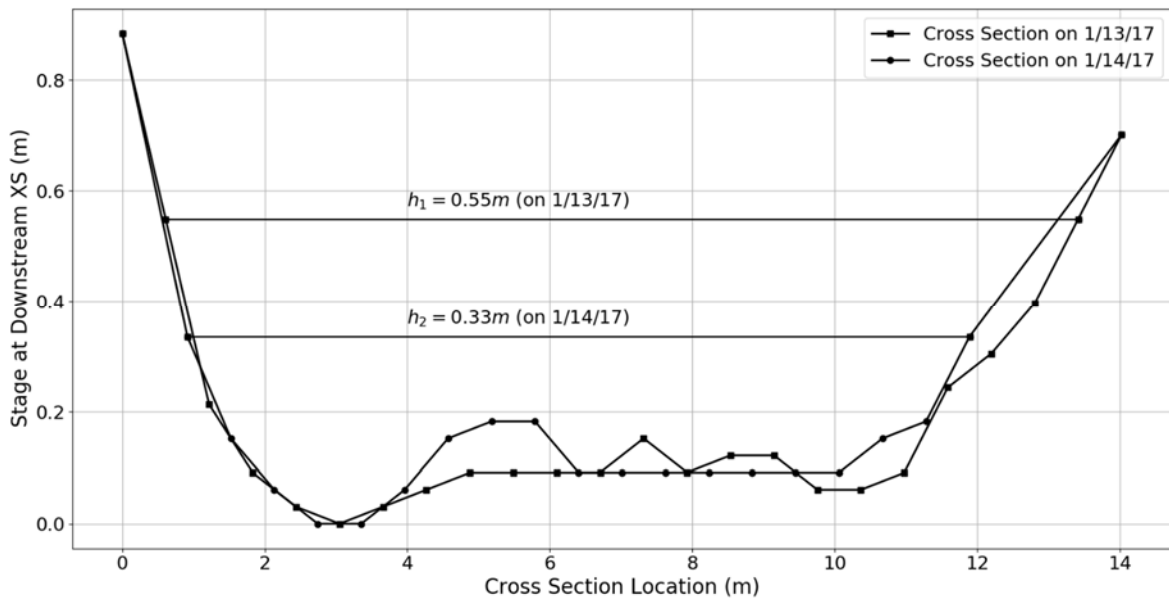


Figure 9. Downstream cross section illustrating large variations in stream stage and width due to variations in upstream flowrate.

In contrast, the upstream streamflow from the 2018 period (Fig. 8c) consistently remain low (< 0.50 m³/s), and hence the Glover and Hunt solutions perform well during this period, predicting streamflow loss accurately during times of pumping and recovery. The solution approaches a steady streamflow loss rate of approximately 0.21 m³/s, which corresponds to the final groundwater pumping rate of this period (see Fig. 8a), and then sharply decreases after

pump shut-off. Of course, the limitations of the 2018 dataset is that no streamflow measurements were taken shortly after the pumps had turned on.

In an effort to test the analytical models against all streamflow loss data, a theoretical pumping period is considered that combines the pumping-effected data from the 2017 and 2018 data sets, i.e. the streamflow loss data measured during periods of low flow in the A-A' and B-B' time periods are superimposed onto a single timeline according to the time since pumping began in that time period. This is performed to isolate the times when streamflow is effected by pumping, and hence when measured streamflow loss can be used to test the analytical models. In general, such an approach should be adopted when testing analytical models against measured streamflow loss. See Table 4. As will be discussed in Section 2.3.3, “low flow” is defined as a flow rate $< 0.54 \text{ m}^3/\text{s}$. A more general streamflow loss equation that estimates loss during time of pumping and non-pumping, and for all times and streamflow rates, is presented in Section 2.3.3.

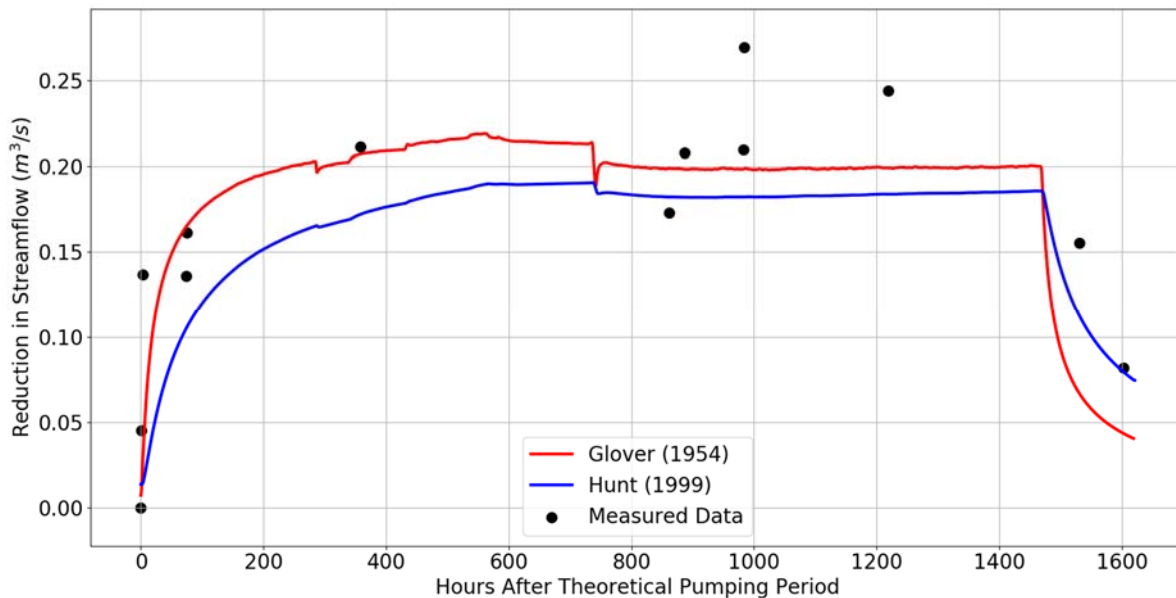


Figure 10. Theoretical pumping period for low upstream streamflow comparing measured data with Glover (1954) and Hunt (1999) solution.

Table 4. Streamflow data that was classified as a ‘low flow’.

Date	Time	Upstream Streamflow (m ³ /s)	Streamflow Loss (m ³ /s)	Low Flow, Q<0.54m ³ /s (Y/N)	Hours since most recent pumping began
1/10/2017	10:00 AM	3.182	0.442	N	-
1/13/2017	9:00 AM	0.305	-0.095	Y	1
1/13/2017	11:00 AM	0.462	-0.05	Y	3
1/13/2017	1:00 PM	0.509	0.041	Y	5
1/16/2017	12:00 PM	0.440	0.041	Y	74
1/16/2017	1:00 PM	0.485	0.066	Y	75
1/20/2017	9:00 AM	1.26	0.228	N	-
1/20/2017	10:00 AM	1.33	0.308	N	-
1/20/2017	11:00 AM	1.33	0.33	N	-
1/28/2017	8:00 AM	0.533	0.116	Y	358
1/28/2017	9:00 AM	0.658	0.149	N	-
1/28/2017	10:00 AM	0.711	0.151	N	-
2/4/2017	8:00 AM	0.911	0.098	N	-
2/4/2017	9:00 AM	0.971	0.142	N	-
2/11/2017	8:00 AM	1.58	0.343	N	-
2/11/2017	9:00 AM	1.66	0.336	N	-
3/2/2018	9:00 AM	0.365	0.077	Y	862
3/3/2018	10:00 AM	0.223	0.113	Y	877
3/7/2018	10:00 AM	0.485	0.114	Y	983
3/7/2018	11:00 AM	0.509	0.174	Y	984
3/17/2018	7:00 AM	0.277	0.148	Y	1219
3/30/2018	7:00 AM	0.241	0.06	Y	1531
4/2/2018	7:00 AM	0.2503	-0.014	Y	1603

Figure 10 shows the measured and simulated streamflow loss for the combined period in comparison with results from Glover and Hunt models. In particular, the reduction of streamflow is plotted relative to the first measured point taken on 13 January 2017 at 9:00 AM MT. Table 3 lists the parameter values used in the models, with λ selected to be 10 m/day (in accordance with the calibrated conductance term for drawdown at Locations A and D). The Glover and Hunt models have a root mean square error of $RMSE = 0.051 \text{ m}^3/\text{s}$ and $RMSE = 0.055 \text{ m}^3/\text{s}$, respectively. This suggests the effects of a streambed clogging layer are not significant along the reach.

2.3.3 General Equation for Streamflow Loss

As seen in Fig. 8, streamflow loss occurs during times of both pumping and non-pumping. Independent of pumping, streamflow loss occurs due to natural gradients between stream stage and water table elevation and also due to changes in streamflow rate resulting in bank storage and seepage through newly inundated unsaturated zones. Using the results of the analytical models, a generalized model to estimate streamflow loss can be developed using Eq. (2.6). In this analysis, ε encompasses the effects of changes in upstream flowrate and channel geometry that allows for the stream to expand during times of high flow, which results in bank storage and unsaturated zone seepage. The generalized streamflow loss model is developed for two reasons: 1) the model can be used to quantify the fraction of streamflow loss attributed to both natural streamflow loss and human-influenced streamflow loss via pumping; and 2) the model can be used to estimate streamflow loss for a stream reach adjacent to a pumping well field no matter the time series of pumping.

A first analysis of $f(\varepsilon)$ for the South Platte River reach in the study region is estimated using the streamflow loss measurements during times in which the pumps are assumed to have negligible effect on streamflow. These five measurements (Fig. 11) are used to create a relationship between streamflow loss and upstream flowrate Q_u , with the following logarithmic equation:

$$f(\varepsilon = Q_u) = 0.28 \ln(Q_u) + 0.17 \quad (2.10)$$

where Q_u is upstream flowrate in m^3/s . $f(\varepsilon = Q_u)$ has a root of $Q_u = 0.54 \text{ m}^3/\text{s}$, indicating that the river does not lose streamflow naturally for flowrates less than approximately $0.54 \text{ m}^3/\text{s}$. This value therefore is designated as “low flow” (see Section 2.3.2). The relationship described by Eq.

(2.10) can be strengthened with more data collection; however, as a first analysis, Eq. (2.10) is adequate for the proposed methodology.

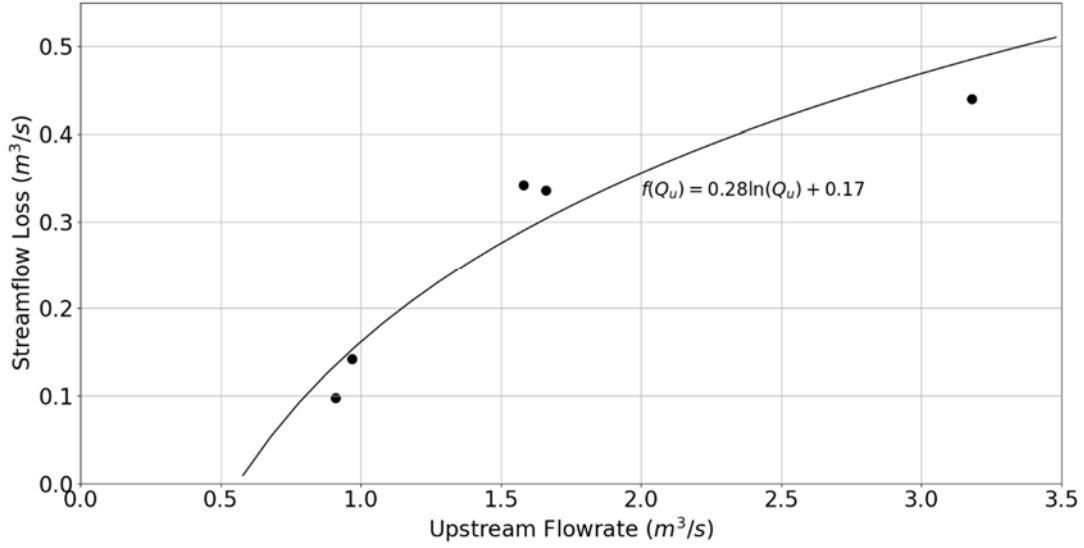


Figure 11. Measured data used to obtain $f(Q_u)$ with streamflow loss as a function of upstream streamflow.

In the previous section, it was shown that the Glover solution was the more accurate model for estimating pumping-induced streamflow depletion for the reach. For this reason, in Eq. (2.9), $g(pumps)$ is given by the Glover model so that a site-specific generalized streamflow loss model can be written as:

$$\Delta Q(Q_w, Q_u) = Q_w \operatorname{erfc} \left(\sqrt{\frac{SL^2}{4Tt}} \right) + 0.28 \ln(Q_u) + 0.17 \quad (2.11)$$

where all parameters have previously been defined. Eq. (2.11) estimates streamflow loss along a reach due to pumping (Q_w) and upstream flow rate (Q_u), with the influence of Q_u likely due to bank storage and unsaturated zone flow caused by changes in Q_u . Also, because Eq. (2.11) is semi-empirical and is not dimensionless, all parameters must be in SI units [m and s]. Fig. 12 illustrates the application of Eq. (2.11) to estimate streamflow loss continuously during the data collection period of 2017, when Q_u was highly variable. During times of low flow ($< 0.49 \text{ m}^3/\text{s}$),

the Hunt solution models streamflow loss with no contribution from Q_u ; for all other times, streamflow loss is a combination of pumping-induced streamflow loss and natural losses. For this application, the model of Eq. (2.11) gives a root mean square error of $RMSE = 0.08 \text{ m}^3/\text{s}$.

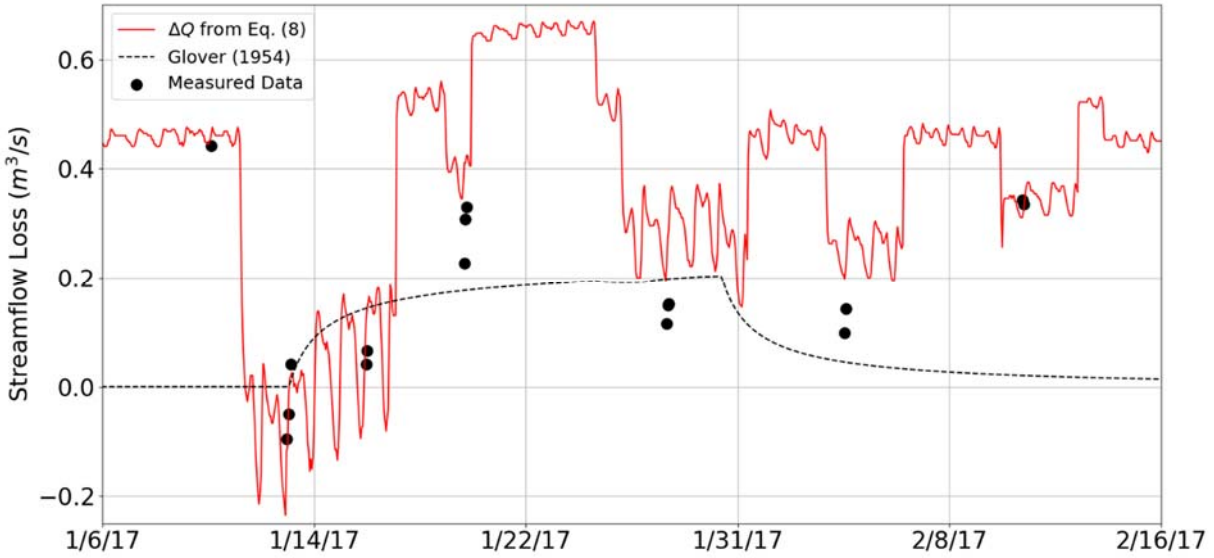


Figure 12. Predicted streamflow loss using Eq. (2.8) compared with Hunt solution.

The general model of Eq. (2.11) can be used to determine the portion of streamflow loss due to pumping wells and other external factors, in this case changes in Q_u . The loss due to pumping ΔQ_{pumps} is:

$$\Delta Q_{pumps}(Q_w, Q_u) = 1 - \frac{f(Q_u)}{\Delta Q(Q_w, Q_u)} \quad (2.9)$$

The loss due to changes in Q_u is the compliment of ΔQ_{pumps} . Fig. 13 shows the portion of streamflow loss from pumping wells and from changes in Q_u for the 2017 data collection time period. Before the pumping wells turn on, all loss is due to Q_u . There is a brief period (2 days) when the streamflow rate drops significantly and the pumps have yet to turn on, and hence very little streamflow loss is occurring. When the pumping wells turn on (and while the upstream streamflow rate remains primarily a ‘low flow’) nearly 100% of losses are due to pumping.

However, this period is short, as four days later Q_u increases from approximately $0.57 \text{ m}^3/\text{s}$ to $2.27 \text{ m}^3/\text{s}$. As a result, only 20% of streamflow losses are predicted to be due to the pumping wells. Even after 14 days of pumping, due to the maintained high Q_u , the pumps are responsible for only approximately 30% of streamflow losses. However, note that the wells are taking more streamflow now than at any point prior to this time and that it is the portion of loss that is relatively low. As Q_u decreases from 26 January 2017 to 31 January 2017, the share of loss due to the wells increases, approaching 90%. After the wells turn off, the share of loss due to pumping decreases, although not monotonically as seen by the small fluctuations due to the changes in Q_u .

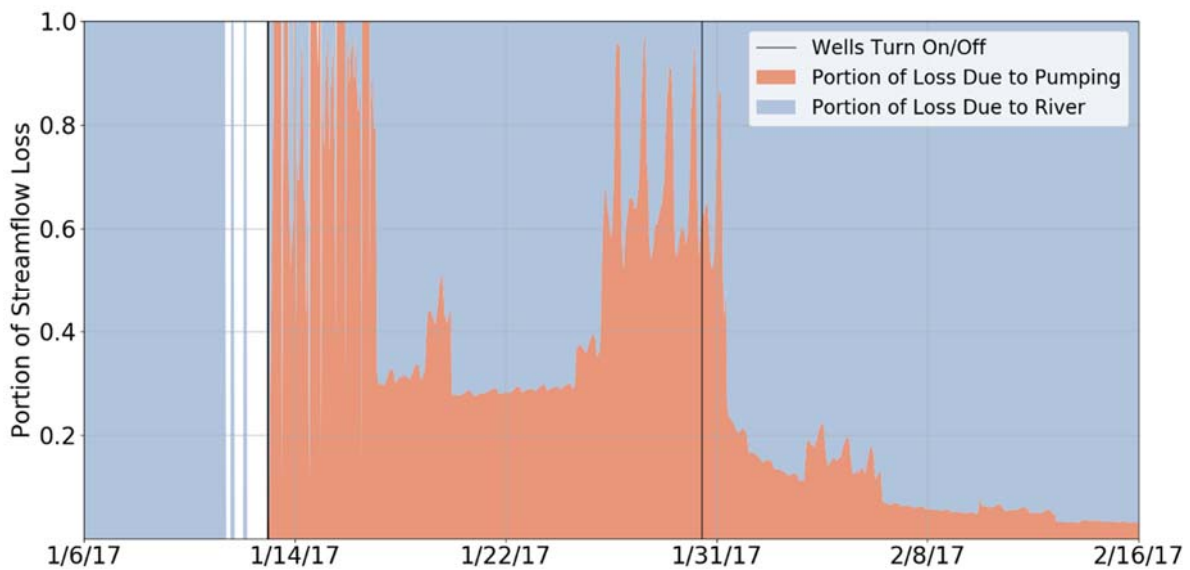


Figure 13. Portion of streamflow loss due to pumps and changes in upstream streamflow in 2017 according to general streamflow loss model (Eq. 2.8).

This same procedure is repeated in for the data collected in 2018 (Fig. 14). Prior to the pumps turning on nearly all streamflow loss is due to the river (a small portion is due to the pumping wells from a previous pumping period). As the pumping wells turn on, coinciding with a sharp decrease in Q_u , nearly all of the streamflow loss is due to pumping. However, unlike the

data from 2017, Q_u remains nearly constant (and low) and therefore the pumping contributes to most of the loss for the entire pumping period. Small deviations in this trend occur near the end of the pumping period due to brief increases in Q_u .

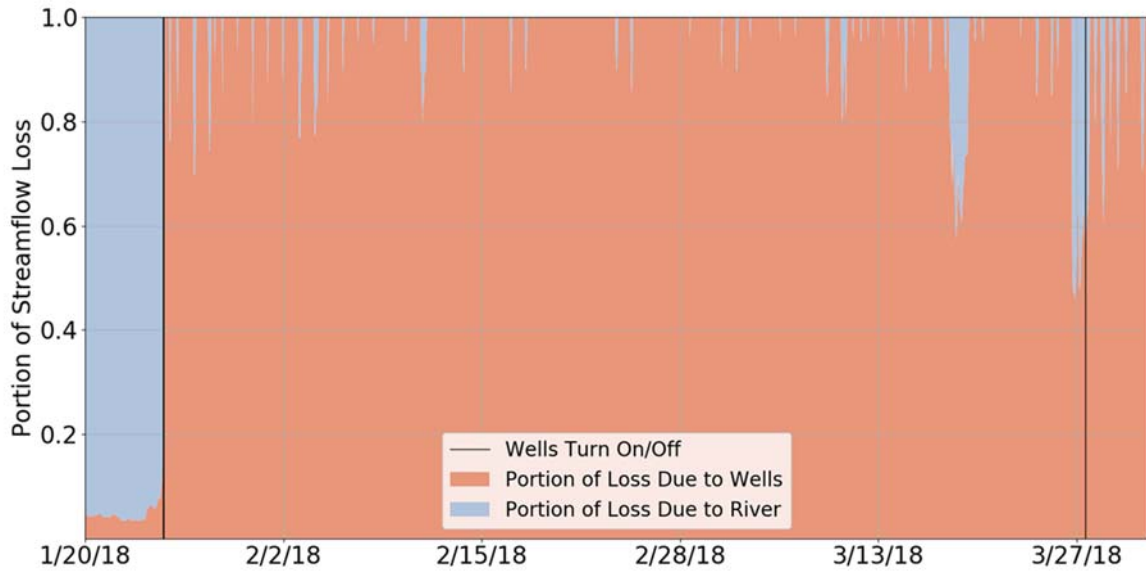


Figure 14. Portion of streamflow loss due to pumps and changed in upstream streamflow in 2018 according to general streamflow loss model (Eq. 2.8).

As seen in Fig. 12 the model of Eq. (2.11) often over-predicts streamflow loss in the reach, although this over-prediction is only high for the measurements taken on 4 February 2017 (measurements are 0.13 to 0.17 m³/s of streamflow loss, and modeled values are 0.23 m³/s of streamflow loss). More field measurements of streamflow loss during periods of non-pumping would provide a more accurate relationship between Q_u and streamflow loss, and hence yield a more accurate estimate of streamflow loss throughout a given time period.

Furthermore, although the method presented is general, the model of Eq. (2.11) is valid only for the reach of the South Platte River in the study region shown in Fig. 3b. Due to the reach's close proximity to an upstream dam, oncoming flood waves do not attenuate significantly before flowing through the reach, resulting in rapid changes in streamflow Q_u . However, in all streams

some level of bank seepage will likely always occur for unsteady increasing flows. Moreover, the regional hydraulic gradient should be closely monitored and quantified to know how the stream naturally interacts with the alluvium, independent of pumping. The general model of Eq. (2.11) is a first approximation to quantify these effects and to determine the true impact of pumping on a case-by-case basis. Given accurate equations for these external factors (bank storage, regional gradients, diversions, inflows, evaporation, etc.) a water budget can be developed with Eq. (2.11) which would allow water resource managers to more accurately quantify the effects of each component contributing to streamflow loss.

2.4 Summary and Conclusions

A stream-aquifer test was performed along a reach of the South Platte River to quantify the effects of pumping on streamflow. For much of the study period between 2017 and 2018, significant streamflow loss occurred along a 2 km reach of the river. For streamflow rates that are sufficiently small and constant, analytical streamflow depletion solutions (Glover, Hunt) are adequate in predicting these losses, with streambed conductivity approximately two orders of magnitude lower than aquifer hydraulic conductivity. However, when streamflow rates were highly variable and large, model results were much different than measured streamflow loss due to bank storage and associated unsaturated zone infiltration contributing to additional streamflow loss. In an attempt to better analytically model these cases, a new general model is proposed that accounts for pumping-induced and background streamflow losses, with contributions from both able to be quantified in time for the study reach.

The following conclusions can be made from this study:

- Analytical models [Glover (1954), Hunt(1999)] are adequate representations of pumping-induced streamflow loss during periods of low flow in the study reach of the South Platte River;
- Analytical models can be tested against measured streamflow loss only if streamflow loss from pumping can be separated from natural streamflow loss (e.g. bank storage from increases in streamflow); and
- A generalized streamflow loss model can be developed that includes the effect of pumping wells and natural processes. This model can be used to estimate streamflow loss for the reach during times of pumping and non-pumping, facilitating water resources management of the stream-aquifer system.

Although the generalized streamflow loss model of Eq. (2.11) is valid only for the reach investigated in this study, the method for developing the model can be applied to any alluvial stream-aquifer system.

REFERENCES

- Arnold, J.G., R. Srinivasan, R.S. Muttiah, J.R. Willaim, 1998, Large area hydrologic modeling and assessment Part 1 Model Development. *Journal of the American Water Resources Association* 34(1): 78-89.
- Bailey, Ryan T., T.K. Gates, M. Admadi, 2014, Simulating Reactive Transport of Selenium Coupled with Nitrogen in a Regional-Scale Irrigated Groundwater System. *Journal of Hydrology*, vol. 515, pp. 29–46., doi:10.1016/j.jhydrol.2014.04.039.
- Beatty, S.J., D.L. Morgan, F.J. McAleer, A.R. Ramsay, 2010, Groundwater contribution to baseflow maintains habitat connectivity for *Tandanus bostocki* (Teleostei: Plotosidae) in a south-western Australian river. *Ecology of Freshwater Fish* 19, pp. 595-608., doi:10.1111/j.1600-0633.2010.004400.x
- Brunke, Matthias, and Tom Gonser., 1997, The Ecological Significance of Exchange Processes between Rivers and Groundwater. *Freshwater Biology*, vol. 37, no. 1, pp. 1–33., doi:10.1046/j.1365-2427.1997.00143.x.
- Chen, Xunhong, M. Burbach, C. Cheng, 2008, Electrical and Hydraulic Vertical Variability in Channel Sediments and Its Effects on Streamflow Depletion Due to Groundwater Extraction. *Journal of Hydrology*, vol. 352, no. 3-4, pp. 250–266., doi:10.1016/j.jhydrol.2008.01.004.
- Colorado Water Conservation Board 2016 Colorado’s Water Plan
(www.colorado.gov/pacific/cowaterplan/plan) (Accessed: 8 December 2016).
- Constanz, J., 1988, Interaction between stream temperature, streamflow, and groundwater exchanges in alpine streams. *Water Resources Research*, 34(7), pp. 1609-1615.

- Fox, Garey A., 2004, Evaluation of a Stream Aquifer Analysis Test Using Analytical Solutions and Field Data. *Journal of the American Water Resources Association*, vol. 40, no. 3, pp. 755–763., doi:10.1111/j.1752-1688.2004.tb04457.x.
- Fox, Garey A., G.V. Wilson, A. Simon, E.J. Langendoen, O. Akay, J.W. Fuchs., 2007, Measuring streambank erosion due to ground water seepage: correlation to bank pore water pressure, precipitation, and stream stage. *Earth Surface Processes and Landforms*. 32, pp. 1558-1573, doi:10.1002/esp.1490
- Fox, Garey A., D.M. Heeren, M.A. Kizer, 2011, Evaluation of a Stream-Aquifer Analysis Test for Deriving Reach-Scale Streambed Conductance. *Transactions of the American Society of Agricultural and Biological Engineers*. 54(2): 473-479.
- Furman, A. (2008), Modeling coupled surface-subsurface flow processes: A review, *Vadose Zone J.*, 7(2), 741-756, doi:10.2136/vzj2007.0065.
- Glover, Robert E., and Glenn G. Balmer., 1954, River Depletion Resulting from Pumping a Well near a River. *Transactions, American Geophysical Union*, vol. 35, no. 3, p. 468., doi:10.1029/tr035i003p00468.
- Hancock, Peter J., A.J. Boulton, W.F. Humphreys, 2005, Aquifers and Hyporheic Zones: Towards an Ecological Understanding of Groundwater. *Hydrogeology Journal*, vol. 13, no. 1, pp. 98–111., doi:10.1007/s10040-004-0421-6.
- Hantush, Mahdi S., 1965, Wells near Streams with Semipervious Beds. *Journal of Geophysical Research*, vol. 70, no. 12, pp. 2829–2838., doi:10.1029/jz070i012p02829.
- Harbaugh, A.W., 2005, MODFLOW-2005, the U.S. Geological Survey modular ground-water model -- the Ground-Water Flow Process: U.S. Geological Survey Techniques and Methods 6-A16.

- Hendricks, Susan P., and David S. White., 1988, Hummocking by Lotic *Chara*: Observations on Alterations of Hyporheic Temperature Patterns. *Aquatic Botany*, vol. 31, no. 1-2, pp. 13–22., doi:10.1016/0304-3770(88)90036-8.
- Hunt, Bruce, J. Weir, B. Clausen, 2001, A Stream Depletion Field Experiment. *Ground Water*, vol. 39, no. 2, pp. 283–289, doi:10.1111/j.1745-6584.2001.tb02310.x.
- Hunt, Bruce, 2003, Unsteady Stream Depletion When Pumping from Semiconfined Aquifer. *Journal of Hydrologic Engineering*, vol. 8, no. 1, pp. 12–19., doi:10.1061/(asce)1084-0699(2003)8:1(12).
- Jenkins, C. T., 1968, Techniques for Computing Rate and Volume of Stream Depletion by Wells. *Ground Water*, vol. 6, no. 2, pp. 37–46, doi:10.1111/j.1745-6584.1968.tb01641.x.
- Keller, Edward A., and G.M. Kondolf., 1990, Chapter 15. Groundwater and Fluvial Processes; Selected Observations. *Groundwater Geomorphology; The Role of Subsurface Water in Earth-Surface Processes and Landforms Geological Society of America Special Papers*, pp. 319–340., doi:10.1130/spe252-p319.
- Kim, Nam Won, I.M. Chung, Y.W. Won, J.G. Arnold, 2008, Development and Application of the Integrated SWAT-MODFLOW Model.” *Journal of Hydrology*, vol. 356, no. 1-2, pp. 1–16., doi:10.1016/j.jhydrol.2008.02.024.
- Myers, Tom, 2013, Remediation scenarios for selenium contamination, Blackfoot watershed, southeast Idaho, USA. *Hydrogeology Journal*, 21, pp. 655-671., doi:10.1007/s10040-013-0953-8.
- Nyholm, T., and S. Christensen. 2000, Stream-flow depletion in a small alluvial stream caused by groundwater abstraction from wells. In “Stream-flow depletion caused by

- groundwater abstraction near alluvial streams,” Ph.D. these, Department of Earth Sciences, University of Aarhus.
- Nyholm, T., S. Christensen, K.R. Rasmussen, 2002, Flow Depletion in a Small Stream Caused by Ground Water Abstraction from Wells. *Ground Water*, 40(4), pp. 425-437.
- Singh, Vijay Pal. *Kinematic Wave Modeling in Water Resources: Surface-Water Hydrology*. John Wiley, 1996.
- Sophocleous, Marios, and Samuel P Perkins., 2000, Methodology and Application of Combined Watershed and Ground-Water Models in Kansas. *Journal of Hydrology*, vol. 236, no. 3-4, pp. 185–201., doi:10.1016/s0022-1694(00)00293-6.
- Sophocleous, Marios, M.A. Townsend, L.D. Vogler, T.J. McClain, E.T. Marks, G.R. Coble, 1988, Experimental Studies in Stream-Aquifer Interaction along the Arkansas River in Central Kansas” Field Testing and Analysis. *Journal of Hydrology*, vol. 98, no. 3-4, 1988, pp. 249–273., doi:10.1016/0022-1694(88)90017-0.
- Spalding, Charles P., and Raziuddin Khaleel., 1991, Review of Analytical Models to Stream Depletion Induced by Pumping: Guide to Model Selection. *Egyptian Journal of Medical Human Genetics*, Elsevier, 6 Apr.,
www.sciencedirect.com/science/article/pii/S0022169418302683.
- Theis, C. V., 1935, The Relation between the Lowering of the Piezometric Surface and the Rate and Duration of Discharge of a Well Using Ground-Water Storage. *Transactions, American Geophysical Union*, vol. 16, no. 2, p. 519., doi:10.1029/tr016i002p00519.
- Theis, C. V., 1941, The Effect of a Well on the Flow of a Nearby Stream. *Transactions, American Geophysical Union*, vol. 22, no. 3, 1941, p. 734.,
doi:10.1029/tr022i003p00734.

3. MODFLOW MODULE FOR SIMULATING STREAM-AQUIFER INTERACTIONS IN WIDTH VARIABLE STREAMS USING ST. VENANT EQUATIONS

3.1 Introduction

Quantifying the magnitude and timing of infiltration fluxes between streams and alluvial aquifers is important for the sustainable development of water resources, understanding and modeling contaminant transport (Brunke and Gonser, 1997), nutrient loading (Myers, 2013; Bailey et al., 2014), stream temperature and quality for aquatic life habitat (Hancock et al., 2005; Beatty et al., 2010), and channel erosion and bank stability (Keller and Kondolf, 1990; Fox et al., 2007). Interactions between surface water and groundwater have long been acknowledged by hydrologists and hydrogeologists, although quantifying the magnitude of water exchange fluxes remains a formidable challenge (Kalbus et al., 2006). This is due to spatial heterogeneity of stream and aquifer properties, the large variation in time scales over which different processes occur, and difficulty in obtaining field data over meaningful spatial and temporal scales, particularly for large-scale water management problems (Sophocleous, 2002).

Significant research efforts have been devoted to developing methods for estimating the exchange rates between surface water and groundwater. Field techniques include using seepage meters (Lee, 1977; Woessner and Sullivan, 1984), heat and solute tracers (Constantz et al., 2001; Constantz and Stonestrom, 2003; Anderson, 2005), grain size analyses (Hazen, 1892; Shepherd, 1989), permeameter tests (Sophocleous et al., 1988; Fox et al., 2011), and pumping tests (Hunt et al., 2001; Nyholm et al. 2002). However, these methods can be labor-intensive and costly to implement on a continual basis. For this reason, models often are used. As the demand for more integrated water management practices increases, so does the demand for increased modeling capabilities, especially in regard to surface water-groundwater interactions (Sophocleous, 2000).

Due to its wide spread availability as an open-source code, abundance of documentation, ease-of-use, and industry acceptance, MODFLOW has become the most commonly used numerical hydrologic model (Furman, 2008). However, certain limitations exist when modeling stream-aquifer interactions with existing MODFLOW stream modules. In particular, streams are modeled as a single line of cells that do not take direct account of stream width. This problem compounds itself on fine-scaled grids, or where cell dimensions are smaller than the stream width. If the MODFLOW cell width is not the same as the stream width, “systematically biased” infiltration fluxes are produced that depend on the cell size instead of the hydraulic properties i.e. the solution becomes grid-dependent. (Brunner et al., 2010). Mehl and Hill (2010) demonstrated that that the net stream flux can vary by as much 122% when coarse grids are applied to streams with widths significantly smaller than the cell size compared to grids with cell size approximately equal to stream width.

A second problem emerging from the MODFLOW river conceptualization relates to streamflow loss. Much focus has been given to the numerical modeling of disconnected streams losing streamflow through an unsaturated soil (Osman and Bruen, 2002; Fox and Durnford, 2003; Brunner et al, 2009). Currently, none of MODFLOW’s stream modules are completely capable of physically modeling unsaturated streamflow losses as they do not consider negative pressure heads at the base of the streambed. When the groundwater head beneath the stream falls below the streambed, MODFLOW’s RIV module assumes gravity flow under the stream that approaches a maximum value which remains proportional to the difference between stream stage and the elevation at the bottom of the streambed. MODFLOW’s SFR2 module improves on previous modules as it uses a kinematic-wave approximation to Richard’s equation for unsaturated flow however it still does not account for negative pressure heads beneath the stream

(Niswonger and Prudic, 2010). As a result, stream seepage can still be underestimated when disconnection occurs under the stream.

Osman and Bruen (2002) illustrated that in reality three flow regimes can exist between a stream and its alluvium: saturated zone flow, transition zone flow, and unsaturated zone flow. Saturated zone flow is characterized by seepage that primarily depends on the location of the water table. Saturated pressure heads within the streambed remain positive so that the pores within the soil do not desaturate. Transition zone flow occurs when the water table has dropped a sufficient distance beneath the streambed such that the soil begins to desaturate. This occurs when the magnitude of the capillary pressure head below the streambed becomes greater than the air entry pressure head (also commonly referred to as the bubbling pressure head or suction head), but not so far that a unit hydraulic gradient develops. The unsaturated zone is defined by a constant maximum capillary pressure head in the vertical direction beneath the streambed that becomes primarily gravity driven. This also results in seepage that is not increased by a further decrease of the water table beneath the stream (Fox and Durnford, 2003). Osman and Bruen (2002) developed a new stream module MOBFLOW which accounts for streamflow loss through an unsaturated soil beneath the stream.

Because MODFLOW streams are contained within their assigned cells, modeled streams become a line of cells that cannot span multiple cells over a given cross section. Not only does this imposition result in inaccurate seepage fluxes but it can inadvertently lead to erroneous groundwater heads near the stream as well. Under a stream, a spatially non-uniform head distribution should be expected which produces variable infiltration fluxes. In general, near the thalweg of the stream, seepage occurs under saturated conditions and near the banks of the stream, unsaturated conditions are more prevalent. If a model only uses the conditions directly

under the thalweg to characterize the entire width of the stream one can expect an underestimation of streamflow loss (Storey et al., 2003). Brunner et al (2010) used HydroGeoSphere (Therrien et al., 2006) (a program that fully couples surface and subsurface calculations in a more physically based manner than MODFLOW) to illustrate that not only does MODFLOW incorrectly predict seepage rates on fine scale models but as a byproduct is also incapable of modeling the geometry of the groundwater mound under the stream.

The primary reason for many of the above problems is that information is inherently lost when a continuous system is discretized. Consider the simple conceptual alluvial system in Fig. 15a. The system is in equilibrium with a flow stage of H_1 and the stream is losing flow to the aquifer as the stream stage is greater than the groundwater head in the underlying aquifer. As the alluvium under the stream is saturated along the entire wetted perimeter of the stream, the loss is assumed to occur through a saturated soil. If the stage in the stream were to rapidly increase to H_2 , in general, the increase in stage could not be instantaneously matched by the groundwater head as groundwater moves orders of magnitude slower than surface water. As a result, despite the groundwater conditions remaining unchanged, an unsaturated zone develops along the stream banks. This unsaturated zone will induce streamflow loss with a greater magnitude than under saturated conditions. If this same conceptual system were to be modeled numerically using the primary MODFLOW stream modules, so that the continuous physical system must become a discrete analog of itself, then the system in shown in Fig. 15b will result.

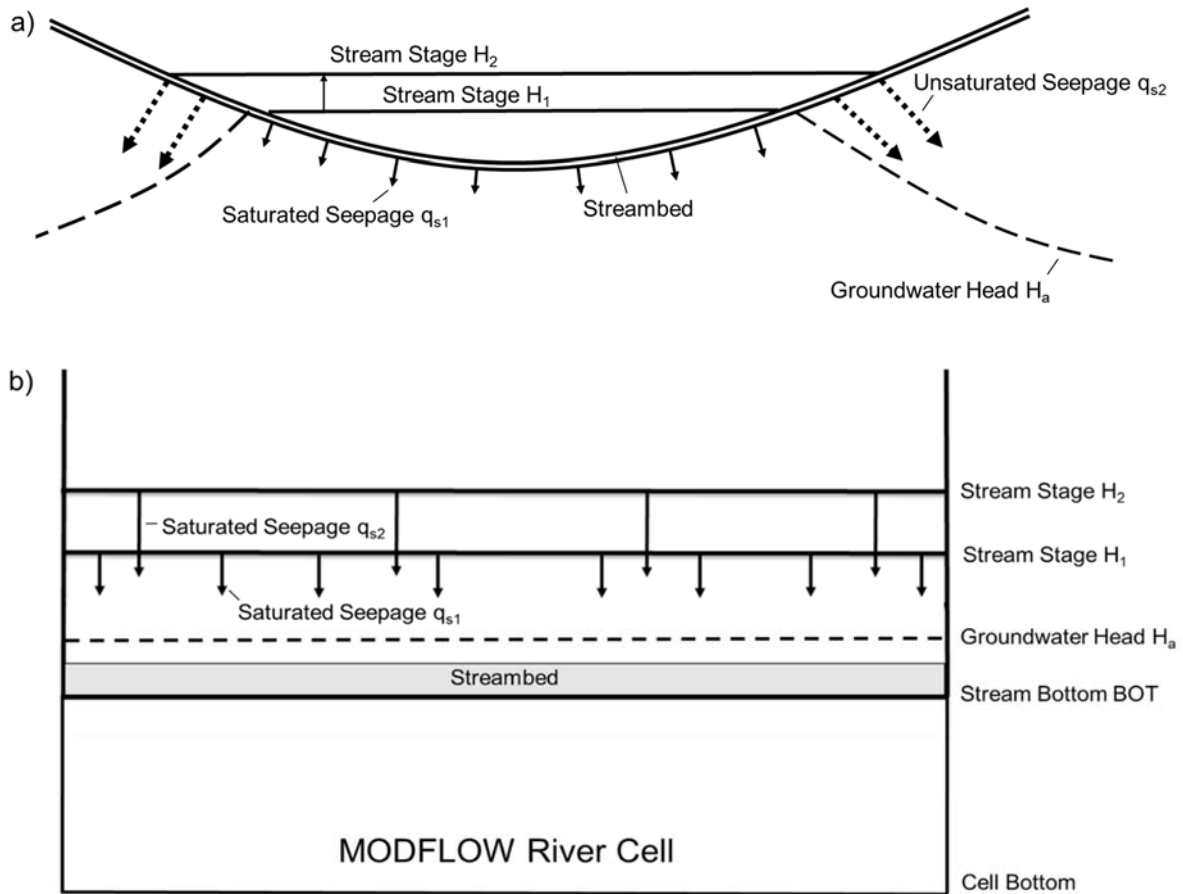


Figure 15. 15a. Physical continuous stream-aquifer system that is losing flow through both a saturated and unsaturated soil after an increase in stream stage; 15b. Numerical discretized stream-aquifer system in which only saturated streamflow loss occurs.

Similarly to the physical continuous system, the discrete system implies that the stream is losing flow under saturated conditions because the groundwater head H_a is below the stream stage but above the streambed. However, now if the stream stage increases from H_1 to H_2 a problem develops because the stream is implicitly assumed to be rectangular and contained to its cell so that all increases in stage cannot manifest in a wider stream. As a result, the unsaturated zone flow that occurs in reality will not be captured in the discrete counterpart.

This is significant because an improved streamflow loss module, such as MOBFLOW (Osman and Bruen, 2002) or SFR2 (Niswonger and Prudic, 2010), will still underestimate streamflow losses if only groundwater head at the thalweg is used to characterize the entire

wetted perimeter of the stream. The limiting dilemma then becomes that even with a more accurate methodology for computing unsaturated zone flow, the unsaturated zone will only develop due to changes in the aquifer and cannot develop due to changes in the surface water.

To overcome this challenge various methods and modules have been developed. It is a common practice to apply adjacent parallel streams with the RIV, STR, or SFR2 modules such that a series of small single-celled rivers create a representative wide river. (Miller et al., 2006). However, stream width must be known a priori for a given flowrate which is 'hard-coded' and will not dynamically adapt based on increased/decreased streamflow from gains/losses due to groundwater exchanges. Stream stages must also be user-defined, obtained from a rating curve, or Manning's equation which cannot be applied in all cases. MODBRNCH (Swain, 1993) was developed by combining MODFLOW with the surface-water code BRANCH (Schaffranek et al., 1981) which computes depth from the one-dimensional St. Venant equations. However stream widths are fixed and seepage is always assumed through a saturated soil.

Rodriguez et al. (2008) linked the United States Army Corps of Engineer's HEC-RAS (Brunner, 1995) model with MODFLOW and applied it to a drainage basin in Argentina. The linked model was ran only under steady-state conditions for a gaining stream so that streamflow loss under unsaturated conditions were not considered. The model could span multiple cells and vary depending on in-stream conditions but because unsaturated zone losses were not accounted for, streamflow losses are predicted to be underestimated. The Surface-Water Routing Process (SWR1) module (Hughes et al., 2012) was developed to account for inflows and outflows from control structures and diversions and routing through ponds, lakes and wetlands. However, while streams can span multiple cells over a cross section, it must be known prior to the simulation

which cells are inundated and the width remains fixed over the simulation. Moreover, unsaturated zone streamflow loss is not accounted for.

More recently, Ou et al. (2013) developed a cross section based, MODFLOW compatible, streamflow routing package, which allows streams to span over multiple cells, referred to as the Cross Section Routing (CSR) module. The module is also capable of modeling inflows and outflows from diversions. CSR was used to illustrate that during large flowrates, combined with pumping near streams, seepage along a cross section can vary greatly. However, CSR does not account for unsaturated streamflow loss and stream stage and flowrate are not computed in a physically based manner but with the Muskingum-Cunge method or a mass-conservation method. Table 5 is a summary of common MODFLOW stream modules and their associated methods of computing stage, width, and streamflow loss.

Table 5. Evaluation of different MODFLOW stream modules.

Module	Method of Computing Stream Stage	Variable Stream Width	Unsaturated Zone Flow
RIV	User-defined	No	No
STR	User-defined	No	No
SFR2	Manning's equation	No	Yes
	User-defined		
	Rating Curve		
MOBFLOW	Manning's equation	No	Yes
	User-defined		
MODBRNCH	1-D St. Venant Equations	No	No
HEC-RAS	1-D St. Venant Equations	Yes	No
SWR1	Dynamic Wave Approximation to 2-D St. Venant Equations	No	No
CSR	Muskingum-Cunge	Yes	No
	Mass conservation		

Note that other hydrologic models exist that are capable of modeling stream-aquifer interactions in a more physically based manner than MODFLOW. Strictly speaking,

MODFLOW is exclusively a groundwater flow model and all surface water-groundwater interactions are linked with MODFLOW in an uncoupled manner. Many fully-coupled models have been developed which jointly solve a form of the St. Venant equations and the groundwater variably-saturated Richard's equation which are then cast into a single global matrix and solved simultaneously. Examples of such models include ParFlow (Maxwell et al., 2014), CATHY (Camporese et al. 2010), HydroGeoSphere (Therrien et al., 2006, Aquanty Inc., 2013), MODHMS (HydroGeoLogic, Inc.), and FIHM (Kumar et al. 2009).

In light of the discussion on the limitations of the existing MODFLOW stream framework, a new stream module, herein referred to as the Dynamic Streamflow module (DSF), has been developed with the primary goal of computing more accurate stream infiltration fluxes. This is done primarily through two mechanisms. First, streams are no longer modeled as a static boundary condition and can adaptively change width based on variable flowrate, flow stage, and channel geometry. DSF calculates river stage from the quasi-steady dynamic wave approximation to the St. Venant equation using an implicit scheme for improved stability. Based on the river's spatially variable channel geometry the flow's top width is computed which in turn determines the cells that are inundated by the stream and therefore interact with the river. That is, streams are not modeled as a single line of cells and can span multiple cells over a cross section. Second, each inundated cell has its own interaction with the river under either saturated or unsaturated conditions depending in the location of the aquifer directly beneath the cell. By allowing infiltration fluxes to be variable across a given cross section more accurate streamflow loss rates can be computed.

DSF has been developed in the FORTRAN language and has been imbedded into the existing MODFLOW program (specifically MODFLOW-NWT). An outline of DSF is presented below.

First, treatment of cross sections and channel geometry are discussed. Second, the hydraulics and numerics of DSF are presented to illustrate how the module computes river stage, cross section top width, and the cells that are inundated by the stream. Finally, the method for determining streamflow and stream seepage is provided and how DSF is embedded within MODFLOW-NWT.

DSF will be evaluated for a small-scale alluvial system and compared against field collected streamflow and groundwater head data. The river running through the alluvium was prone to large fluctuations in streamflow leading to large changes in stream width. DSF's ability to dynamically change stream width will be shown to produce more accurate streamflow losses due to these changes.

3.2 Development of Dynamic Streamflow Module

3.2.1 Overview of the DSF Module

The new Dynamic Streamflow stream module (DSF) for MODFLOW simulates the exchange of water between a stream and an alluvial aquifer using a line of grid cells that span the cross section of a stream. Fig. 16 shows DSF cross sections with adjacent cross sections alternating colors between red and blue and which are projected upon an example MODFLOW grid. Stream banks (in black) are defined by the user and should approximately represent the largest possible stream width expected for the largest flowrate during the simulation period, with widths varying between these defined banks during the simulation. The width of the stream can also vary along the reach. Each cross section is uniquely defined by its line of cells, with each cell provided unique hydraulic properties (hydraulic conductivity, streambed thickness, air entry pressure head, Brooks and Corey parameter). Stream lines are assumed approximately

orthogonal to each cross section. Details for calculating flow depth, flow rate, and cell-specific seepage.

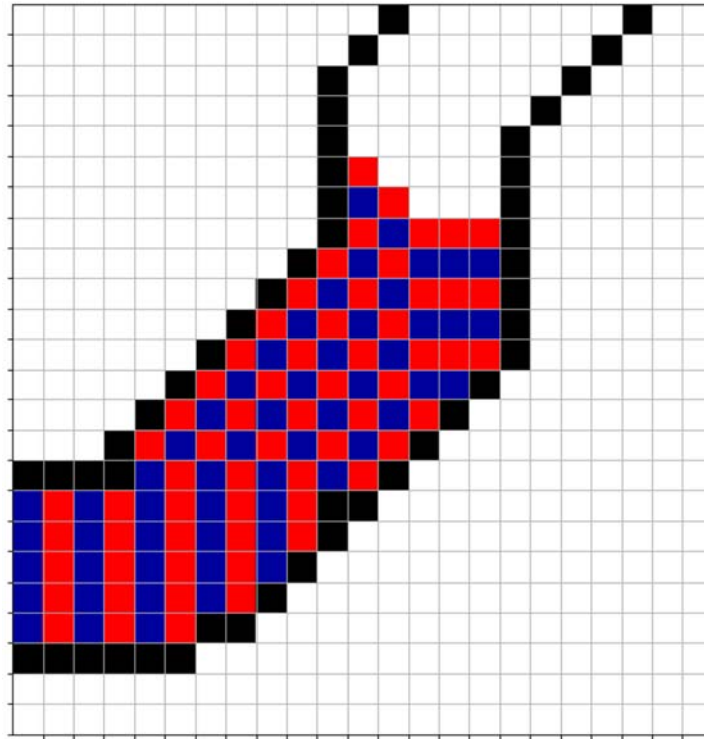


Figure 16. Example DSF cross sections projected on MODFLOW grid. Cross sections alternate between red and blue and black cells represent largest possible stream banks over simulation period.

In the current version of the module, all cross sections are assumed trapezoidal. Of course, rectangular and triangular cross sections can be obtained when the side slopes or bottom width are zero, respectively. The four vertices making up the trapezoid must be identified which are used with linear interpolation used to determine bottom width and side slopes.

3.2.2 Determining Flow Depth

DSF uses the quasi-steady dynamic wave approximation to the St. Venant equations to calculate flow depth. Applying arguments of specific energy to the conservation of momentum equation gives:

$$\frac{\partial h}{\partial x} = \frac{S_0 - S_f}{1 - Fr^2} \quad (3.1)$$

where h is flow depth [L], x is the downstream direction [L], S_0 is bed slope [L/L], S_f is the rate of energy loss (friction slope) [L/L], and Fr is the Froude number [-]. For improved stability, Eq. (3.1) is numerical solved with a first-order implicit Euler scheme, given as:

$$h_{i+1} = h_i + \Delta x \left[\frac{S_0 - S_f}{1 - Fr^2} \right]_{i+1} \quad (3.2)$$

where subscript i is positive in the upstream direction. The friction slope S_f is computed using Manning's equation, although other friction or conveyance equations could be implemented instead. The bed slope S_0 is computed with a four-point method. The Froude number Fr is computed from its definition and assuming a trapezoidal channel. These three functions are given below.

$$S_{f_{i+1}} = \left[\frac{Q_i n_{i+1}}{\phi A_{i+1} R_{i+1}^{2/3}} \right]^2 \quad (3.3)$$

$$S_{0_{i+1}} = \frac{-z_{i+3} + 8z_{i+2} - 8z_i + z_{i-1}}{12\Delta x} \quad (3.4)$$

$$Fr_{i+1} = \frac{Q_i^2 T_{i+1}}{g A_{i+1}^3} \quad (3.5)$$

A , R , and T are the flow area, hydraulic radius, and top width, respectively. As all cross sections in the DSF module are assumed trapezoidal, these geometric parameters take the form:

$$A_{i+1} = b_{i+1} h_{i+1} + 0.5 h_{i+1} (m_{i+1}^L + m_{i+1}^R) \quad (3.6)$$

$$R_{i+1} = \frac{A_{i+1}}{P_{i+1}} = \frac{A_{i+1}}{b_{i+1} + h_{i+1} \left(\sqrt{1 + (m_{i+1}^L)^2} + \sqrt{1 + (m_{i+1}^R)^2} \right)} \quad (3.7)$$

$$T_{i+1} = b_{i+1} + h_{i+1}(m_{i+1}^L + m_{i+1}^R) \quad (3.8)$$

where b is the bottom width of the trapezoidal cross section [L] and m^L and m^R are the side slopes of the left and right bank, respectively [L/L]. If the channel is rectangular then $m^L = m^R = 0$ and if the channel is triangular $b = 0$. Manning's n defines the flow resistance [T/L^{1/3}], ϕ is a unit correction factor that is 1.49 for English units and 1 for SI units, and g is the gravitational force due to gravity. When Eq. (3.2) is evaluated with Eqs. (3.3), (3.4), and (3.5) a nonlinear equation emerges in solving for h_{i+1} due to A , R , and T all being a function of h_{i+1} . A bisection algorithm is implemented to find the root of the following equation:

$$f(h_{i+1}) = h_{i+1} - h_i - \Delta x \left[\frac{S_0 - S_f}{1 - Fr^2} \right]_{i+1} = 0 \quad (3.9)$$

That is, h_{i+1} is sought such that Eq. (3.9) is satisfied, or within a prescribed tolerance ε such that $|f(h_{i+1})| < \varepsilon$. A realistic interval $[a, b]$ in which h_{i+1} lies within must also be specified. The lower bound must always be critical depth $a = y_c$ at the current cross section as the flow is assumed to remain subcritical. The upper bound b represents the largest expected depth at the cross section. A downstream boundary condition h_l must also be specified and can vary on a case-by-case basis. As DSF imposes subcritical flow, the downstream boundary condition is always a multiple j of the critical depth at the downstream boundary condition, $h_l = j \cdot y_c, j > 1$.

3.2.3 Determining Flowrate and Seepage

At a given cross section $i+1$, a flow depth h_{i+1} is computed using the process discussed in Section 3.2.2. The cells that are inundated (and where streamflow interactions can occur) are determined from the computed top width of the cross section T_{i+1} . Each cell that is inundated is then evaluated independently to determine the nature of the stream-aquifer interaction.

The equations to solve depend on whether the groundwater head in the cell of interest is above or below the streambed. DSF incorporates the methodology outlined by Fox and Durnford (2002), which used the Brooks and Corey equation (Brooks and Corey, 1964) to approximate unsaturated hydraulic conductivity. Transition regime flow is ignored within DSF because the range of groundwater heads over this flow regime is relatively small and the time in which it occurs is also very fast (Fox, 2003). Fox (2003) also reported that simulation results did not significantly change when transition flows were not included in the module. The following relationships are used to determine infiltration flux between the stream and alluvium. Saturated zone flow occurs when the groundwater head H_a [L] is above the streambed BOT [L] with the specific discharge q_s [L/T] given as:

$$q_s = K_{sb} \frac{H_r - H_a}{m} \quad (3.10)$$

where m is the streambed thickness [L] K_{sb} is the saturated streambed hydraulic conductivity [L/T], and H_r is the stream stage [L]. Unsaturated zone flow is assumed to occur when groundwater head is below the streambed. In this case, a system of equations is solved to determine the specific discharge through the streambed:

$$q_s = \begin{cases} K_{sb} \left[1 + \frac{h_{cu} + H_r}{m} \right] \\ K_a \left[\frac{h_e}{h_{cu}} \right]^\eta \end{cases} \quad (3.10)$$

where h_{cu} is the maximum capillary pressure head that exists within the soil [L], h_e is the air entry pressure head [L], K_a is the vertical hydraulic conductivity of the alluvium beneath the streambed [L], and η is referred to as the Brooks and Corey exponent [-]. Each variable or parameter is evaluated for each inundated cell so that, in general, each cell can have its own set of parameters (K_{sb} , m , h_e , η). In reference to Figure 17, neither BOT nor H_a is constant along a

cross section, leading to the possibility of both saturated and unsaturated flow regimes occurring along a single cross section. Subsequently as a result, a given cross section can have multiple flow regimes occurring. Values of K_a are read in from the MODFLOW UPW (or LPF) package and can vary from cell to cell.

The specific discharge q_s is multiplied by the horizontal projection of the cross sectional area of the cell to determine the volumetric seepage flux Q_s flowing into or out of the cell. Currently, DSF does not account for horizontal seepage through the side slopes. Streamflow losses are added to the first layer in which the water table exists. As seen in Figure 17, in general, some cells will be losing flow through both saturated and unsaturated soils. In this case, DSF determines the horizontal projected area governed by each regime and computes the specific and volumetric discharge for each area. For example, in the conceptual case in Figure 17, the stream would be losing flow to row 3 (layer 2) through an unsaturated soil through only a portion of the entire cell area. The stream would be losing flow through both a saturated and unsaturated soil to row 4 (layer 2). Rows 5-11 (layer 2) would all gain flow from the stream through a saturated soil through the entire cell area and row 12 (layer 2) would gain flow from the stream through both a saturated and unsaturated soil over only part of the cell area.

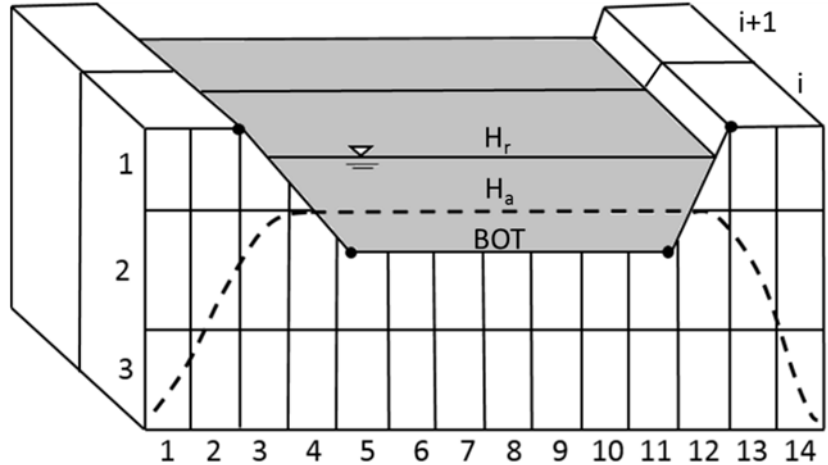


Figure 17. Schematic of DSF cross section in relation to MODFLOW grid (after Ou et al., 2013).

After the volumetric seepage flux for each cell is computed along a cross section the sum of losses and gains determines the total net loss Q_{seep} for that cross section. That is, in reference to Figure 17, the sum of losses from rows 3-12 would determine Q_{seep} . Therefore the streamflow rate at the next cross section Q_{i+1} is equal to the streamflow rate at the current cross section Q_i plus the net streamflow loss.

$$Q_{i+1} = Q_i + Q_{seep} \tag{3.11}$$

This process is repeated for every cross section to the final upstream cross section, which will have a computed streamflow rate Q_f and is compared to the known actual upstream flowrate Q_u . If Q_f is equal to Q_u or within an acceptable tolerance, then the assumed initial downstream flow Q_a is deemed correct. Otherwise, the downstream flowrate is updated until convergence is achieved using an interval halving method, with a solution assumed within the interval $[0, j \cdot Q_u]$. The lower bound on the downstream streamflow is always 0 (i.e. all streamflow is lost over the reach) and the upper bound is a multiple j of the known upstream flowrate (i.e. the reach gains j times the upstream flowrate). A value of 2 is recommended.

The DSF procedure is illustrated as a flowchart in Figure 18. For each stress period a known upstream flowrate is provided to DSF. Computing downstream to upstream, stream stages are then calculated using the methodology of Section 3.2.2. At each cross section, streamflow losses or gains from groundwater are determined using the methodology of Section 3.2.3. When the final upstream cross section is reached, the computed upstream flowrate is evaluated, and if need be, updated using the interval halving method algorithm of Section 3.2.3. This process is repeated for every stress period.

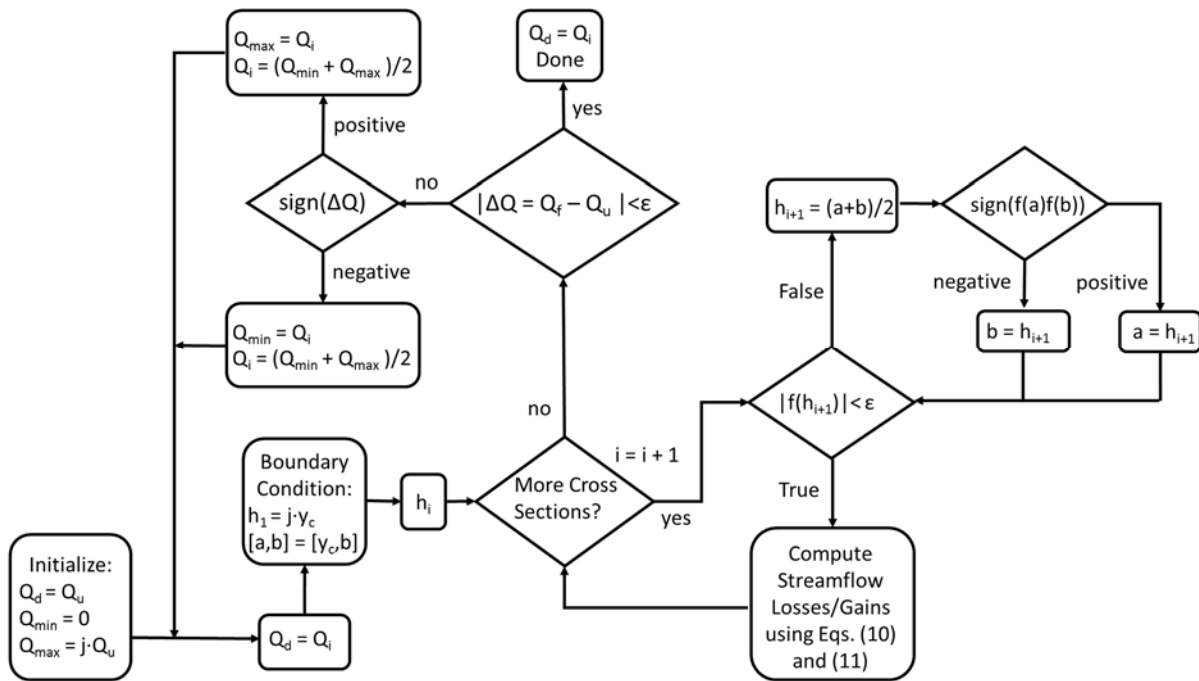


Figure 18. Logical flowchart illustrating the methodology of computing stream stage and flowrate within DSF.

3.2.3 DSF within MODFLOW

The DSF module is written in the FORTRAN language and embedded into MODFLOW-NWT (Niswonger et al., 2011). When active, the module reads in required input (cross section geometry and hydraulic parameters) and computes volumetric infiltration rates for the inundated cells. These stresses are then added to the MODFLOW source/sink volumetric flux array using

the WEL package (the WEL package must therefore always be activated when using DSF).

Figure 5 illustrates the general process. For each stress period, MODFLOW will determine if the DSF module is active. If so, the DSF calculations will proceed using the methodology discussed in Sections (3.2.2) and (3.2.3) and illustrated in Figure 19. When the DSF calculations are complete, the results are treated as stresses and added to the WEL package.

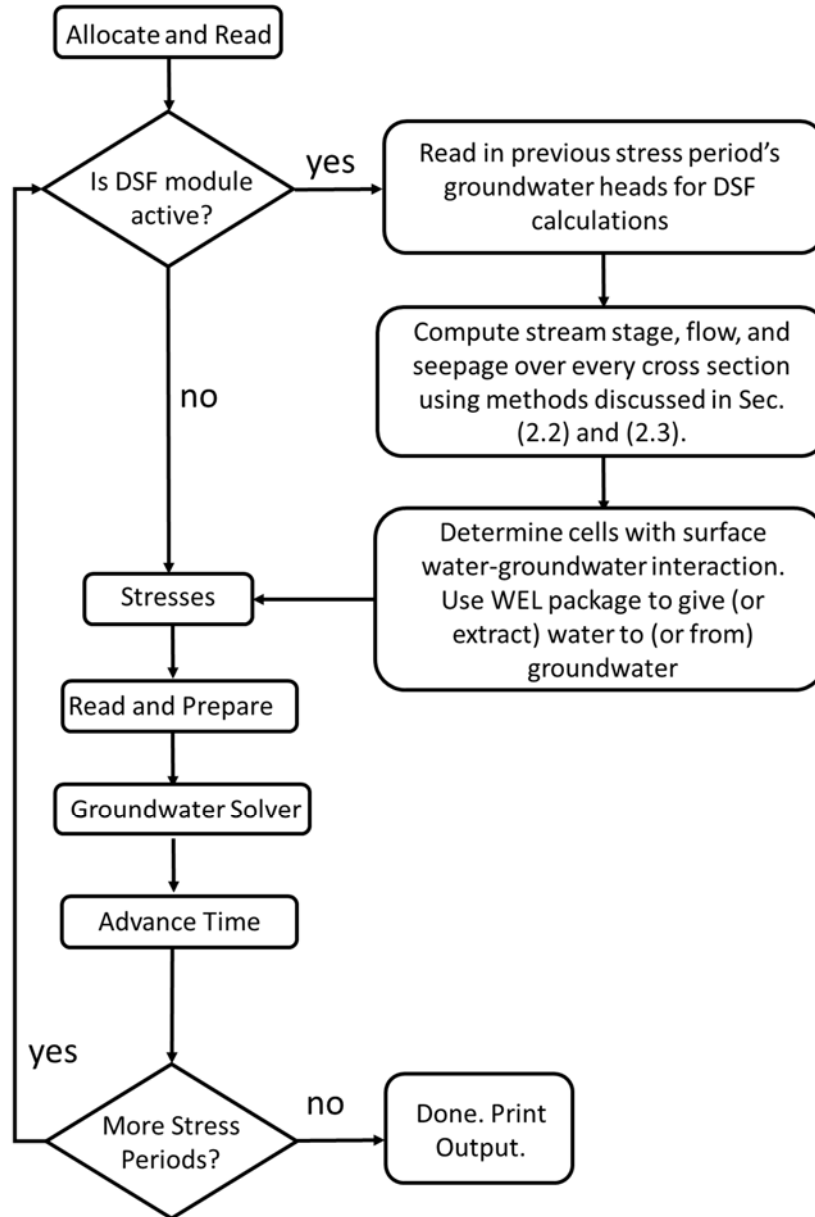


Figure 19. General framework of MODFLOW-NWT when DSF module is active.

3.3 Application of DSF

3.3.1 Field Site

A field test was conducted to illustrate DSF's capabilities and improved accuracy in computing streamflow loss. The study was conducted along a reach of the South Platte River south of Denver, Colorado (Fig. 20a) from December 2016 to February 2017. The river flows through a shallow alluvium consisting of fine gravels and coarse sands with an average thickness of 14 m. The reach is approximately 2 km downstream of Chatfield Reservoir, which released water at rates up to 3.5 m³/s during the study period. Also upstream of the reach, but downstream of the Reservoir, is the Centennial Waste Water Treatment Plant (WWTP) which releases effluent into the river at rates ranging from 0.15 to 0.55 m³/s. Releases from Chatfield Reservoir varied over approximately weekly cycles, whereas releases from the WWTP occurred over hourly cycles.

This reach of the South Platte River is characterized by a series of pools and riffles. The pools have depths up to 3 m. The streambed primarily consists of medium to fine sands. Bank stabilization efforts are prevalent along much of the east bank, preventing the river from expanding over the floodplain. The west bank is more natural and with shallow side slopes, which allows for the river to expand laterally and inundate banks during times of high streamflow. Stream widths varied between 7 and 40 m along the reach, depending on location and streamflow rate. No inflows or outflows of surface water occurred over the reach and any direct evaporation or precipitation onto the River were assumed negligible over the 2 km reach.

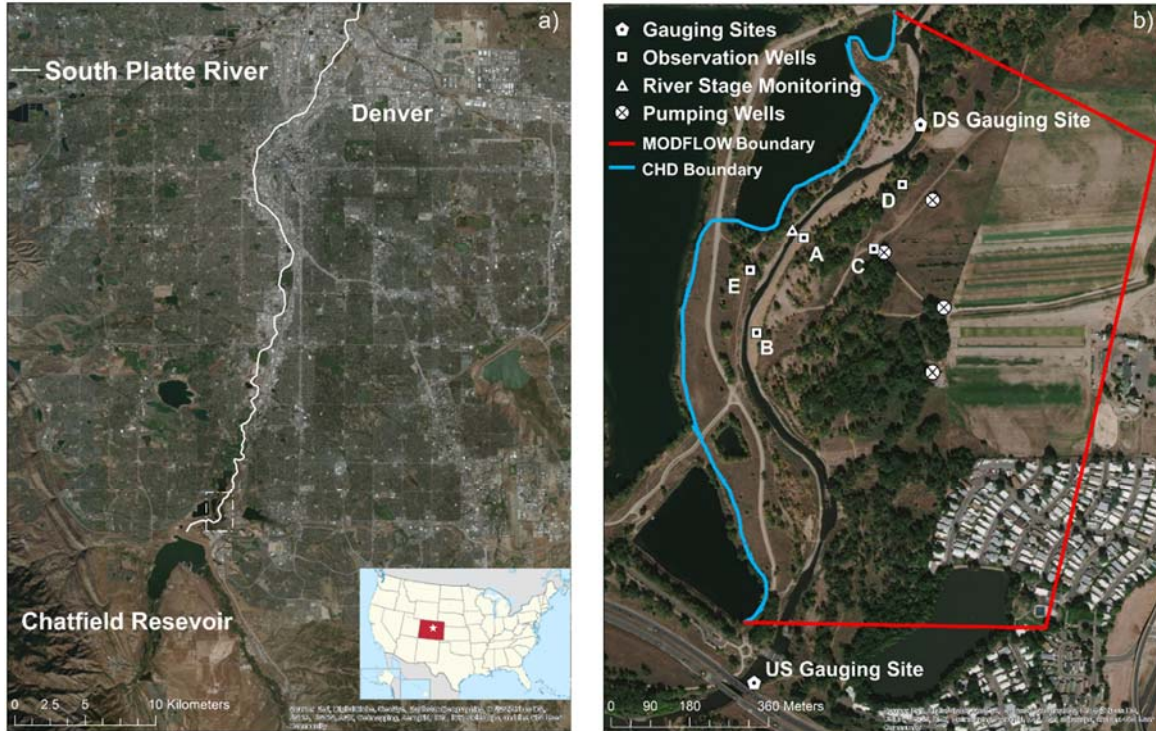


Figure 20. 20a (Left): Location of study site and relative proximity to Chatfield Reservoir and City of Denver; 20b (Right): Map of South Platte River reach where streamflow and groundwater levels were monitored, showing five monitoring well locations, four pumping wells, two streamflow gauging sites, and location where river stage was monitored. MODFLOW model boundary and boundary conditions shown in red and blue, respectively.

The reach was adjacent to a pumping well field which consisted of four high-capacity pumping wells (Fig. 20b) each with a capacity of approximately $0.064 \text{ m}^3/\text{s}$. The pumping wells are owned and operated by the Centennial Water and Sanitation District, and are located between 122 and 259 m from the River.

3.3.2 Field Data Collection

Both streamflow and groundwater levels were monitored during the study period. Streamflow was monitored coming into and leaving the reach to determine streamflow loss. Upstream streamflow was obtained from the City of Littleton, who operates a stream gauge with reported values every 15 minutes. A hydrograph is shown in Fig. 21 which shows the streamflow traveling through the reach over the study period. The horizontal axis is hours after 20 December

2016 11:00 AM MT. The small fluctuations are due to changes in the WWTP release and the large fluctuations are due to changes in the release from Chatfield Reservoir. Downstream streamflow was measured at discrete times using an acoustic Doppler velocimeter (ADV).

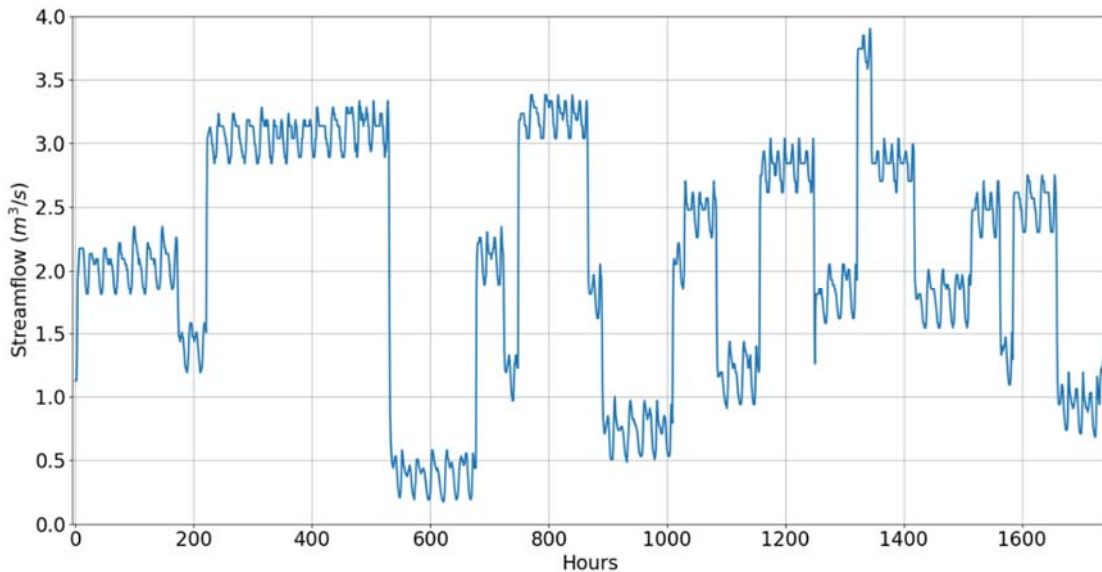


Figure 21. Hydrograph of South Platte River over the study period.

3.3.3 Development of MODFLOW Model

Two MODFLOW models were created to compare against measured streamflow and groundwater head data. Each model was identical with the only distinction that one model used the DSF module to model the river whereas the other model used the SFR2 module. For both models, the alluvium was modeled with two layers, 1035 rows, and 877 columns producing a horizontal grid size of 1x1 meter. Horizontal hydraulic conductivity ranged from 144 to 240 m/day throughout the alluvium with larger values near the stream. Specific yield ranged from 0.13 to 0.35 with larger values near the stream which produced more stable results in the DSF module. Vertical hydraulic conductivity was assumed to be 0.01% of the horizontal hydraulic conductivity for each cell. A constant head boundary condition was prescribed along the western

flank of the model, as the study site was adjacent to three gravel ponds which were reported to be unlined (see Fig. 20b).

The hydraulic properties of the stream were calibrated using the Parameter Estimation and Uncertainty Analysis (PEST) program (Doherty, 2015) to have a variable hydraulic conductivity ranging from 6.76×10^{-3} to 9.95 m/day with a mean value of 4.97 m/day. For the DSF module, the downstream boundary condition was placed at the beginning of a downstream riffle sequence where flow depth was assumed to be 5% greater than critical depth. Table 6 provides the necessary input parameters for both the DSF and SFR2 modules. Note: The SFR2 module is capable of calculating river stage using Manning’s equation however, because this reach consisted of a series of pools with adverse slopes, Manning’s equation was not valid. Therefore, this aspect of the SFR2 module was not utilized and river stages were prescribed for each stress period based on computed river stages from Eq. (3.2).

Table 6. Necessary stream module parameters used for the DSF and SFR2 modules.

Parameter	SFR2	DSF
Streambed hydraulic conductivity	Varies over reach Average: 4.97 m/day	Varies over reach and cross sections Average: 4.97 m/day
Stream width	10 m	Variable
Streambed thickness	1 m	Varies over cross section 1-2 m
Brooks and Corey exponent	0.3	0.3
Saturated water content	0.35	Na
Manning n	Na	Varies over reach Average: 0.03
Method for calculating stage	User defined.	Equation (3.2)

The model consisted of 1740 stress periods each with a length of 1 hour. The four pumping wells began pumping on the stress period 576 and turned off on stress period 975. They collectively pumped at an average rate of 0.27 m³/s over this period.

3.3.4 Model Results

3.3.4.1 Groundwater Head

An examination of the simulated groundwater heads when applying DSF provides an initial insight into stream-aquifer interactions. Simulated groundwater heads at Location A and C are compared with measured data (see Fig. 20b). Location C shows that in areas relatively far from the stream that the model is capable of providing very accurate results (Fig. 22). Deviations between simulated and observed values could most likely be resolved if more variation in hydraulic conductivity was modeled.

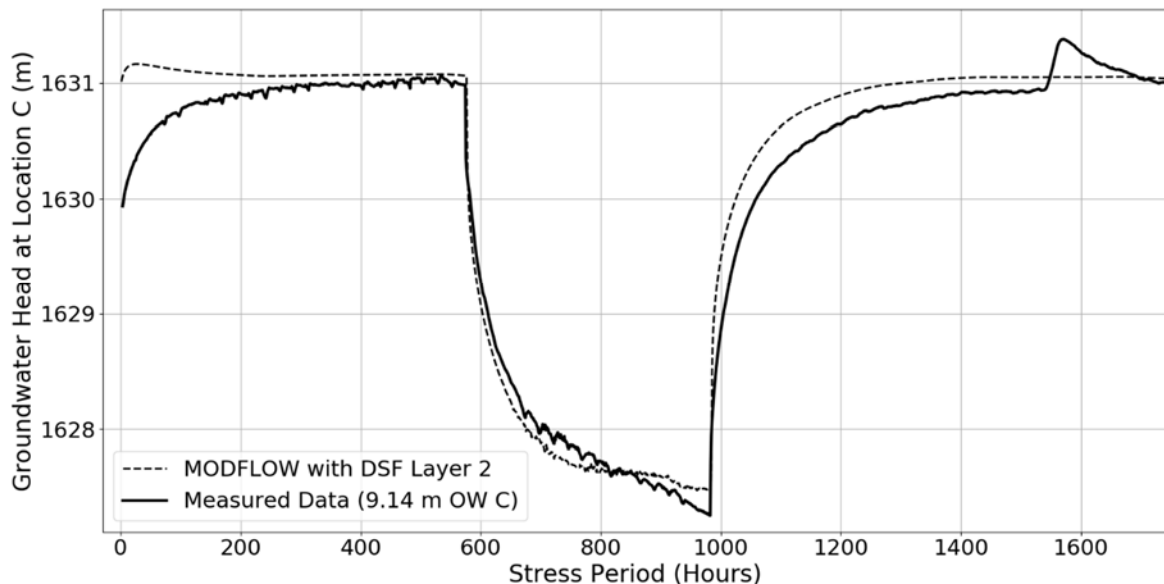


Figure 22. Simulated and observed groundwater heads at Location C.

Simulated groundwater heads are also provided in Fig. 23 for Location A. The simulated results fit the trends at two different depths within the aquifer (2.44 and 4.27 m below ground surface). In particular, the data suggest that the groundwater head near the river is largely dependent upon changes in the stream stage. This is seen by the small changes in head corresponding nearly exactly to the changes in streamflow (see hydrograph in Fig. 21). For these

small changes in groundwater head, which are the result of interactions with the nearby river, to be modeled accurately, it is vital that accurate infiltration fluxes between the river and the alluvium are attainable. The closeness of fit between model output and observed values suggests that DSF is capable of providing these values.

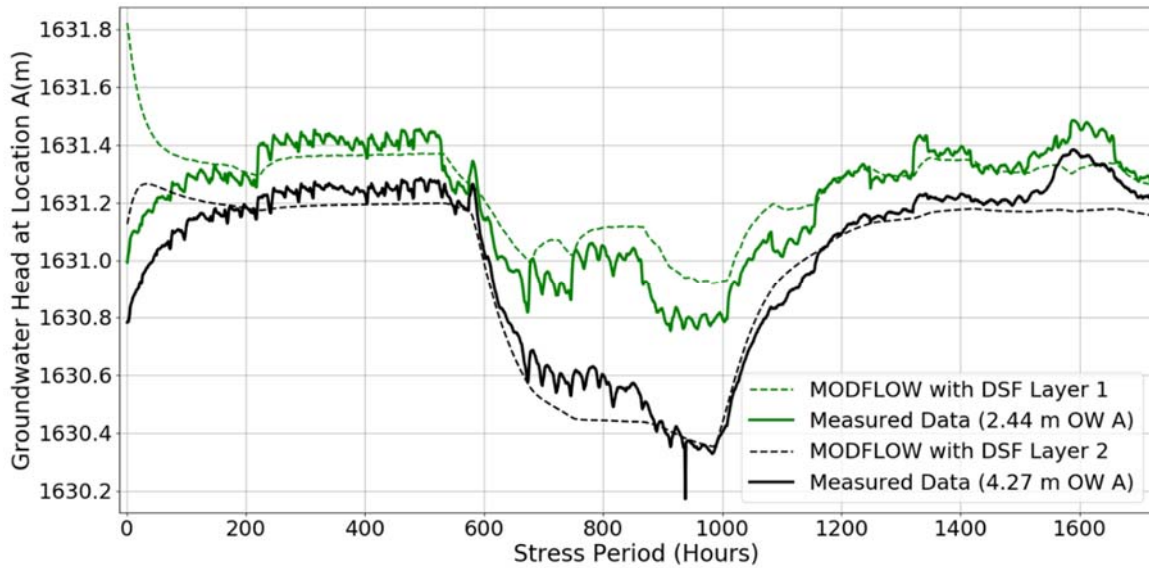


Figure 23. Simulated and observed groundwater heads at Location A.

3.3.4.2 Streamflow Loss

Fig. 24 shows simulated streamflow loss for each stream module, DSF and SFR2, in comparison with the measured streamflow loss. The RMSE of the DSF and SFR2 modules are 0.14 and 0.15 m³/s, respectively. However, if measured streamflow losses on stress period hour 505, 1271, and 1272 are neglected then the RMSE of the DSF and SFR2 modules are 0.07 and 0.11 m³/s, respectively. These three measurements were taken during the largest streamflow rates during the simulation period (see Fig. 21) and so it is possible that equipment measurement errors were augmented. It is also possible that because neither DSF nor SFR2 accounts for horizontal seepage that neither module is well suited to simulate these high flow events.

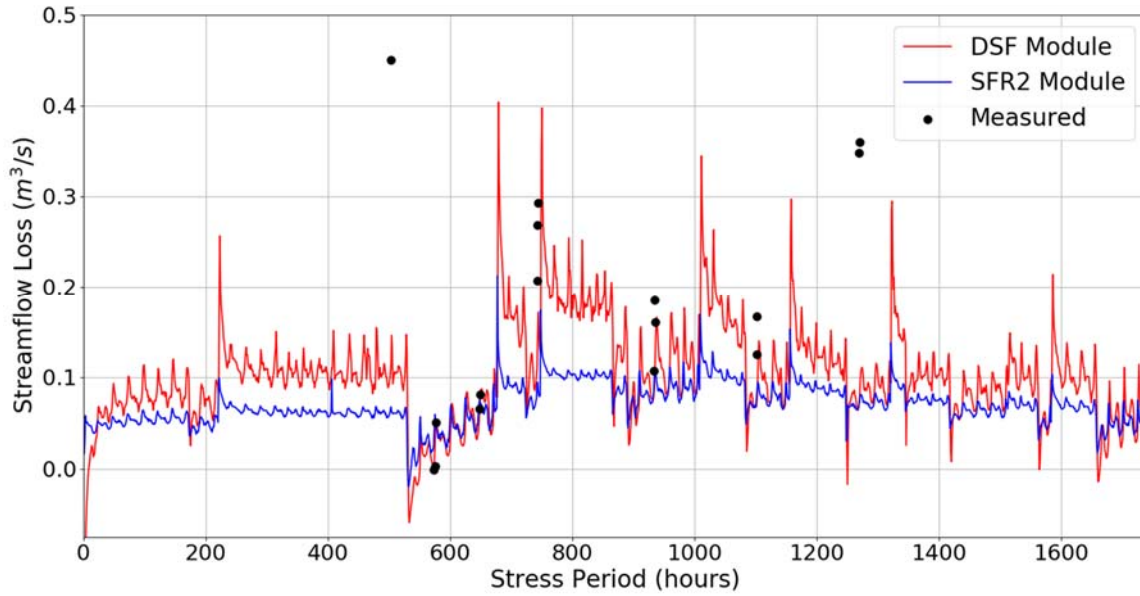


Figure 24. Computed streamflow loss with DSF and SFR2 modules evaluated against measured data.

However for all measurements, the DSF module performs more accurately than the SFR2 module due to its ability to dynamically change stream width due to changes in streamflow rate. This is seen by DSF's capability in modeling both low and high streamflow rates. Whereas the range of losses is relatively limited in the SFR2 simulation, the DSF module possesses a larger range of predicted values due to its ability to adaptively increase stream width. This phenomena can be shown visually, as seen in Fig. 25, where the number of cells that are inundated by the river decreases for decreased streamflow. Fig. 25a is at stress period hour 500 (with a streamflow rate of $2.94 \text{ m}^3/\text{s}$) and Fig. 25b at stress period hour 550 (with a streamflow rate of $0.26 \text{ m}^3/\text{s}$). The large decrease in streamflow directly manifests in a large decrease in stream width for all reaches. The decrease in stream width has a direct impact on streamflow loss rate as well. In reference to Fig. 24, streamflow loss decreases from $0.09 \text{ m}^3/\text{s}$ to $-0.004 \text{ m}^3/\text{s}$ (i.e. a gaining stream) over this 50 hour period. This decrease is the consequence of a smaller wetted perimeter for streamflow loss to occur, combined with a decrease in river stage.

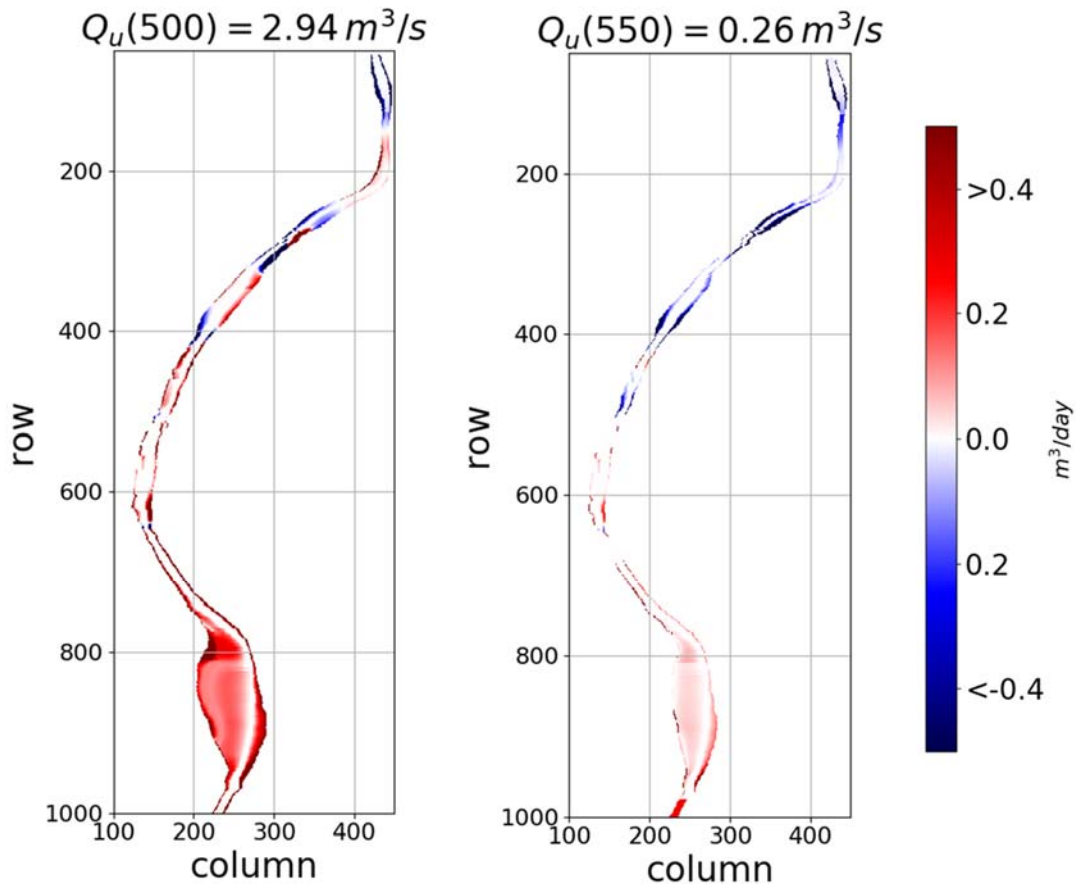


Figure 25. 25a (Left): Inundation map of river during times of high flow at stress period hour 500; 25b (Right): Inundation map of river during times of low flow at stress period hour 550.

The largest decreases in stream width occur in the upstream reaches of the river, as seen in Fig. 26. As previously mentioned, the west bank of the river did not have significant bank stabilization efforts put into place to manage the river. As a result, the river's side slopes were relatively small so that increases in streamflow resulted in large increases in stream width. In particular, it is seen that the increase in streamflow resulted in an increase stream width of approximately 10 m over some cross sections.

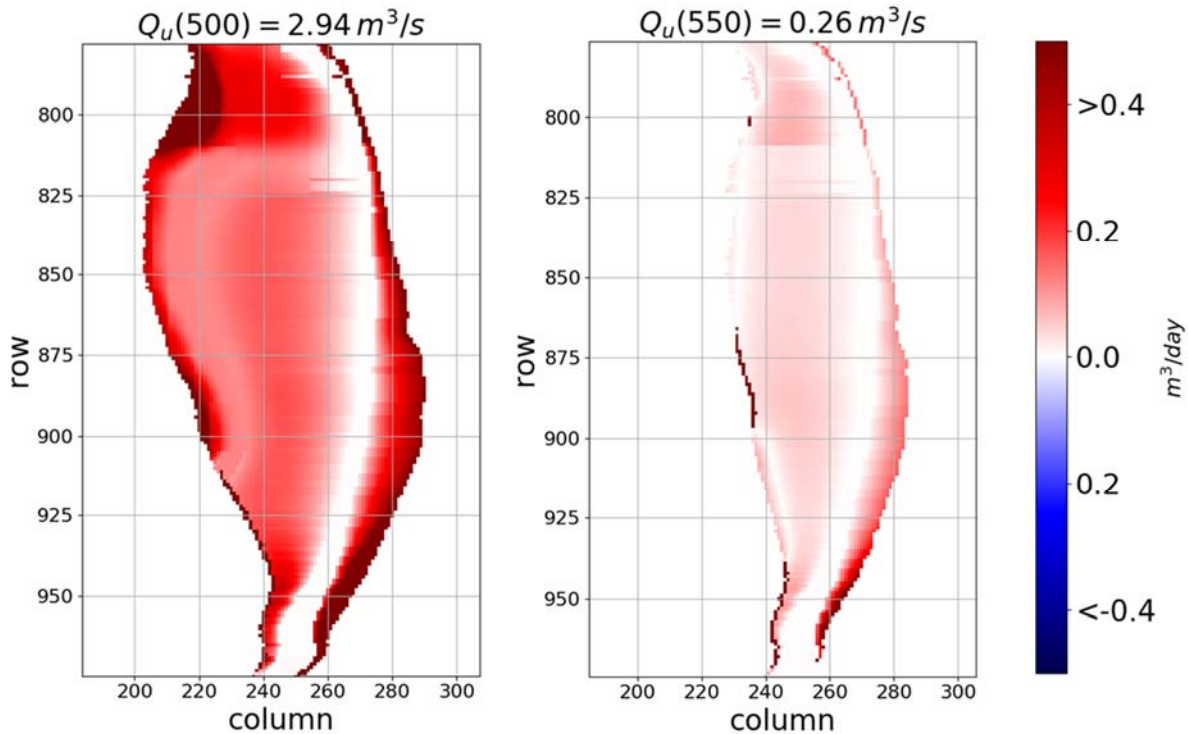


Figure 26. 26a (Left): Inundation map of upstream reach during times of high flow at stress period hour 500; 26b (Right): Inundation map of upstream reach during times of low flow at stress period hour 550.

DSF also provides insight into where streamflow loss primarily occurs along a cross section. Fig. 26 illustrates that in general, the river loses most of its streamflow along its banks where unsaturated zones are more likely to develop. This is seen by the darker red regions. Fig. 27 shows a downstream reach in which, similar to the upstream reach of Fig. 26, during times of high flow the reach is losing flow with unsaturated zone flow near its banks. When the streamflow decreases, not only does the stream width decrease, but the river transitions from a losing stream to a gaining stream. Fig. 28 is of a cross section through row 200 in which the river stage drops significantly due to a decrease in streamflow. While the groundwater head also drops due to the decrease in infiltration from the river, it does not decrease as much as the stream stage so that the area transitions to a gaining reach.

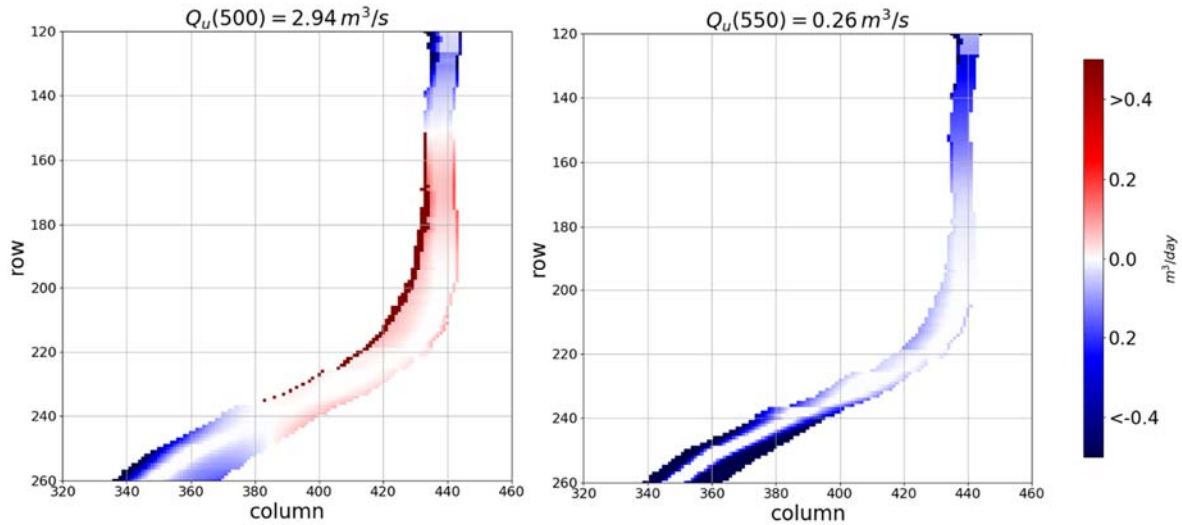


Figure 27. 27a (Left): Inundation map of downstream reach during times of high flow at stress period hour 500; 27b (Right): Inundation map of downstream reach during times of low flow at stress period hour 550.

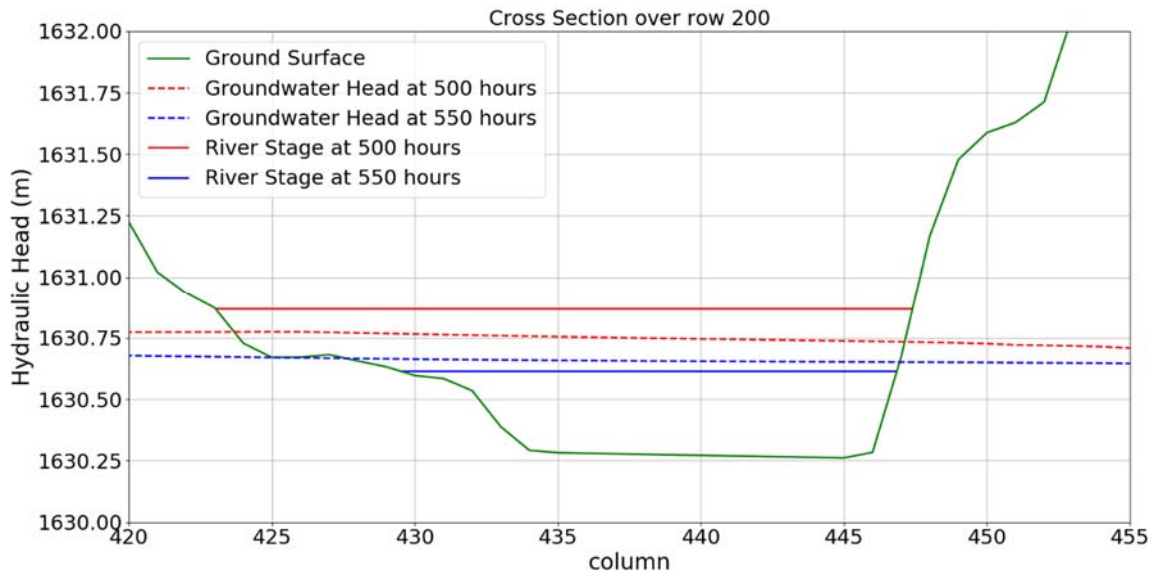


Figure 28. Cross section over row 200 showing the transition from a losing to a gaining stream due to a decrease in streamflow.

3.3.4.3 Effect of Pumping Wells

The ability of the DSF module to calculate non-uniform seepage along a cross section proves important in the evaluation of pumping-induced streamflow loss. Fig. 29 shows a contour map of heads and simulated streamflow loss over inundated areas at stress period hour 950 when

pumps were simulated (corresponding to 374 hours of pumping) versus when they were not simulated. The approximately parallel contour lines (relative to the river) imply that a gradient has developed that will induce streamflow loss. By inspecting the shades of colors representing magnitude of streamflow loss, it is seen that the east bank is where much of the streamflow is occurring for almost every cross section.

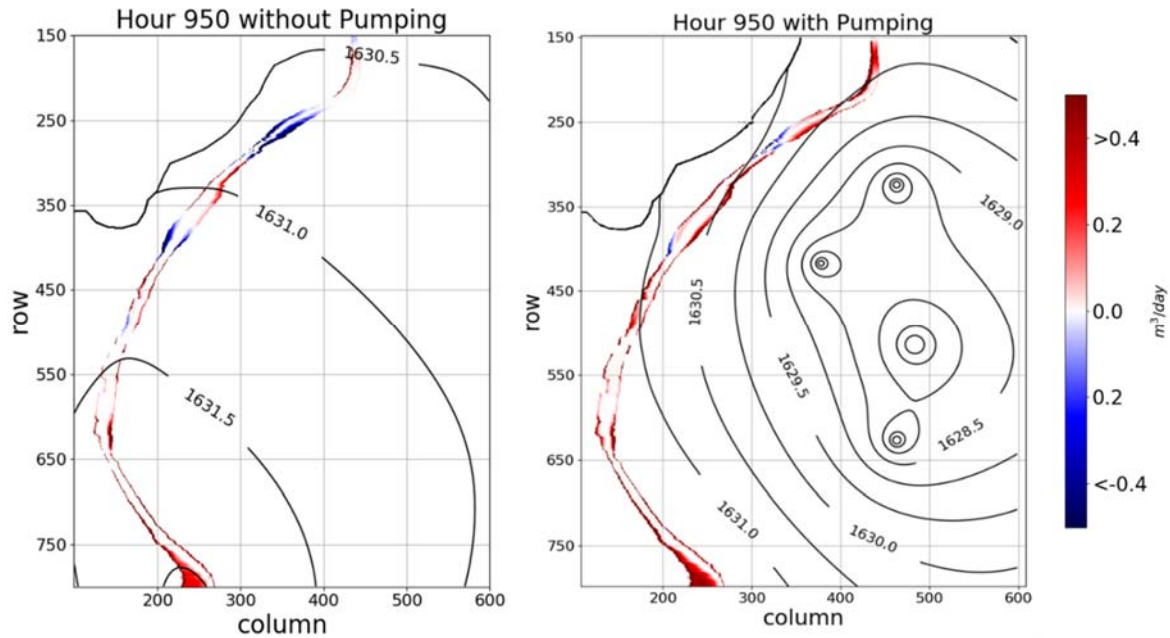


Figure 29. 29a (Left): Inundation map and contour lines of groundwater head of downstream reach at stress period hour 950 when pumps are not operating; 29b (Right): Inundation map and contour lines of groundwater head of downstream reach at stress period hour 950 when pumps were modeled.

This is further confirmed in Fig. 30 which shows the groundwater profile at the cross section through row 370 at stress period hour 950. One profile is when pumps are simulated (blue) and one profile is when the pumps are neglected (red). The result is that along the right bank nearly 3 m of unsaturated zone flow is induced due to the pumping wells.

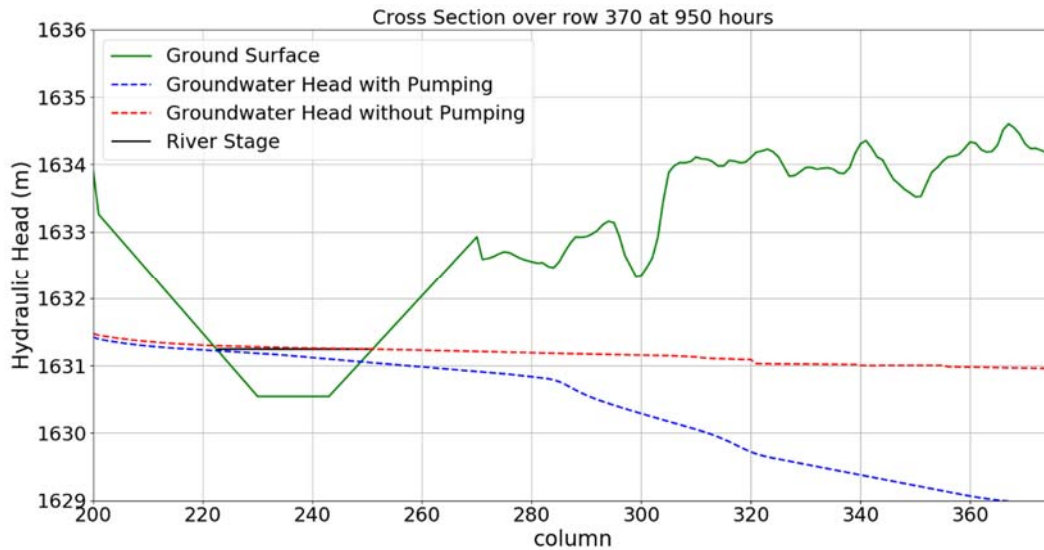


Figure 30. Groundwater profile over row 370 when pumps are simulated (in blue) and ignored (in red).

The implication of this is that the simulated pumping-induced streamflow loss using DSF is relatively greater than the simulated pumping-induced streamflow loss using SFR2 as seen in Fig. 31. On closer inspection of Fig. 30 it is seen that along the thalweg of the stream, the streambed remains saturated (as the groundwater head is above the streambed), but along the right bank an unsaturated zone has developed.

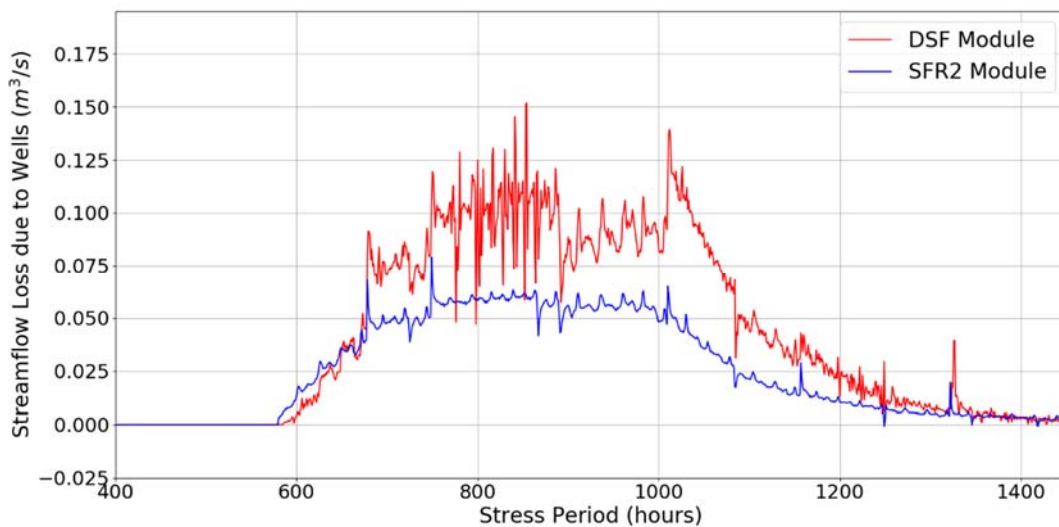


Figure 31. Pumping-induced streamflow loss.

While DSF will model this unsaturated zone accordingly, SFR2 will compute seepage assuming a saturated soil along the entire wetted perimeter of the stream. As a result, the loss due to the wells will be underestimated. Moreover, for increases in stage, the length of inundation over an unsaturated soil will also increase. This explains the large relative increase in pumping-induced streamflow loss at stress period hour 680 when streamflow increases from 0.5 to 2.0 m³/s over an hour.

3.4 Conclusions

A new MODFLOW stream module was developed to better model stream-aquifer interactions in small scale alluvial systems where MODFLOW cells have dimensions smaller than the width of the stream. The module uses the quasi-steady one-dimensional dynamic wave approximation to the St. Venant equations to obtain stream stage. The stream width can span multiple cells and the associated stream-aquifer fluxes are not assumed constant over a cross section. Streamflow loss can occur through a saturated or unsaturated soil. It was shown that in a fine scale model that the module is more accurate in predicting streamflow losses than existing stream modules due to its capability in estimating unsaturated zone losses along newly inundated stream banks. The module also provided insight into alluviums impacted by pumping wells, revealing that most streamflow loss occurs along the banks of the stream near the pumping wells.

REFERENCES

- Anderson, Mary P. "Heat as a Ground Water Tracer." *Ground Water*, vol. 43, no. 6, 2005, pp. 951–968., doi:10.1111/j.1745-6584.2005.00052.x.
- Bailey, Ryan T., T.K. Gates, M. Admadi, 2014, Simulating Reactive Transport of Selenium Coupled with Nitrogen in a Regional-Scale Irrigated Groundwater System. *Journal of Hydrology*, vol. 515, pp. 29–46., doi:10.1016/j.jhydrol.2014.04.039.
- Beatty, S.J., D.L. Morgan, F.J. McAleer, A.R. Ramsay, 2010, Groundwater contribution to baseflow maintains habitat connectivity for *Tandanus bostocki* (Teleostei: Plotosidae) in a south-western Australian river. *Ecology of Freshwater Fish* 19, pp. 595-608., doi:10.1111/j.1600-0633.2010.004400.x
- R. H. Brooks And A. T. Corey. "Hydraulic Properties of Porous Media and Their Relation to Drainage Design." *Transactions of the ASAE*, vol. 7, no. 1, 1964, pp. 0026–0028., doi:10.13031/2013.40684.
- Brunke, Matthias, and Tom Gonser., 1997, The Ecological Significance of Exchange Processes between Rivers and Groundwater. *Freshwater Biology*, vol. 37, no. 1, pp. 1–33., doi:10.1046/j.1365-2427.1997.00143.x.
- Brunner, Gary W. *HEC-RAS River Analysis System: User's Manual*. US Army Corps of Engineers, Institute for Water Resources, Hydrologic Engineering Center, 2002.
- Brunner, Philip, et al. "Hydrogeologic Controls on Disconnection between Surface Water and Groundwater." *Water Resources Research*, vol. 45, no. 1, 2009, doi:10.1029/2008wr006953.

- Brunner, Philip, et al. "Modeling Surface Water-Groundwater Interaction with MODFLOW: Some Considerations." *Ground Water*, vol. 48, no. 2, 2010, pp. 174–180., doi:10.1111/j.1745-6584.2009.00644.x.
- Constantz, Jim, et al. "Analysis of Streambed Temperatures in Ephemeral Channels to Determine Streamflow Frequency and Duration." *Water Resources Research*, vol. 37, no. 2, 2001, pp. 317–328., doi:10.1029/2000wr900271.
- Fox, G.A. An improved unsaturated flow module for MODFLOW's RIVER package. In: Ramirez JA, editor: Proceedings of the 23rd Annual American Geophysical Union Hydrology Days, Colorado State University, Fort Collins, Colorado, 2003.
- Fox, Garey A., and Deanna S. Durnford. "Unsaturated Hyporheic Zone Flow in Stream/Aquifer Conjunctive Systems." *Advances in Water Resources*, vol. 26, no. 9, 2003, pp. 989–1000., doi:10.1016/s0309-1708(03)00087-3.
- Fox, Garey A., G.V. Wilson, A. Simon, E.J. Langendoen, O. Akay, J.W. Fuchs., 2007, Measuring streambank erosion due to ground water seepage: correlation to bank pore water pressure, precipitation, and stream stage. *Earth Surface Processes and Landforms*. 32, pp. 1558-1573, doi:10.1002/esp.1490
- Fox, Garey A., D.M. Heeren, M.A. Kizer, 2011, Evaluation of a Stream-Aquifer Analysis Test for Deriving Reach-Scale Streambed Conductance. *Transactions of the American Society of Agricultural and Biological Engineers*. 54(2): 473-479
- Furman, A., 2008, Modeling coupled surface-subsurface flow processes: A review, *Vadoze Zone J.*, 7(2), 741-756, doi:10.2136/vzj2007.0065.

- Hancock, Peter J., A.J. Boulton, W.F. Humphreys, 2005, Aquifers and Hyporheic Zones: Towards an Ecological Understanding of Groundwater. *Hydrogeology Journal*, vol. 13, no. 1, pp. 98–111., doi:10.1007/s10040-004-0421-6.
- Hazen, Allen. 1892. Some physical properties of sands and gravels. Mass. State Board of Health, Ann. Rept. pp. 539-556.
- Hughes, J.D., Langevin, C.D., Chartier, K.L., and White, J.T., 2012, Documentation of the Surface-Water Routing (SWR1) Process for modeling surface-water flow with the U.S. Geological Survey Modular Ground-Water Model (MODFLOW-2005): U.S. Geological Survey Techniques and Methods, book 6, chap. A40 (Version 1.0), 113 p.
<https://pubs.er.usgs.gov/publication/tm6A40>
- Hunt, Bruce, J. Weir, B. Clausen, 2001, A Stream Depletion Field Experiment. *Ground Water*, vol. 39, no. 2, pp. 283–289., doi:10.1111/j.1745-6584.2001.tb02310.x.
- Kalbus, E., et al. “Measuring Methods for Groundwater, Surface Water and Their Interactions: a Review.” *Hydrology and Earth System Sciences Discussions*, vol. 3, no. 4, 2006, pp. 1809–1850., doi:10.5194/hessd-3-1809-2006.
- Keller, Edward A., and G.M. Kondolf., 1990, Chapter 15. Groundwater and Fluvial Processes; Selected Observations. *Groundwater Geomorphology; The Role of Subsurface Water in Earth-Surface Processes and Landforms Geological Society of America Special Papers*, pp. 319–340., doi:10.1130/spe252-p319.
- Lee, David Robert. “A Device for Measuring Seepage Flux in Lakes and Estuaries.” *Limnology and Oceanography*, vol. 22, no. 1, 1977, pp. 140–147., doi:10.4319/lo.1977.22.1.0140.

- Mehl, Steffen, and Mary C. Hill. "Grid-Size Dependence of Cauchy Boundary Conditions Used to Simulate Stream-Aquifer Interactions." *Advances in Water Resources*, vol. 33, no. 4, 2010, pp. 430–442., doi:10.1016/j.advwatres.2010.01.008.
- Miller, Calvin D., et al. "Stream Depletion in Alluvial Valleys Using the SDF Semianalytical Model." *Ground Water*, vol. 45, no. 4, 2007, pp. 506–514., doi:10.1111/j.1745-6584.2007.00311.x.
- Myers, Tom, 2013, Remediation scenarios for selenium contamination, Blackfoot watershed, southeast Idaho, USA. *Hydrogeology Journal*, 21, pp. 655-671., doi:10.1007/s10040-013-0953-8.
- Niswonger, R.G. and Prudic, D.E., 2005, Documentation of the Streamflow-Routing (SFR2) Package to include unsaturated flow beneath streams--A modification to SFR1: U.S. Geological Survey Techniques and Methods, Book 6, Chap. A13, 47 p.
- Nyholm, T., S. Christensen, K.R. Rasmussen, 2002, Flow Depletion in a Small Stream Caused by Ground Water Abstraction from Wells. *Ground Water*, 40(4), pp. 425-437.
- Osman, Yassin Z, and Michael P Bruen. "Modelling Stream-Aquifer Seepage in an Alluvial Aquifer: an Improved Loosing-Stream Package for MODFLOW." *Journal of Hydrology*, vol. 264, no. 1-4, 2002, pp. 69–86., doi:10.1016/s0022-1694(02)00067-7.
- Ou, Gengxin, et al. "Development of a Cross-Section Based Streamflow Routing Package for MODFLOW." *Environmental Modelling & Software*, vol. 50, 2013, pp. 132–143., doi:10.1016/j.envsoft.2013.09.012.
- Rodriguez, Leticia B., et al. "Fully Conservative Coupling of HEC-RAS with MODFLOW to Simulate Stream-Aquifer Interactions in a Drainage Basin." *Journal of Hydrology*, vol. 353, no. 1-2, 2008, pp. 129–142., doi:10.1016/j.jhydrol.2008.02.002.

- Schaffranek, R., Baltzer, R., Goldberh, D., 1981. A model for Simulation of Flow in Singular and Interconnected Channels. U.S. Geological Survey p. 110 number Book 7, Chapter C3 in Techniques of Water-Resources Investigations.
- Shepherd, Russell G. “Correlations of Permeability and Grain Size.” *Ground Water*, vol. 27, no. 5, 1989, pp. 633–638., doi:10.1111/j.1745-6584.1989.tb00476.x.
- Sophocleous, Marios, M.A. Townsend, L.D. Vogler, T.J. McClain, E.T. Marks, G.R. Coble, 1988, Experimental Studies in Stream-Aquifer Interaction along the Arkansas River in Central Kansas - Field Testing and Analysis. *Journal of Hydrology*, vol. 98, no. 3-4, 1988, pp. 249–273., doi:10.1016/0022-1694(88)90017-0.
- Sophocleous, M. “From Safe Yield to Sustainable Development of Water Resources; the Kansas Experience.” *Journal of Hydrology*, vol. 235, no. 1-2, 2000, pp. 27–43., doi:10.1016/s0022-1694(00)00263-8
- Sophocleous, Marios. “Interactions between Groundwater and Surface Water: the State of the Science.” *Hydrogeology Journal*, vol. 10, no. 2, 2002, pp. 348–348., doi:10.1007/s10040-002-0204-x.
- Stonestrom, David Arthur., and Jim Constantz. *Heat as a Tool for Studying the Movement of Ground Water near Streams*. U.S. Dept. of the Interior, U.S. Geological Survey, 2003.
- Storey, Richard G., et al. “Factors Controlling Riffle-Scale Hyporheic Exchange Flows and Their Seasonal Changes in a Gaining Stream: A Three-Dimensional Groundwater Flow Model.” *Water Resources Research*, vol. 39, no. 2, 2003, doi:10.1029/2002wr001367.
- Swain, E.D., 1993, Documentation of a Computer Program (Streamlink) to represent Direct-Fflow connections in a Coupled Ground-water and Surface-water Model. Technical Report 93-4011. U.S. Geological Survey, Tallahassee, Florida.

Therrien, R., R.G. McLaren, E.A. Studickym and S.M Panday. 2006. *Hydrogeosphere*.

Waterloo, Canada: Groundwater Simulations Group, University of Waterloo.

Woessner, William W., and Kevin E. Sullivan. “Results of Seepage Meter and Mini-Piezometer

Study, Lake Mead, Nevada.” *Ground Water*, vol. 22, no. 5, 1984, pp. 561–568.,

doi:10.1111/j.1745-6584.1984.tb01425.x.

4. A COMPARISON OF ANALYTICAL AND NUMERICAL METHODS: A SYNTHESIS

4.1 Introduction

This chapter provides a synthesis of the methods and results used in the previous chapters. In particular, results from analytical and numerical models are compared directly with the goal of assessing not only the accuracy and validity of each approach but also to provide suggestions on when each method is appropriate to use under various circumstances.

4.2 Groundwater Head Distribution

In this analysis, two methods were employed for modeling groundwater head distributions. In Chapter 2, time series of drawdowns were analyzed to determine the effects of pumping on groundwater head at specified points in space. The model that was used was the analytical Hunt (1999) drawdown solution. Without further explanation, Hunt's solution is given as (see Chapter 2 for a review of limiting assumptions and parameter definitions):

$$\phi(x, y, t) = \frac{Q_w}{4\pi T} \left\{ E_1 \left[\frac{(L-x)^2 + y^2}{4Tt/S} \right] - \int_0^\infty e^{-\theta} E_1 \left[\frac{\left(L + |x| + \frac{2T\theta}{\lambda} \right)^2 + y^2}{\frac{4Tt}{S}} \right] d\theta \right\} \quad (4.1)$$

Drawdown was also computed numerically in Chapter 3 with MODFLOW (coupled with the DSF stream module). Figs. 32-35 shows the comparison between each modeling approach at Locations A, C, D, and E compared against field measured data. The data is plotted on a semi-logarithmic abscissas and the ordinate is in terms of drawdown (not hydraulic head with respect to a specified datum as was done in Chapter 3). This was done to remove the effects from variations in the non-uniform head distribution prior to pumping in the MODFLOW model. Fig. 32 is of the time variant drawdown at the 4.24 m observation well at Location A. While Hunt's equation is able to model the general trend of the drawdown curve it is not able to capture the

deviations in this trend to changes in stream stage and the ensuing stream fluxes. Of course, the DSF module used in MODFLOW is designed to accurately simulate these fluxes and so the numerical drawdown curve is able to model changes in drawdown due to factors beyond pumping, especially seen at later times.

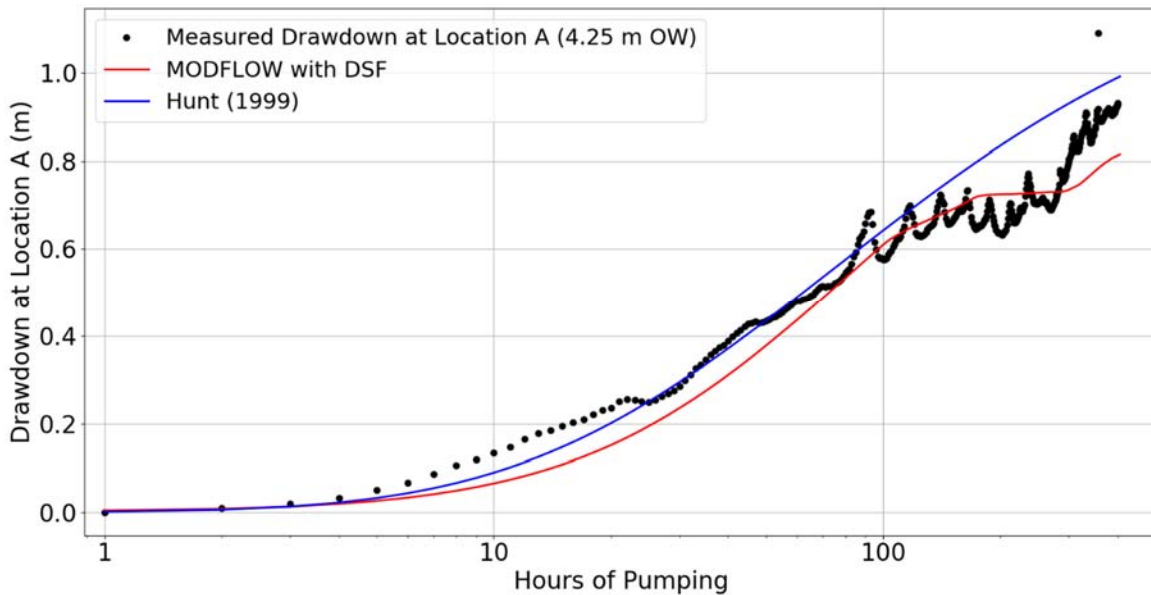


Figure 32. Drawdown predictions from Hunt (1999) solution and MODFLOW DSF at Location A.

The same qualitative comparison between the two solutions at Location A can also be applied at Location E, on the opposite side of the river (Fig. 33). Again, while the Hunt solution models the general trend of the drawdown, the numerical solution is better suited to capture fluctuations in this trend. Based on the drawdown analysis at Location A and E it would appear that if time variant drawdown predictions are required (and not just the average drawdown trend over pumping) then the numerical model is the preferred model to provide these results.

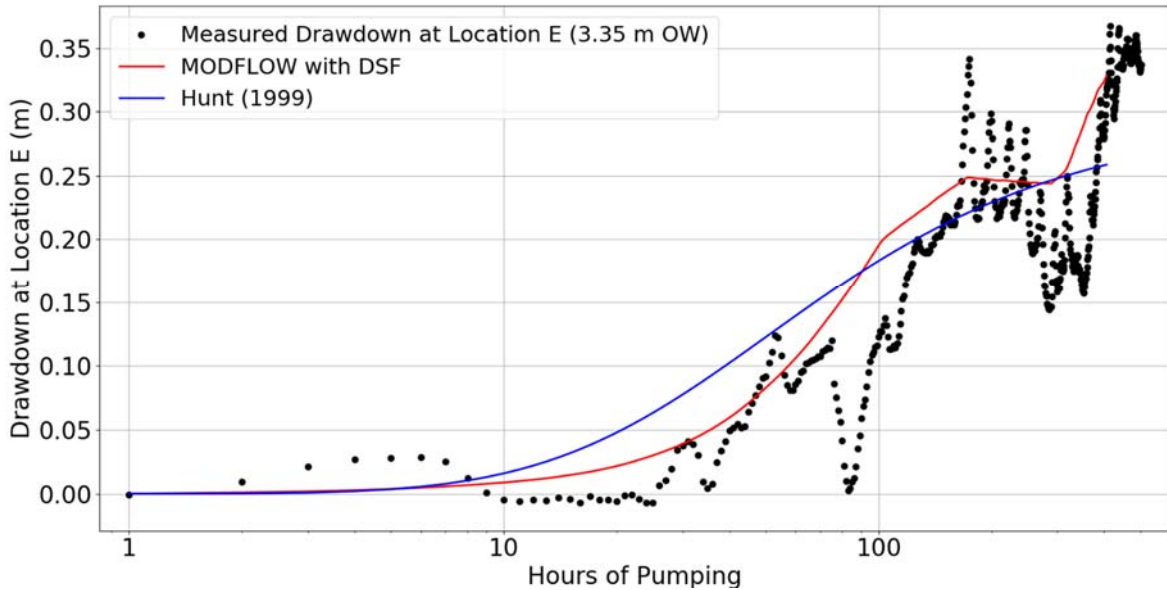


Figure 33. Drawdown predictions from Hunt (1999) solution and MODFLOW DSF at Location E.

However, if the drawdown at the 9.14 m observation well at Location D is compared the MODFLOW solution begins to deviate from the measured drawdown at later times and the analytical Hunt model provides more accurate results (Fig. 34). The reason for this is that the alluvium is most likely exhibiting delayed yield affects which are not being modeled accurately in the MODFLOW model. As mentioned in Chapter 3, the specific yield near the river was assigned a slightly higher than normal value (0.35) in the MODFLOW to obtain more stable results using the DSF module. Based on the analytical modeling in Chapter 2 the average specific yield in the alluvium is approximately 0.2. The larger specific yield value within MODFLOW will lead to under predictions in pumping-induced drawdown. Similarly, this same effect is seen at the 9.14 m well at Location C (Fig. 35). During early times (prior to 200 hours of pumping) the MODFLOW produced drawdown curve provides extremely accurate results. However, during later times, the numerical solution begins to flatter as the measured drawdown

continues to increase. Moreover, at these later times, the Hunt solution proves to be the more accurate solution.

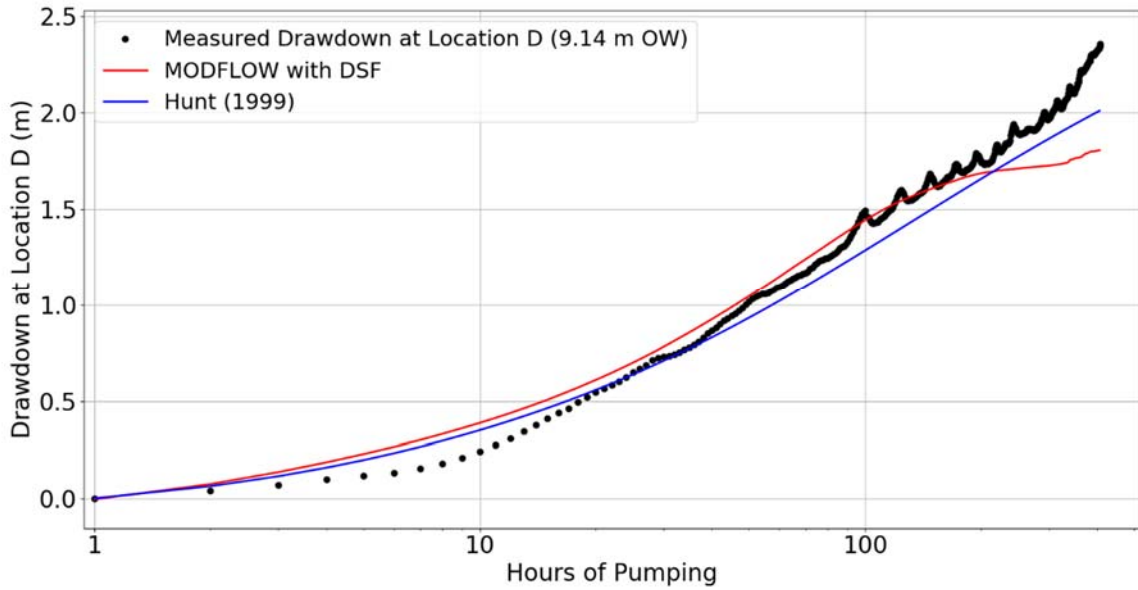


Figure 34. Drawdown predictions from Hunt (1999) solution and MODFLOW DSF at Location D.

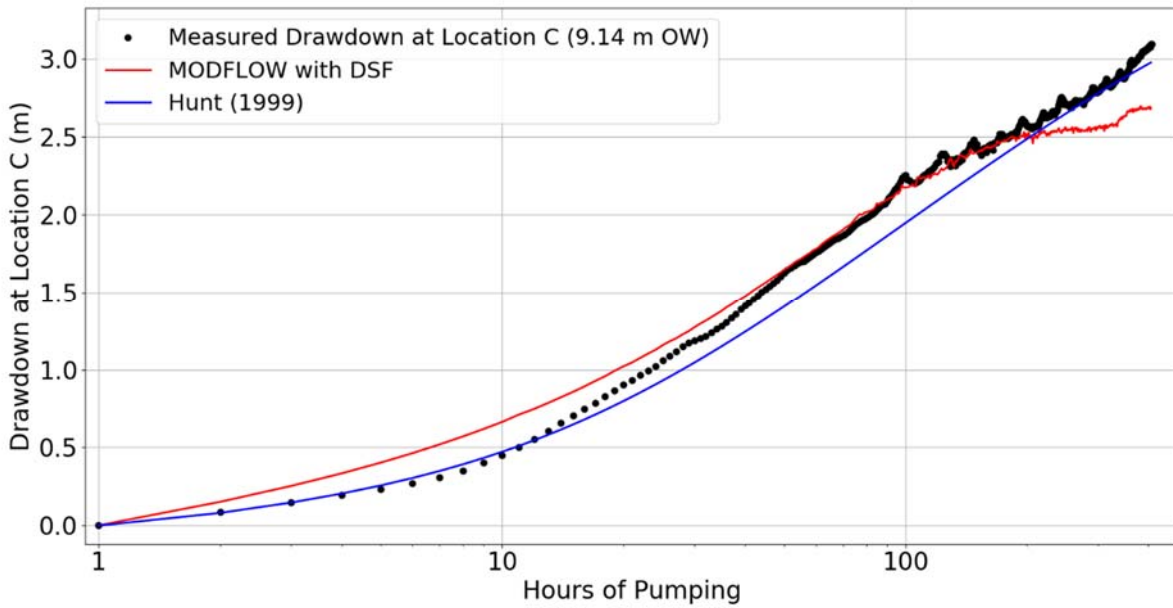


Figure 35. Drawdown predictions from Hunt (1999) solution and MODFLOW DSF at Location C.

Table 7 summarizes the RMSE between the two modeled drawdowns and the measured data at all four locations. At all locations except Location A, the Hunt solution produces a smaller error than MODFLOW when predicting drawdown. First, it should be noted that, as discussed in Chapter 2, each Hunt drawdown curve was independently calibrated and so the same parameter set was not used for each module. The drawdown curves in the MODFLOW model were all simultaneously computed using the same parameter set. Moreover, the Hunt drawdown curves all assume a uniform initial head distribution and a uniform alluvial bottom, both assumptions of which are not true in reality. Other violations are the treatment of the river as a straight line and the neglecting of boundary conditions, as the Hunt solution assumes an infinite aquifer. Therefore, the Hunt solution is inherently flawed when applied to this system despite producing more accurate results (at least in a least squares sense). That is to say, colloquially, “it is right for the wrong reasons”. That being said, as a first analysis tool it is extremely viable.

Table 7. Root Mean Square Error (RMSE) of drawdown predictions of Hunt (1999) solution and MODFLOW DSF.

Location	MODFLOW with DSF	Hunt (1999)
RMSE at Location A (m)	0.0681	0.1118
RMSE at Location E (m)	0.0606	0.0564
RMSE at Location D (m)	0.2274	0.1345
RMSE at Location C (m)	0.1855	0.1488

At all locations but Location E the drawdown at later times are greater when simulated with the Hunt solution than with the MODFLOW model. Fig. 36 is a plot of the difference between the predicted drawdown using the Hunt solution and MODFLOW projected onto the study area (hashed circles are the four pumping wells) after 400 hours of pumping. The solid turquoise line is the actual river modeled within MODFLOW and the dashed turquoise line is the representative straight river modeled with the Hunt solution. As seen by the contour lines, except at locations

very near to the pumping wells, the computed drawdown from the Hunt solution exceeds the computed drawdown obtained from MODFLOW. Near the two most northern pumping wells the difference between the two models ranges from 0.05 to 0.2 m. Similar magnitudes of difference also exist in the eastern regions of the study area. However, in the southern areas of the study area the difference between the two models grows very quickly and approaches 0.5 m.

The reason for this is due to how the river is modeled in the Hunt model. In reference to Fig. 36, the actual river arcs around all of the pumping wells and observation wells. However the Hunt solution assumes a straight river which creates a representative river which lies farther away from the southernmost pumping wells than in reality. Subsequently, the source of water coming from the river is not as strongly felt and drawdown will over predicted. The MODFLOW model (with the DSF module) models the exact location of the river and does not have this problem. As a result, the difference between the two models in this area are very large. Therefore, in this sense, the numerical model is preferred over the Hunt model as refined spatial geometry can be well modeled.

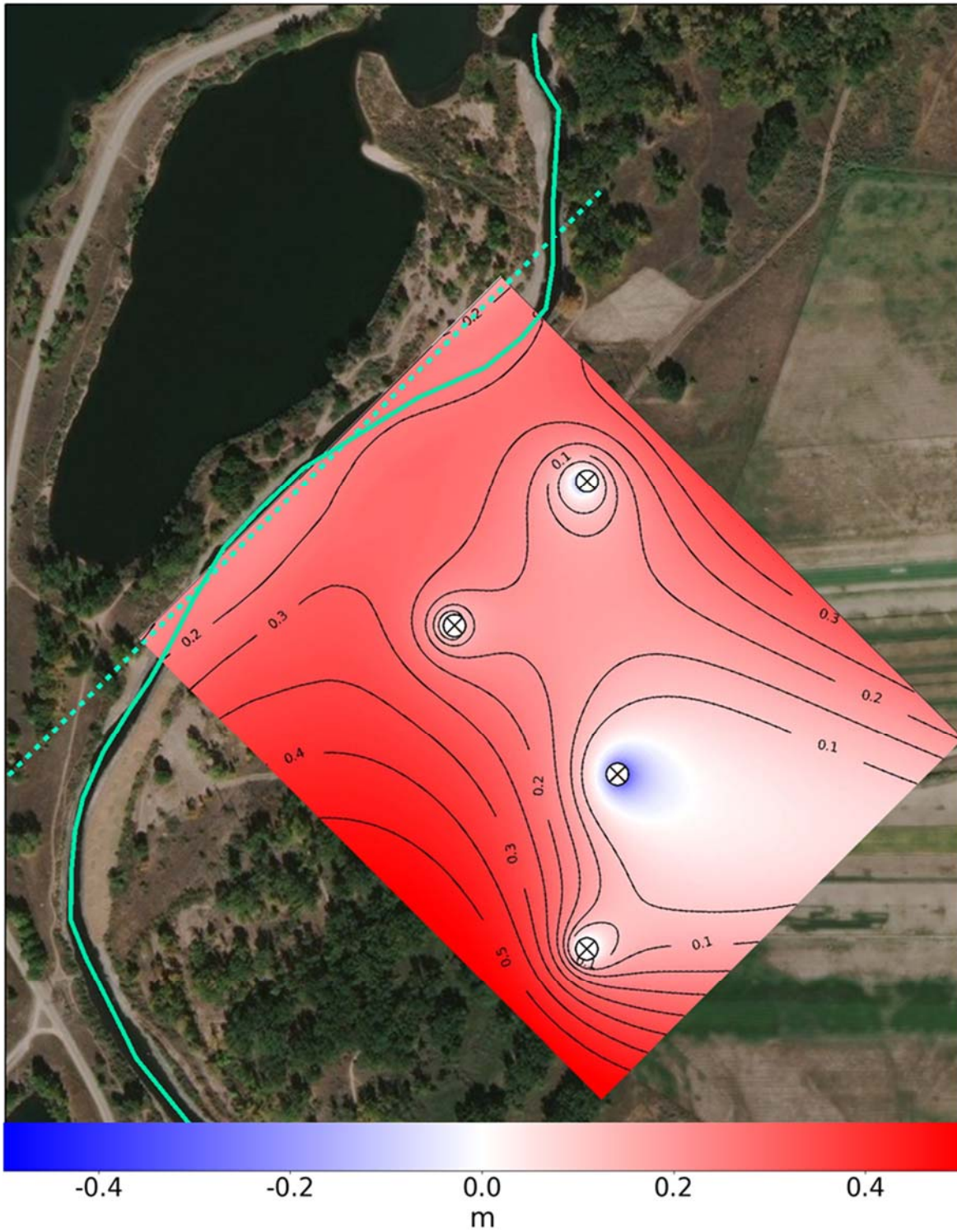


Figure 36. Contour map of the difference in drawdown (m) predictions between Hunt (1999) solution and MODFLOW DSF.

4.3 Streamflow Loss

In Chapter 2 it was shown that for low constant streamflows that the Hunt streamflow depletion equation is an accurate model for this particular reach of the South Platte River. However when the streamflow is high and variable, its limiting assumptions (namely, constant stream width and stage) are violated and the model becomes invalid. A semi-analytical solution was proposed in which losses due to changing stream stage and width are also accounted for so that a general streamflow loss equation can be obtained (Eq. 2.8). In essence, what the semi-analytical model accomplishes is the allowance of a streamflow depletion equation accounting for exclusively hydrostatic mechanisms (pumping wells) to also account for hydrodynamic mechanisms (streamflow). This is accomplished with the empirical term added to a pumping equation. It was shown that given sufficient data characterizing these background losses that the semi-analytical method was very adequate in predicting streamflow losses for all river conditions.

In Chapter 3, streamflow loss was modeled using the numerical model, MODFLOW. The existing river packages (specifically SFR2) was shown to struggle in predicting streamflow losses due to the constraint that a river cannot span multiple cells within the existing stream modules. A new stream module DSF which overcome these limitations was developed and was shown to be more accurate than the SFR2 module. Like the semi-analytical method proposed in Chapter 2, the DSF module in effect allows for a hydrostatic model (MODFLOW) to account for hydrodynamic effects (through the DSF module). Note that DSF is not directly accounting for hydrodynamic forces, just the effects of them.

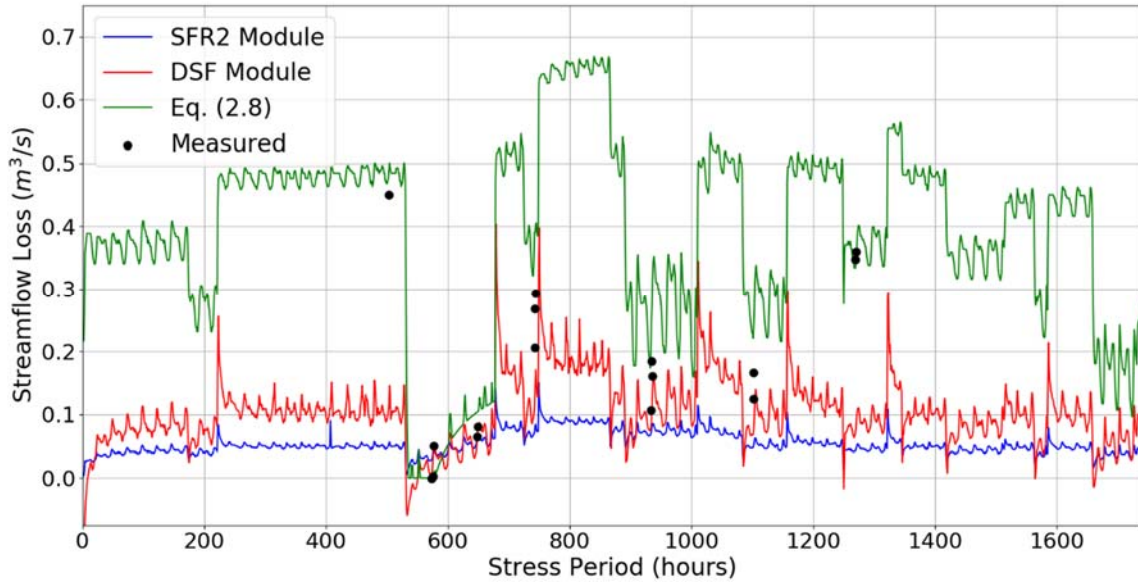


Figure 37. Predicted streamflow loss from the SFR2 module, the DSF module, and Eq. (2.8) compared with field collected data.

Fig. 37 shows the computed streamflow loss from three models: the semi-analytical approach given in Chapter 2, the DSF module, and the SFR2 module. Because the model of Eq. (2.8) was developed using streamflow data during times of large upstream flow, it is the best suited model for predicting streamflow during these times. In general, Eq. (2.8) over predicts streamflow loss during times of lower flow (also corresponding to pumping times) for the reasons discussed in Chapter 2. During these times, the DSF module is the most accurate model. The SFR2 module is limited in the range of values it can predict and is not an accurate model for the circumstances (highly variable flowrates) defining this reach and study period. Table 8 gives the RMSE of the three modules.

Table 8. Root Mean Square Error (RMSE) of predicted streamflow loss of the SFR2 module, DSF module, and Eq. (2.8).

MODEL	RMSE (m ³ /s)
SFR2	0.17
DSF	0.14
Eq. (2.8)	0.08

The large errors for DSF and SFR2 modules are due to the large differences between observed data and modeled output for the first and last two measured data points. If these three points are neglected in the error calculations then the RMSE of the three modules then become (Table 9):

Table 9. Root Mean Square Error (RMSE) of predicted streamflow loss of the SFR2 module, DSF module, and Eq. (2.8) when streamflow loss data collected during times of largest streamflow are neglected.

MODEL	RMSE (m ³ /s)
SFR2	0.11
DSF	0.07
Eq. (2.8)	0.09

where, the DSF module is now the more accurate solution.

Fig. 38 compares the pumping-induced streamflow loss when computed with the DSF module and Eq. (2.8). The pumping-induced losses in Eq. (2.8) are obtained from the Hunt solution. It is interesting to note that while obviously each module produces the same general trend, the Hunt solution predicts more pumping-induced streamflow loss. This is perhaps unexpected as the Hunt solution assumes a straight river that will have a greater average effective distance from the pumping wells than the arced river that DSF models. Moreover, unsaturated zone are not modeled with the Hunt solution and which are of course modeled within the DSF module. The two most likely reasons for these unexpected results are the effects of

boundary conditions and large specific yields near the river in the MODFLOW model. As shown in Fig. 20b, the MODFLOW model was developed with a constant head boundary along the ponds on the western flank of the model domain. This prevents greater drawdown due to the pumping wells and further streamflow loss. Moreover, as discussed in Chapter 3, the specific yield near the river was assigned to be approximately 0.35 while the rest of the alluvium had an assumed specific yield value of 0.13 - 0.2 (as the Hunt equation also assumed in Chapter 2). While the larger specific yield values near the river produced more stable results, this also creates an unrealistic condition where drawdown near the river occurs relatively slowly.

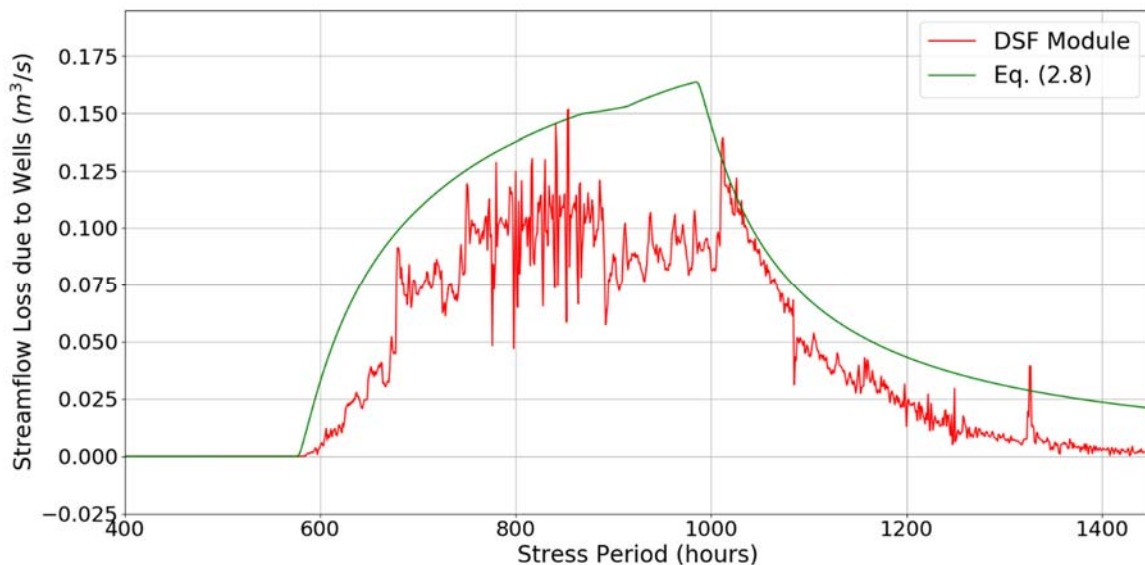


Figure 38 - Comparison of pumping-induced streamflow loss using DSF module and Eq. (2.8).

Despite this, Fig. 39 shows the portion of streamflow loss due to the pumping wells computed with the DSF module and Eq. (2.8) and the results are quite similar. Apart from early times (when the total loss due to the pumping wells is small) the predicted portion of the pumping induced streamflow loss on the total streamflow loss between the two models is very similar. Small deviations exist due to more subtle intricacies (channel geometry, boundary

conditions) being modeled within MODFLOW and not in the analytical modeling. The implications of these similarities are very important. First, the likeness of the two model outputs, which were obtained and developed in very different and independent manners, suggests that results provide an accurate portrayal of what is occurring in the alluvium. That is to say, that the empirical equation describing background losses in Chapter 2 is reliable and the physics and numerics upon which DSF is based (Chapter 3) are accurate. Second, this further suggests the importance of determining the existing or background streamflow losses when trying to determine pumping-induced streamflow loss. Fig. 39 shows that for this particular reach of the South Platte River often (especially during times of high flow) pumping only contributes up to 20-60% of streamflow loss.

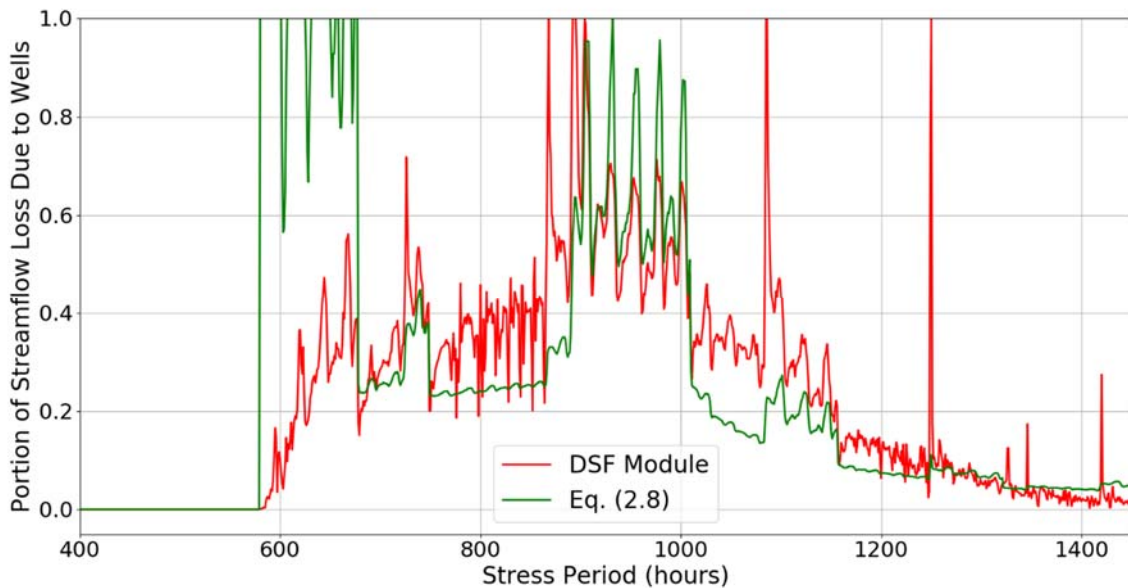


Figure 39. Portion of streamflow loss due to pumping wells when computed with Eq. (2.8) and the DSF module.

5. CONCLUSIONS AND FUTURE WORK

5.1 Analytical Solutions

The Glover and Hunt streamflow depletion equations in their current forms were not well suited for predicting streamflow loss along this reach of the South Platte River. This is because streamflows varied greatly over the study period leading to expanded stream widths and induced bank seepage. As streamflow loss was occurring due to other factors beyond the pumping wells, it was impossible to use the analytical solutions to assess the effect of pumping on streamflow. When the Hunt solution was modified to account for these background losses, a new semi-analytical equation was produced which was capable of modeling all streamflow loss. The semi-analytical equation also allowed for losses due to pumping to be separated from losses independent of pumping. As a first analysis, it was shown that for this particular reach of the South Platte River that losses external to pumping contributed to as much as 60% of streamflow losses. In general, if analytical streamflow depletion equations are to continue to be used in water management, the methodology outlined in Chapter 2 should be applied to account for all streamflow losses, regardless of pumping.

Hunt's drawdown equation was very adequate in predicting drawdown from pumping wells, statistically, performing better than MODFLOW. Due diligence should be taken in assuring that limiting assumptions are not violated in the physical world when applying the Hunt drawdown equation. In particular, along this reach, the Hunt drawdown solution predicted drawdown inaccurately when modeled stream geometry did not align with the physical stream geometry.

5.1.1 Future Work on Analytical Solutions

Deviations from analytical model output and observed data were the result of changes in the surface water conditions. An analytical model that can account for changes in river conditions

(whether it be in river width or stage) could prove to be an improvement in accounting for these differences. There seems to have been a move away from analytical models in favor of numerical models in hydrologic modeling. While numerical models are inherently more robust and capable of solving a wider variety of problems, the work shown in this study proves the value of analytical solutions when applied in the correct circumstances. Analytical models are difficult to derive but their value is immense.

5.2 Numerical Solutions

The developed MODFLOW model for the study site could not accurately predict streamflow losses with the existing stream modules. The DSF module was shown to be an improvement over existing MODFLOW stream modules and was capable of not only simulating more accurate streamflow loss rates but also groundwater heads near the stream. Confirming the analytical modeling work, DSF suggests that the pumping wells only make up to half of the total streamflow loss occurring along this reach of the South Platte River.

5.1.1 Future Work for DSF Module

Discrepancies between simulated streamflow loss and measured streamflow loss using DSF still existed for large flows. The author believes this to be the result of horizontal seepage occurring that is not modeled within DSF. Future work on improving DSF will include these fluxes to determine their impact on a losing stream. Moreover, DSF should be altered to account for inflows and outflows from surface water diversions, have a more sophisticated solver which allows for the computation of supercritical flows, and to model the full transient version of the dynamic wave approximation of the St. Venant equations to account for flood wave attenuation through a reach.

5.3 Overall Conclusions

The following conclusions can be made from the study:

- Current methods, both analytical and numerical, in determining pumping-induced streamflow loss are not well suited for systems in which hydrodynamic drivers are a major determinant in hyporheic flows.
- A generalized semi-analytical streamflow loss model can be developed that includes the effect of pumping wells and natural processes. This model can be used to estimate streamflow loss for the reach during times of pumping and non-pumping, facilitating water resources management of the stream-aquifer system.
- A new MODFLOW stream module was also developed which considers variable width streams that span multiple cells over a cross section.
- Both proposed models performed more accurately than existing methods.